

**POLYTECHNIQUE MONTRÉAL**

affiliée à l'Université de Montréal

**Lightning induced overvoltages caused by non-vertical lightning  
and earth current behavior**

**MASASHI NATSUI**

Département de génie électrique

Thèse présentée en vue de l'obtention du diplôme de *Philosophiæ Doctor*

Génie électrique

Juillet 2020

# **POLYTECHNIQUE MONTRÉAL**

affiliée à l'Université de Montréal

Cette thèse intitulée :

## **Lightning induced overvoltages caused by non-vertical lightning and earth current behavior**

présentée par **Masashi NATSUI**

en vue de l'obtention du diplôme de *Philosophiæ Doctor*

a été dûment acceptée par le jury d'examen constitué de :

**Houshang KARIMI**, président

**Jean MAHSEREDJIAN**, membre et directeur de recherche

**Akihiro AMETANI**, membre et codirecteur de recherche

**Keyhan SHESHYEKANI**, membre

**Genevieve LIETZ**, membre externe

## DEDICATION

*À ma femme, mon fils, et mes parents.*

*To my wife, my son, and my parents.*

## ACKNOWLEDGEMENTS

First and foremost, I would like to express my great appreciation to my supervisor Prof. Jean Mahseredjian for all his helpful guidance, valuable discussions, and continuous support during my doctoral research at Polytechnique Montréal.

I am sincerely grateful to Prof. Akihiro Ametani for his outstanding motivation, great patience, and continuous encouragement throughout my study. His advice with deep insight and comprehensive knowledge were very helpful in all aspects of my research work.

Discussion and assistance provided by Prof. Ilhan Kocar were much appreciated.

All colleagues at the department for their friendship and support, Isabel Lafaia, Baki Cetindag, Louis Filliot, Xiaopeng Fu, Fidji Diboune, Serigne Seye, Thomas Kauffmann, Anas Abusalah, Ming Cai, Jesus Morales, Miguel Martinez, Anton Stepanov, Reza Hassani, Aboutaleb Haddadi, David Tobar, Nazak Soleimanpour, Maryam Torabi, Amir Sadati, and Willy Mimbe.

I also extend my gratitude to Nippon Steel Corporation for giving me a great opportunity to study at Polytechnique Montréal.

Finally, I would like to thank my family: my wife Eriko Natsui, my son Sosuke Natsui, and my parents Tsuguo Natsui and Shigeiko Natsui for their constant support and encouragement.

## RÉSUMÉ

Les surtensions induites par la foudre deviennent un sujet important dans le domaine des réseaux de distribution. Une évaluation précise des tensions induites est très essentielle pour la protection contre la foudre. Un problème des évaluations existantes est qu'un canal de foudre vertical et une terre parfaitement conductrice, qui ne sont pas réalistes, sont supposés dans la plupart des cas. Ces hypothèses nécessitent des recherches plus approfondies pour une évaluation précise de la tension induite.

L'objectif principal de cette thèse est de révéler et résumer (1) les influences de la foudre non verticale sur les surtensions induites par la foudre dans les réseaux de distribution et (2) le comportement du courant de foudre dans une terre avec pertes, pour une évaluation précise des tensions induites.

Pour (1), les circuits du modèle FDTD pour représenter la foudre non verticale sont construits et les influences de la foudre non verticale sur les tensions induites sont étudiées avec diverses conditions telles que la forme d'onde du courant de foudre, la géométrie du canal de foudre, l'état de la terre et la distribution ligne, etc. De plus, le mécanisme des changements est discuté en comparaison avec une formule analytique. Il est clair que l'inclinaison de la foudre vers la ligne augmente considérablement les tensions induites. Les tensions atteignent plus de deux fois plus que celles du boîtier vertical. L'inclinaison le long de la ligne ne montre que des différences mineures sur la tension de crête alors qu'elle rend le profil de tension le long de la ligne asymétrique. Des tendances similaires sont observées même lorsque l'on suppose une ligne triphasée réaliste avec mises à la terre et parafoudres. Les connaissances acquises dans cette thèse indiquent clairement que les influences de la foudre non verticale doivent être prises en compte pour une évaluation précise des surtensions induites par la foudre.

Pour (2), les circuits du modèle FDTD sont validés par rapport aux résultats expérimentaux dans des articles publiés, et les influences de la distance de la foudre, de la position de la foudre sur la ligne, de la structure de mise à la terre, de la position du fil neutre, etc. sont étudiées par la FDTD. Il est confirmé que le couplage électromagnétique foudre-terre influence le courant de surface de la terre et l'augmentation du potentiel de terre (GPR) qui en résulte pendant une période transitoire, et donc l'inclinaison de la foudre rend le courant et le GPR différents du cas vertical. L'effet de

couplage doit être pris en compte pour des études précises du courant de terre et du GPR. Lorsqu'il y a une ligne de distribution à proximité, une grande partie du courant de foudre circule dans la ligne à proximité via ses mises à la terre. Bien que le courant lui-même ne fasse pas de grande différence sur la tension induite, cela provoquerait des problèmes de surtension de foudre dans la ligne.

## ABSTRACT

Lightning induced overvoltages are becoming one of the most important topics in the field of distribution networks. An accurate evaluation of the induced voltages is essential for the design of lightning protection. One problem of existing evaluations is that a vertical lightning channel and a perfectly conducting earth, which are not realistic, are assumed in most cases. These assumptions require further careful investigations for an accurate induced-voltage evaluation.

The main objective of this thesis is to reveal and summarize (1) the influences of non-vertical lightning on the lightning induced overvoltages in the distribution systems and (2) lightning current behavior in a lossy earth, for an accurate evaluation of the induced voltages.

For (1), FDTD model circuits to represent the non-vertical lightning are built and influences of the non-vertical lightning on the induced voltages are investigated with various conditions such as lightning current waveform, lightning-channel geometry, earth condition, and distribution-line configuration etc. In addition, the mechanism of the changes is discussed in comparison with an analytical formula. It is made clear that lightning inclination toward the line significantly increases the induced voltages. The voltages reach values that are more than two times larger than those of the vertical case. The inclination along the line shows only minor differences on the peak voltage while it makes the voltage profile along the line asymmetric. Similar trends are observed even when a realistic three-phase line with groundings and arresters is assumed. The knowledge obtained in this thesis clearly indicates that the influences of non-vertical lightning should be considered for an accurate evaluation of lightning induced overvoltages.

For (2), FDTD model circuits are validated in comparison with experimental results in published papers, and influences of lightning distance, lightning-struck position to the line, grounding structure, neutral wire position etc. are investigated by FDTD. It is confirmed that lightning-to-earth electromagnetic coupling influences the earth surface current and resulting ground potential rise (GPR) in a transient period, and thus the lightning inclination makes the current and GPR different from the vertical case. The coupling effect should be considered for accurate earth current and GPR studies. When there is a distribution line nearby, a large portion of lightning current flows into the nearby line via its groundings. Although the current itself does not make a large difference to the induced voltage, it would cause lightning surge problems in the line.

## TABLE OF CONTENTS

DEDICATION .....	III
ACKNOWLEDGEMENTS .....	IV
RÉSUMÉ.....	V
ABSTRACT.....	VII
TABLE OF CONTENTS .....	VIII
LIST OF TABLES .....	XIII
LIST OF FIGURES.....	XIV
LIST OF SYMBOLS AND ABBREVIATIONS.....	XXI
LIST OF APPENDICES .....	XXIII
CHAPTER 1 INTRODUCTION.....	1
1.1 Motivation .....	1
1.2 Thesis outline .....	2
1.3 Contributions.....	4
1.3.1 Lightning induced overvoltages caused by non-vertical lightning .....	4
1.3.2 Earth current behavior.....	5
CHAPTER 2 BASICS AND DEVELOPMENTS OF LIGHTNING INDUCED OVERVOLTAGE EVALUATIONS.....	7
2.1 Evaluation methods for lightning induced overvoltages.....	7
2.1.1 Analytical method .....	8
2.1.2 Transmission-line (TL) method .....	10
2.1.3 Numerical electromagnetic analysis (NEA) method.....	12
2.2 Lightning induced overvoltages with non-vertical lightning .....	14
2.2.1 Studies of non-vertical lightning between 1977-2000 .....	15



2.2.2	Induced voltages by non-vertical lightning.....	16
2.2.3	Lightning induced overvoltage and LEMP with lightning tortuosity .....	18
2.2.4	LEMP study by non-vertical lightning.....	19
2.3	Conclusion.....	20
CHAPTER 3 PRELIMINARY STUDY OF LIGHTNING INDUCED OVERVOLTAGES AND EARTH CURRENTS BY INCLINED LIGHTNING.....		21
3.1	Model circuit .....	21
3.2	Lightning induced voltages by inclined lightning.....	24
3.2.1	Influence of angle $\theta$ .....	24
3.2.2	Influence of angle $\varphi$ .....	26
3.2.3	Influence of rise time $T_f$ .....	27
3.2.4	Influence of return stroke velocity $\beta$ .....	29
3.3	Earth surface current by inclined lightning.....	29
3.4	Concluding remarks .....	32
CHAPTER 4 LIGHTNING INDUCED OVERVOLTAGES CAUSED BY INCLINED LIGHTNING .....		34
4.1	Lightning induced voltage in a single-conductor line by inclined lightning.....	34
4.1.1	Models.....	34
4.1.2	Lightning induced voltages caused by inclined lightning above a perfectly conducting earth .....	37
4.1.3	Influence of earth resistivity on induced voltage .....	41
4.1.4	Influence of lightning current waveforms on the induced voltage.....	45
4.1.5	Mean value of the induced voltage by inclined lightning .....	47
4.2	Lightning induced voltage in a three-phase distribution line by inclined lightning.....	48

4.2.1	FDTD model circuit .....	48
4.2.2	Induced voltages due to inclined lightning .....	49
4.3	Concluding remarks .....	51
CHAPTER 5	LIGHTNING INDUCED OVERVOLTAGES CAUSED BY NON-VERTICAL LIGHTNING .....	53
5.1	Induced voltages by bent lightning channels .....	53
5.1.1	FDTD model circuit .....	53
5.1.2	Induced voltages by bent lightning .....	55
5.2	Voltages by non-vertical lightning-like channel .....	63
5.2.1	Computationally generated lightning-like channel .....	63
5.2.2	Induced voltage .....	65
5.2.3	Incident electric field to the distribution line .....	66
5.3	Concluding remarks .....	67
CHAPTER 6	FUNDAMENTAL EARTH CURRENT BEHAVIOR AND RESULTING GROUND POTENTIAL RISE .....	68
6.1	Experiment for impulse current applied to grounding electrode.....	69
6.1.1	Test circuit.....	69
6.1.2	Test and FDTD results .....	71
6.2	FDTD Computation for earth current and GPR .....	72
6.2.1	FDTD model circuit for the current and GPR computation.....	72
6.2.2	Difference between lightning to earth and conducting pole .....	74
6.2.3	Influence of grounding electrode on earth current .....	75
6.2.4	Influence of grounding electrode on GPR.....	77
6.2.5	Distribution of earth currents and GPR.....	79

6.2.6	Influence of coupling between the lightning and earth .....	81
6.3	Effect of distribution line .....	83
6.3.1	Model circuit .....	83
6.3.2	Transient current and voltage .....	85
6.4	Concluding remarks .....	89
CHAPTER 7 NEARBY LIGHTNING SURGES FLOWING INTO A DISTRIBUTION LINE VIA GROUNDINGS .....		90
7.1	Experimental circuit .....	91
7.1.1	Test circuit.....	91
7.1.2	FDTD modeling .....	93
7.1.3	FDTD simulation in comparison with measured results .....	94
7.2	Investigation of lightning characteristics based on FDTD simulation .....	95
7.2.1	Current distribution .....	96
7.2.2	Voltage characteristics .....	99
7.2.3	Effect of lightning position .....	100
7.2.4	Effect of pole grounding resistance.....	103
7.2.5	Inclined lightning channel.....	105
7.2.6	Effect of neutral wire configuration .....	107
7.2.7	Return stroke current of 30 kA.....	109
7.3	EMTP Simulation.....	111
7.3.1	Modeling of test circuit .....	111
7.3.2	Simulation results .....	112
7.4	Concluding remarks .....	113
CHAPTER 8 CONCLUSIONS.....		115

8.1	Summary of thesis.....	115
8.1.1	Influences of non-vertical lightning on lightning induced overvoltages.....	115
8.1.2	Earth current behavior.....	116
8.2	Future work.....	117
8.2.1	Correction method for existing standards.....	117
8.2.2	Further verification and comparison with field test results.....	117
8.2.3	Statistical analysis of the non-vertical lightning influences.....	118
	<b>BIBLIOGRAPHY.....</b>	<b>119</b>
	<b>APPENDIX A LIST OF PUBLICATIONS.....</b>	<b>136</b>

## LIST OF TABLES

Table 3.1 Lightning channel modeling in FDTD .....	22
Table 4.1 Peak voltages and mean values .....	47
Table 6.1 Grounding resistance.....	85
Table 7.1 Arrester characteristic .....	92
Table 7.2 Grounding resistance.....	92
Table 7.3 Peak currents and voltages with the time of occurrence. ....	96

## LIST OF FIGURES

Figure 3.1 FDTD experimental configuration: Lightning channel base is located at the center of the working space and the distance between the base and a 10 m-height overhead line is 50 m. Lightning inclination angle $\theta$ and $\varphi$ vary from $+45^\circ$ to $-90^\circ$ and $0^\circ$ to $+90^\circ$ , respectively. ...	23
Figure 3.2 Return stroke current waveforms.....	24
Figure 3.3 Induced voltages on the overhead line with the inclined lightning of angle $\theta$ with $\varphi = 0^\circ$ : $\beta = 1.00$ , $T_f = 1.0 \mu\text{s}$ .....	25
Figure 3.4 Influence of the inclination angle $\theta$ with $\varphi = 0^\circ$ on the peak induced voltages: $\beta = 1.00$ , $T_f = 1.0 \mu\text{s}$ .....	25
Figure 3.5 Induced voltages due to the inclined lightning for various angle $\varphi$ with $\theta = 0^\circ$ : $\beta = 1.00$ , $T_f = 1.0 \mu\text{s}$ .....	26
Figure 3.6 Influence of the inclination angle $\varphi$ with $\theta = 0^\circ$ on the peak induced voltages: $\beta = 1.00$ , $T_f = 1.0 \mu\text{s}$ .....	27
Figure 3.7 Comparisons of the induced voltage waveforms between $T_f = 1.0 \mu\text{s}$ and $0.1 \mu\text{s}$ : $\beta = 1.00$ , $\theta = +45^\circ$ , $\varphi = 0^\circ$ .....	28
Figure 3.8 Comparison of the influence of the lightning inclination on the peak voltages between $T_f = 1.0$ : $\beta = 1.00$ , $\theta = +45^\circ$ .....	28
Figure 3.9 Influence of the lightning inclination angle $\theta$ with $\varphi = 0^\circ$ on the peak voltages between $T_f = 1.0 \mu\text{s}$ and $0.1 \mu\text{s}$ : $\beta = 0.33$ .....	29
Figure 3.10 Earth-surface current-density waveforms in the earth of $\rho_e = 0, 100$ , and $2000 \Omega\text{m}$ for $\theta = 0^\circ$ and $+45^\circ$ with $\varphi = 0^\circ$ : $\beta = 1.00$ .....	30
Figure 3.11 Peak values of the earth-surface current density caused by the lightning inclined at $\theta = 0^\circ$ and $+45^\circ$ with $\varphi = 0^\circ$ : $\beta = 1.00$ .....	31

Figure 3.12 Horizontal differential voltages between the earth surface under the measuring point of the overhead line and the surface of 50 m behind in the $y$ -direction: $\beta = 1.00$ , $\rho_e = 2000 \Omega\text{m}$ , $\varphi = 0^\circ$ .....	32
Figure 3.13 Peak differential voltages between the earth surface under the measuring point of the overhead line and the surface of 50 m behind in the $y$ -direction: $\beta = 1.00$ , $\varphi = 0^\circ$ .....	32
Figure 4.1 Model circuit.....	36
Figure 4.2 Return-stroke current waveforms. ....	36
Figure 4.3 Lightning induced voltages on a single-conductor overhead line caused by inclined lightning: $1/200 \mu\text{s}$ , $x = 0 \text{ m}$ , $d = 100 \text{ m}$ , $\rho_e = 0 \Omega\text{m}$ , comparison with an analytical formula [132]. ....	38
Figure 4.4 Influence of lightning inclination on voltage components of the induced voltage calculated by an analytical formula [132]: $x = 0 \text{ m}$ , $1/200 \mu\text{s}$ , $d = 100 \text{ m}$ , $\rho_e = 0 \Omega\text{m}$ . $U_{FDTD}$ is computed with FDTD and the others are computed with the analytical formula. ....	39
Figure 4.5 Peak induced voltages at $x = 0$ as a function of the angles $\theta$ and $\varphi$ computed by FDTD: $1/200 \mu\text{s}$ , $d = 50, 100, \text{ and } 1000 \text{ m}$ , $\rho_e = 0 \Omega\text{m}$ . ....	40
Figure 4.6 Peak voltage profiles along the line for the various angles $\theta$ and $\varphi$ computed by FDTD: $1/200 \mu\text{s}$ , $d = 100 \text{ m}$ , $\rho_e = 0 \Omega\text{m}$ . ....	41
Figure 4.7 Lightning induced voltages on a single-conductor line above a lossy earth caused by inclined lightning: $1/200 \mu\text{s}$ , $x = 0 \text{ m}$ , $d = 100 \text{ m}$ , in comparison with a TL method [71] for vertical lightning. ....	42
Figure 4.8 Peak voltages at $x = 0 \text{ m}$ for the lossy earth as functions of the angle $\theta$ and $\varphi$ computed by the FDTD: $1/200 \mu\text{s}$ , $d = 100 \text{ m}$ . ....	43
Figure 4.9 Peak voltage profiles along the line above the lossy earth for the various angles $\theta$ and $\varphi$ computed by the FDTD: $1/200 \mu\text{s}$ , $d = 100 \text{ m}$ . ....	44
Figure 4.10 Lightning induced voltages by current waveforms of $0.25/100$ and $5.5/200 \mu\text{s}$ : $x = 0 \text{ m}$ , $d = 100 \text{ m}$ , $\rho_e = 100 \Omega\text{m}$ , in comparison with a TL method [71] for vertical lightning....	45

Figure 4.11 Peak voltage ratios for lightning current waveforms of 0.25/100 and 5.5/200 $\mu\text{s}$ as a function of angle $\theta$ computed by the FDTD: $x = 0$ m. ....	46
Figure 4.12 FDTD model circuit of a multi-phase distribution line. ....	48
Figure 4.13 Lightning induced voltages at $x = 0$ m by the vertical lightning with various line configurations: single-phase (S) and multi-phase (M) overhead lines with utility poles (P), a shield wire with groundings (G), and arresters (A): 1/200 $\mu\text{s}$ , $d = 100$ m, in comparison with analytical formula[132] and the TL method [71] for the cases of (S).....	49
Figure 4.14 Lightning induced voltages at $x = 0$ m on the phase-b wire of MPG and MPGA lines due to the incline lightning: 1/200 $\mu\text{s}$ , $d = 100$ m. ....	50
Figure 4.15 Peak voltages at $x = 0$ m in MPG and MPGA lines as a function of the angle $\theta$ : 1/200 $\mu\text{s}$ , $d = 100$ m. ....	51
Figure 5.1 Model circuit. ....	54
Figure 5.2 Return stroke current. ....	55
Figure 5.3 Lightning induced voltages on a single-conductor overhead line by bent lightning with various bent heights and inclined angles $\theta$ : Case A, 1/200 $\mu\text{s}$ , $\rho_e = 0 \Omega\text{m}$ , $d = 50$ m, $\varphi = 0^\circ$ .56	
Figure 5.4 Lightning induced voltages on a single-conductor overhead line by bent lightning with various bent heights and inclined angles $\theta$ : Case B, 1/200 $\mu\text{s}$ , $\rho_e = 0 \Omega\text{m}$ , $d = 50$ m, $\varphi = 0^\circ$ .57	
Figure 5.5 Lightning induced voltages on a single-conductor overhead line by bent lightning with various bent heights and inclined angles $\varphi$ : Cases A and B, 1/200 $\mu\text{s}$ , $\rho_e = 0 \Omega\text{m}$ , $d = 50$ m, $\theta = 0^\circ$ . ....	58
Figure 5.6 Lightning induced voltages on a single-conductor overhead line by bent lightning with various bent heights and inclined angles $\theta$ : Case A, 1/200 $\mu\text{s}$ , $\rho_e = 1000 \Omega\text{m}$ , $d = 50$ m, $\varphi = 0^\circ$ . ....	59
Figure 5.7 Lightning induced voltages on a single-conductor overhead line by bent lightning with various bent heights and inclined angles $\theta$ : Case A, 1/200 $\mu\text{s}$ , $\rho_e = 1000 \Omega\text{m}$ , $d = 100$ and 300 m, $\varphi = 0^\circ$ . ....	61



Figure 5.8 Lightning induced voltages on a single-conductor overhead line by bent lightning with various bent heights and inclined angles $\theta$ : Case A, $5.5/200 \mu\text{s}$ , $\rho_e = 1000 \Omega\text{m}$ , $d = 300 \text{ m}$ , $\varphi = 0^\circ$ .	62
Figure 5.9 A lightning path generated by a probabilistic calculation based on an electric potential distribution [155], [156]. Yellow lines show lightning leaders which progress from cloud to ground, and a red line indicates a return stroke path after the leader attaches to the ground.	64
Figure 5.10 Lightning induced voltages on a single-conductor overhead line by 1) the computationally-generated and 2) simply-inclined lightning channels: $1/200 \mu\text{s}$ , $d = 50 \text{ m}$ , inclined angles $\theta = 11.5^\circ$ , and $\varphi = 0.5^\circ$ .	65
Figure 5.11 Incident electric field at $h = 10 \text{ m}$ (the line height) and $x = 50 \text{ m}$ (50-m distant from the line center) generated by 1) the computationally-generated and 2) simply-inclined lightning channels: $1/200 \mu\text{s}$ , $d = 50 \text{ m}$ , inclined angles $\theta = 11.5^\circ$ , and $\varphi = 0.5^\circ$ .	66
Figure 6.1 Test circuit of earth current and GPR measurements for a 30 m-length grounding electrode.	69
Figure 6.2 FDTD model circuit for earth current and GPR measurements.	71
Figure 6.3 Measured and FDTD computed results of earth currents and GPRs. Dotted lines show measured results in the test [22] and solid lines show FDTD computed results.	72
Figure 6.4 Model circuit for FDTD computation.	73
Figure 6.5 Earth-surface current density due to lightning to a ground and to a pole: $L = 0 \text{ m}$ , current of y component.	74
Figure 6.6 GPR at the earth surface due to lightning to a ground and to a pole: $L = 0 \text{ m}$ .	75
Figure 6.7 Current density $J$ for various electrode lengths $L$ : current of y component.	75
Figure 6.8 Peak earth current density as a function of electrode length $L$ : current of y component.	76
Figure 6.9 GPR waveforms with various electrode lengths $L$ .	78
Figure 6.10 GPR peak values as a function of electrode length $L$ .	78

Figure 6.11 Current density peaks as a function of distance $r$ from the source: current of $y$ component. ....	80
Figure 6.12 Current density peaks as a function of depth $d$ from the earth surface: current of $y$ component. ....	81
Figure 6.13 Influence of the lightning-to-earth electromagnetic coupling on the earth surface current. The electromagnetic field from the lightning channel to the earth surface is calculated by the Cooray-Rubinstein formula explained in [65], [67], and the current density is calculated by (6.1). ....	82
Figure 6.14 Model circuit for an investigation of a distribution line. ....	84
Figure 6.15 Currents flowing through a pole grounding ( $I_g$ ), a neutral wire ( $I_n$ ) and a phase wire ( $I_p$ ) for $L = 0$ m. ....	85
Figure 6.16 Transient GPR waveforms at Pole-1 foot ( $r = 10$ , $d = 0$ ) for various grounding structures of Pole 1: $L = 0$ m. ....	86
Figure 6.17 Earth-surface current distribution for Case 3 with and without Pole-1 as a function of distance from the lightning base.....	87
Figure 6.18 Distribution of earth surface current density $J_s$ in $x$ - $y$ plane at $t = 3.6 \mu\text{s}$ : lightning channel base ( $x = 0$ m, $y = 0$ m), Pole-1 of the distribution line ( $x = 0$ m, $y = 10$ m): $\rho_e = 100 \Omega\text{m}$ . ....	87
Figure 6.19 GPR peak values of current and GPR at Pole 1: $L = 0$ m. ....	88
Figure 6.20 Grounding current ( $I_g$ ) waveforms for various electrode length $L$ . ....	88
Figure 7.1 Test circuit for transient current measurements due to a lightning strike to ground near a distribution line.....	91
Figure 7.2 Return stroke current ( $I_L$ ) of FPL0350-1. ....	92
Figure 7.3 An example of grounding representation at Pole 15 in FDTD. ....	92
Figure 7.4 Measured and FDTD/EMTP computed results of ground lead current ( $I_g$ ) at each pole. ....	95

Figure 7.5 Currents $I_g$ , $I_n$ , and $I_a+I_b+I_c$ at pole 15, 10, and 1 computed by FDTD. ....	97
Figure 7.6 Phase-to-neutral voltages ( $V_a-V_n$ , $V_b-V_n$ , and $V_c-V_n$ ) at pole 15, 10, and 1 computed by FDTD. ....	98
Figure 7.7 Voltage $V = V_a-V_n$ , $dV/dt$ , current $I_a$ , and arrester capacitance calculated by $I_a$ divided by $dV/dt$ at Pole 14 in the initial transient. ....	99
Figure 7.8 Ground lead current and phase-to-neutral voltages at Pole 15 when the lightning channel is inclined $90^\circ$ in the opposite direction to the line and placed 1-m above the earth surface in the FDTD.....	100
Figure 7.9 Simulated results of currents and voltages in Cases A1 and A2. ....	102
Figure 7.10 Peak currents and phase-a voltages for various lightning positions. ....	103
Figure 7.11 Structure of Pole 15 grounding in Cases 0, B1, and B2. ....	103
Figure 7.12 Currents and voltages at Pole 15 in Case B1 and B2.....	104
Figure 7.13 Peak ground lead currents and phase-a voltages for different grounding resistances ( $R_g$ ) at Pole 15.....	104
Figure 7.14 Lightning channel inclination. ....	105
Figure 7.15 Influence of the lightning inclination on the ground-lead current ( $I_g$ ) at Pole 15.....	106
Figure 7.16 Influence of the lightning inclination on the phase-a voltage ( $V_a-V_n$ ) waveform. ...	106
Figure 7.17 Influence of the lightning inclination on the amplitude of the ground lead current ( $I_g$ ) and phase-a voltage ( $V_a-V_n$ ) of Pole 15 at peak and at $50 \mu s$ . ....	107
Figure 7.18 Study cases of the neutral wire position. ....	108
Figure 7.19 Effect of the neutral wire position on the peak phase-a voltage ( $V_a-V_n$ ).....	108
Figure 7.20 Peak phase-to-neutral voltages ( $V_a-V_n$ , $V_b-V_n$ , and $V_c-V_n$ ) in the cases of the neutral wires A9 (full length, Pole 15 to 1) plus: 1) A13 (full length), and 2) A13 (partial length, Pole 15 to 10). ....	108
Figure 7.21 Peak currents and phase-a voltages for various lightning positions with a return stroke current of 30 kA. ....	110

Figure 7.22 Current and voltage waveforms at Pole 10 in Case A2 with a return stroke current of 30 kA. ....	110
Figure 7.23 A comparison of the voltage waveforms at Pole 1 in Case A2 between return stroke currents of 8.4 and 30 kA. ....	110
Figure 7.24 Effect of the neutral wire position on the peak phase-a voltage $ V_a - V_n $ with a return stroke current of 30 kA. ....	111
Figure 7.25 EMTP model circuit. ....	112

## LIST OF SYMBOLS AND ABBREVIATIONS

This list presents the symbols and abbreviations used in the thesis in alphabetical order, along with their meanings.

< Symbols >

$\beta$	Ratio of lightning return-stroke velocity to the light speed
$d$	Distance/depth in Chapter 6
$\varepsilon_r$	Relative earth permittivity
$e_m$	An induced voltage generated by a vertical vector potential
$h$	Distribution line height
$h_A, h_B$	Bent heights of bent lightning channels in Chapter 5.
$I_0$	Return-stroke current amplitude
$I_a$	Current on a phase-a wire
$I_b$	Current on a phase-b wire
$I_c$	Current on a phase-c wire
$I_g$	Current on a grounding or a ground lead wire
$I_n$	Current on a neutral wire
$I_p$	Current on a phase wire
$I_L$	Lightning current
$J$	Earth current density
$\theta$	Lightning inclination angle toward a distribution line
$\varphi$	Lightning inclination angle along a distribution line
$L$	Grounding electrode length in Chapter 6
$\rho_e$	Earth resistivity

$r$	Distance from a grounding in Chapter 6
$T_f$	Rise time of a lightning return-stroke current (an exponential function is assumed)
$t_{d10-90}$	A wave-front duration time of which a lightning current rises from 10 to 90 %
$t_h$	A decay time of which lightning current decreases from peak to half
$U$	Total induced voltage
$V_a$	Voltage of a phase-a wire
$V_b$	Voltage of a phase-b wire
$V_c$	Voltage of a phase-c wire
$V_n$	Voltage of a neutral wire
$V_{s1}$	Traveling-wave voltage propagating from the left to the right on a distribution line
$V_{s2}$	Traveling-wave voltage propagating from the right to the left on a distribution line
$y_{min}$	Distance of which lightning may become a direct stroke to a distribution line

#### <Abbreviations>

EMTP	Electromagnetic transient program (software)
FDTD	Finite-difference time-domain method
FEM	Finite element method
GPR	Ground potential rise
LEMP	Lightning electromagnetic pulse
MoM	Method of moments
NEA	Numerical electromagnetic analysis
PCE	Perfectly conducting earth
TCS	Traveling-current-source model
TL	Transmission line

## LIST OF APPENDICES

Appendix A	List of publications.....	136
------------	---------------------------	-----

## CHAPTER 1 INTRODUCTION

### 1.1 Motivation

Power quality issues such as voltage stability in power systems are becoming more important especially in the field of distribution systems, because increasing numbers of electronic/digital devices including home appliances and renewable energy equipment are being installed on the systems [1]-[11]. Concerning voltage stability, “lightning” is one of the main causes of harmful overvoltages in distribution systems. In particular, indirect lightning is a more frequent event than direct lightning to distribution lines because the distribution lines have a medium line-height compared to other structures in their vicinity. The indirect lightning, which strikes near a distribution system, radiates an electromagnetic field which causes lightning induced overvoltages on the system, as is well-known [12]-[22]. An accurate evaluation of the induced voltages is, therefore, very important to protect distribution systems and power system devices.

Because real lightning experiments such as rocket-triggered lightning observations [23]-[24] are quite expensive, an accurate calculation of lightning induced overvoltages is one of the most important topics in this field. A number of analytical and numerical calculation methods have been proposed since the middle of the 20th century. However, in most cases, the lightning channel is assumed to be straight and vertical to the ground, because existing analysis techniques are mainly based on transmission line (TL) theory which cannot easily handle non-uniform conductors in a three-dimensional space [25]-[29]. In addition, a perfectly conducting earth is generally assumed due to the theoretical premise. In reality, a lightning channel is neither straight nor vertical, and the lightning current flows into a lossy earth. Therefore, these assumptions require further careful investigations for an accurate evaluation of lightning induced overvoltages.

This thesis focuses on revealing and summarizing (1) influences of non-vertical lightning on the lightning induced overvoltage in distribution systems and (2) lightning current behaviour in a lossy earth by using a finite-difference time domain (FDTD) computation method. The advantage of the method is that it can directly calculate Maxwell’s equations, i.e. it can handle an arbitrary configuration of the lightning channel and ground. Results computed by the FDTD are also compared with those by existing analytical/TL-based methods and measured results of induced-voltages/earth-currents in published papers.



## **1.2 Thesis outline**

This thesis is composed of eight chapters.

### **◆CHAPTER 1 – INTRODUCTION**

This chapter introduces the motivation for this research, highlights its contributions, and summarizes the contents of each chapter.

### **◆ CHAPTER 2 – BASICS AND DEVELOPMENTS OF LIGHTNING INDUCED OVERVOLTAGE EVALUATIONS**

Basics and developments of three evaluation methods (analytical, transmission-line (TL), numerical) for lightning induced overvoltages, especially in terms of non-vertical lightning and lossy earth, are summarized. Further, early studies of the lightning induced overvoltages with non-vertical lightning are reviewed.

### **◆CHAPTER 3 – PRELIMINARY STUDY OF LIGHTNING INDUCED OVERVOLTAGES AND EARTH CURRENTS BY INCLINED LIGHTNING**

A 3D-finite-difference time-domain (FDTD) method is employed to build a simple model circuit for a lightning-induced voltage study, and influences of inclined lightning on the induced voltage and earth current behavior are investigated as a preliminary study. The effects of the earth resistivity, lightning current waveform, and return stroke velocity as well as lightning inclination angles are summarized. It is clearly demonstrated that the induced voltage and earth current are greatly influenced by the inclined lightning.

### **◆ CHAPTER 4 – LIGHTNING INDUCED OVERVOLTAGES CAUSED BY INCLINED LIGHTNING**

Lightning induced overvoltages due to inclined lightning are investigated by the FDTD with more practical conditions which refer to published standards (IEEE/IEC) and papers. A single conductor line and a realistic multi-phase line (three-phase conductors with a shield wire, utility poles,

groundings, and arresters) are modeled and several investigations including a comparison with analytical and TL approaches are performed. Influences of the inclined lightning on the induced voltage are comprehensively summarized.

#### ◆CHAPTER 5 – LIGHTNING INDUCED OVERVOLTAGES CAUSED BY NON-VERTICAL LIGHTNING

Influences of non-uniform lightning geometry on the induced voltages are investigated by considering “bent” and “computationally-generated” channels in the FDTD computation. It is successfully demonstrated that the lightning channel geometry at low altitude is important for the induced voltages. In addition, it is confirmed that zig-zag non-vertical lightning can be represented by simply-inclined lightning in induced-voltage studies.

#### ◆CHAPTER 6 – FUNDAMENTAL EARTH CURRENT BEHAVIOR AND RESULTING GROUND POTENTIAL RISE

Fundamental behavior of an earth current flowing in a lossy earth is investigated. Measured results of the earth current in a published paper are compared with FDTD computed results to validate the FDTD model. Then, earth current distribution in the earth and the resulting ground potential rise (GPR) are investigated with various grounding conditions of a lightning-struck object. One important point is that the lightning channel is modeled in the FDTD working space to consider its influence on the earth surface current. In addition, the effect of a nearby distribution-line pole on the earth current distribution is revealed.

#### ◆CHAPTER 7 – NEARBY LIGHTNING SURGES FLOWING INTO A DISTRIBUTION LINE VIA GROUNDINGS

A rocket-triggered lightning experiment for lightning near a distribution line is reproduced by the FDTD. Lightning induced overvoltages and lightning current distributions flowing from the earth to the line via line groundings are investigated. The investigation includes not only measured

results but also non-observed voltage/current behavior computed by the FDTD. Further, the influence of inclined lightning on the induced voltage and the effect of neutral wire configuration on suppressing the induced voltages are summarized.

## ◆CHAPTER 8 – CONCLUSIONS

The results obtained in this thesis and expected future work are summarized.

### **1.3 Contributions**

The main achievements and contributions of this research are summarized here.

#### **1.3.1 Lightning induced overvoltages caused by non-vertical lightning**

##### **1.3.1.1 FDTD model circuit for induced voltages caused by non-vertical lightning**

FDTD model circuits to investigate lightning induced overvoltages caused by non-vertical lightning are built. The non-vertical lightning channel can be easily modeled by a series of current sources, which allows us to have flexibility of lightning parameters (e.g., current waveform, return stroke velocity etc.) and to obtain an undistorted electromagnetic field radiated from the channel. The validity of the non-vertical lightning model is confirmed in comparison with resulting induced voltages computed by the FDTD and an analytical formula for inclined lightning.

##### **1.3.1.2 Comprehensive parametric investigation of non-vertical lightning influences on the distribution-line voltages by FDTD**

Lightning induced overvoltages with non-vertical lightning were recently investigated in published papers in which the difference in induced voltages generated by vertical and non-vertical lightning was demonstrated (will be reviewed in Chapter 2). However, the investigations focused mainly on showing the difference, in other words, the difference has not been investigated and summarized parametrically and comprehensively.

This thesis has investigated and summarized the influences of the non-vertical lightning on the induced voltages by the FDTD with various conditions such as lightning parameters, lightning channel geometry, earth condition, voltage measuring point, and distribution-line configuration including a realistic three-phase line with poles, arresters, and groundings. When the non-vertical lightning is considered, the induced voltages in particular conditions are nearly two times higher than those obtained using the vertical-lightning assumption. Further, the induced voltage profile along a distribution line becomes asymmetric due to the lightning inclination along the line.

The influences explained above should be considered in lightning-induced overvoltage protection in power systems.

### **1.3.1.3 Mechanism of the induced-voltage changes by the non-vertical lightning**

FDTD-computed induced voltages are compared with those calculated by analytical and transmission-line based approaches to analyze the mechanism of the changes caused by the non-vertical lightning. It is made clear from the analytical-formula viewpoint that lightning inclination toward a distribution line increases both traveling-wave-voltage and vector-potential contributions to the induced voltages. Lightning inclination along the line causes no significant difference to the final induced voltages at the line center, while the traveling-wave voltages which propagate to the right and left of the line are significantly increased or decreased due to the inclination. The change finally results in an asymmetric voltage profile along the line.

## **1.3.2 Earth current behavior**

### **1.3.2.1 Earth surface current and resulting GPR by non-vertical lightning**

FDTD studies on non-vertical lightning reveal that the non-vertical lightning also influences the amplitude of an earth surface current and resultant ground potential rise (GPR) under the distribution line. Both the current and GPR induced by the non-vertical lightning increase by a factor of approximately two compared to those induced by vertical lightning.

### **1.3.2.2 Fundamental lightning-current distribution flowing in a lossy earth and influence of lightning-to-earth coupling**

Although some papers regarding groundings, earth current, and GPR have been published, only a few papers investigated an earth-surface current and GPR including a lightning channel in a 3D model circuit. The lightning channel geometry above the earth would influence the earth current as observed in an inclined lightning study. Thus, in this thesis, a 3D FDTD model circuit which includes groundings, the earth, and a vertical lightning channel in a working space is built, and fundamental earth current behavior and interactions between the lightning channel and the earth are investigated. It is confirmed that initial transient peaks of the earth surface current and GPR are significantly influenced by electromagnetic coupling between the lightning channel and the earth even though vertical lightning is assumed.

### **1.3.2.3 Nearby lightning current flowing into a distribution line via its groundings**

When there is a distribution line near a lightning-struck point, the lightning current is absorbed by the distribution line through its groundings. Firstly, the studies in this thesis clearly demonstrate the phenomenon. Then, an experimental result for lightning near a distribution line in a published paper is reproduced by the FDTD. The investigations undertaken using the FDTD model clarified the influences of lightning distance, lightning-struck position to the line, grounding structure, neutral wire position, and lightning inclination on the induced voltages/currents in the distribution line.

## CHAPTER 2      **BASICS AND DEVELOPMENTS OF LIGHTNING INDUCED OVERVOLTAGE EVALUATIONS**

### **2.1 Evaluation methods for lightning induced overvoltages**

Lightning induced overvoltages have been studied since the beginning of the 20th century, and Wagner and MacCann proposed a fundamental theory for analytical calculation in 1942 [33]. The theory was based on a concept, which is widely accepted nowadays, that a lightning return stroke generates a lightning electromagnetic pulse (LEMP) for exciting distribution lines. One problem of this theory was that the formulation did not consider the contribution of a vector potential on the induced voltages. In 1958, Rusck [34] presented an analytical formulation including both scalar and vector potentials as a voltage-inducing source. A vertical lightning channel and a perfectly conducting earth were assumed in the modeling. This method is adopted in IEEE Std.1410-2010 [12] as the “Rusck model”. Presently, several improved analytical formulas have been developed as discussed later.

From the 1960s, numerical evaluation methods based on transmission line (TL) theory have been developed [35]. In the initial stage, these theories also require the above-mentioned assumptions. However, numerous contributions have been made to relax or remove the restrictions. Nowadays, the TL method is the most common approach to calculate lightning induced overvoltages in power systems [25].

Since around the 1990s, numerical electromagnetic-analysis (NEA) methods such as the method of moments (MoM) [36], finite-element method (FEM) [37], and finite-difference time-domain method (FDTD) [38] have been applied to the lightning-induced overvoltage evaluations. These approaches initially appeared in the field of structure mechanics and communication engineering, and were applied to power systems engineering later. These methods are currently becoming a promising approach to evaluate lightning induced overvoltages under complex conditions in which the TL methods cannot handle easily [17].

This chapter reviews (1) basics and developments of the above-mentioned evaluation methods, especially for non-vertical lightning and lossy earth, and (2) previous studies regarding non-vertical lightning. Because recent lightning studies have been developed interactively by the above-mentioned methods, reference papers are firstly classified and numbered as follows.

<i>Analytical methods</i>	[39]-[49]
<i>Transmission-line (TL) method</i>	[49]-[87]
<i>Numerical electromagnetic analysis (NEA) method</i>	[88]-[124]
<i>Lightning-induced overvoltage study with non-vertical lightning</i>	[125]-[148]

## 2.1.1 Analytical method

### 2.1.1.1 Basics

Although the recent numerical computational approaches are widely used for lightning induced overvoltage investigations, analytical solutions still have strong advantages for engineering design [12] and parametric studies (e.g. [39]) as they yield theoretical insight which sometimes becomes obscured in numerical simulations.

The first important achievement in the analytical formulation was made by the Rusck model [34] as mentioned above. In the formulation, the electromagnetic (EM) field was calculated under the assumptions of vertical lightning, a perfectly conducting earth, a single infinite conductor and a stepwise lightning current. Also, the intensity of the induced electric and magnetic fields between the line and ground was approximated by the value at the ground surface, i.e. the height dependencies of the fields are ignored. The formulation of the induced voltage was based on the coupling equations proposed by Rusck, and the total induced voltage on the line was calculated by the contribution of scalar and vertical vector potentials between the line and ground.

Other formulas based on different lightning models and coupling equations have been proposed by Chowdhuri and Gross [40], Liew and Mar [41], and Høidalen [42] in 1967, 1986 and 2003, respectively. In 2009, Andreotti *et al.* [43] demonstrated a rigorous formulation by adopting more general coupling equations proposed by Tayler [35]. The height dependency of the electric- and magnetic-field intensity between the line and ground were also considered. The accuracy of the

proposed formula was validated by “LIOV code” (a TL-method based program) [69]. Also, the author compared existing formulas, and endorsed the validity of the Rusck model to calculate the induced voltages on distribution lines. The results of the Rusck and Andreotti models showed good agreement for a distribution-line height of  $h = 10$  m. However, the Rusck model overestimated peak voltages for a transmission-line height of  $h = 30$  m.

### 2.1.1.2 Earth resistivity

The formulas mentioned above still require the assumption of the vertical lightning and perfectly conducting earth. For taking into account the lossy earth, a simple practical correction based on the results of numerical evaluation methods was proposed by Darveniza [44] in 2007, and adopted in IEEE Std.1410–2010 [12].

$$h_{\text{eff}}(\rho) = h + k\sqrt{\rho} \quad k = 0.15 \text{ in [44] and } 0.25 \text{ [12]} \quad (2.1)$$

Note that the correction is derived from the results of earth resistivity  $\rho = 100, 400, \text{ and } 1000 \Omega\text{m}$ . Thus, the applicable range should be carefully considered for higher values of earth resistivity. The validity of the correction was confirmed by the FDTD method by Rizk *et al.* in 2016 [120]. The author also mentioned that the peak value of the induced voltage with Darveniza’s correction was underestimated in higher earth resistivity as is expected.

Analytical extensions for the earth resistivity have shown recent progress. One was made by Andreotti *et al.* in 2013 [46]-[47] by means of implementing the Cooray-Rubinstein approximation [65] to his formulas. The result was validated in comparison with numerical evaluation methods. The other one was proposed by Piantini and Member in 2017 [48], which considers the frequency dependence of a line so-called ground transient resistance  $\zeta'_g$  [49]. The accuracy of the formula was confirmed by a small-scale experiment.

### 2.1.1.3 Lightning inclination

A lightning induced overvoltage calculation for inclined lightning was demonstrated by Sakakibara in 1989 [126] using the same assumptions as the Rusck model. The voltages were calculated by the combination of analytical LEMP formulas and Agrawal coupling [51]. Then, in 2009, a closed-form solution for arbitrary inclined lightning was developed by Matsubara and Sekioka [132]. In



2012, Andreotti mentioned that his method [46] was extended to the arbitrary-shape lightning by numerical superposition [138]. These methodologies and obtained knowledge will be discussed later in Section 2.1.2.

The recent developments in the analytical methods allow us to calculate the lightning induced overvoltages with the earth resistivity and lightning inclination. However, there is a limitation that the formulas cannot handle complex line systems such as a multi conductor line with groundings. Thus, one application of the analytical methods is the validation of other numerical calculation models. In this thesis, the results calculated by the FDTD method will be compared with the Matsubara-Sekioka formula [132] and discussed from the analytical-formula viewpoint.

## **2.1.2 Transmission-line (TL) method**

### **2.1.2.1 Basics**

As mentioned before, the TL method is the most common approach to calculate lightning induced overvoltages in power systems. The advantage of the method is the capability to deal with more realistic and complex network configurations/conditions than those assumed in the analytical methods. The method is composed of two computation steps: (1) LEMP (lightning electromagnetic pulse) calculation and (2) its coupling to transmission lines [25]. An initial concept of this method was developed in the 1980s. It adopted EM-field-radiation formulas from a dipole antenna derived by Master and Uman [50] and a field-to-line coupling model proposed by Agrawal [51]. These formulations were equivalently or explicitly based on the assumption of vertical lightning and a perfectly conducting earth. The following improvements have been made to consider more realistic lightning and ground conditions.

### **2.1.2.2 Return stroke model**

A lightning return stroke model describes the spatial and temporal distribution of the lightning channel. In general, the lightning channel is assumed as vertical antenna on a perfectly conducting earth (or a dipole). Several return stroke models (so-called TL, MTL, MTLE, BG, and TCS) have been proposed [52]-[56]. The differences among them are the expression of the lightning return-stroke velocity and current decay with height. In 1998, Rakov and Uman [57] reviewed the models

from the viewpoint of the peak and entire shape of the calculated electric field, and ranked MTL as first and MTLE as second.

### **2.1.2.3 Extension for earth resistivity in LEMP calculation**

When the formulas proposed by Master and Uman [50] are adopted for LEMP, a perfectly conducting earth is automatically assumed by representing a lightning channel as a dipole. The assumption is, within a few kilometers from the lightning to lines, considered as reasonable for the vertical electric field and horizontal magnetic field [50], [58]. On the other hand, the horizontal electric field is noticeably influenced by the earth resistivity [59]. A rigorous technique, the so-called “Sommerfeld integral” to take into account the influence of the lossy earth, had been proposed in 1909 [60]. Because the integral was a slow-converging calculation, several approximate formulas [61]-[65] to mitigate the calculation time were developed around the 1990s. In 1996, F. Rachidi *et al.* [67] reviewed these formulas and concluded that the Cooray-Rubinstein formula [65] was the most reasonable and reliable to express the Sommerfeld integral. Nowadays, the formula has become somewhat of a de facto standard in lightning-induced overvoltage studies to take into account the lossy earth (e.g. [12], [17], [67]).

Recently, a computer program called “LIOV code” was developed by research groups in Switzerland and Italy [69]. The code adopts the MTL return-stroke model (vertical lightning), Cooray-Rubinstein formula, and Agrawal coupling for the calculation, and is therefore capable of simulating lightning induced voltages on multi-conductor lines above a lossy earth. The line coupling equations are solved by a finite-difference time-domain (FDTD) technique. Note that this FDTD means a discretized calculation for coupling equations and is different from a full-wave FDTD method explained in the next section. The code was applied to a study in IEEE Std.1410–2010 [12] and referred to by CIGRE Technical Brochure [16]. Also, an optional module using the LIOV code is available for EMTP [70].

### **2.1.2.4 Extension for earth resistivity in coupling calculation**

A general coupling model for two wires was firstly presented by Taylor *et al.* in 1965 [35], and was developed for a multi-conductor systems by Agrawal in 1980 [50]. Because the coupling theories themselves only describe the interaction between the incident EM field and the line

conductors, they are independent from the influence of the finite earth conductivity. The effect of lossy earth for the incident field is already considered in a LEMP calculation. For traveling-wave voltages on transmission lines, the effect can be taken into account by considering earth return impedance  $Z_g'$  in the total line impedance  $Z'$  as is well-known [7]. The study of the earth return impedance is another area of significant interest in power system transients and numerous developments have been made since the 1920s (e.g., [72]-[79]).

In lightning induced overvoltage studies, most of the published papers do not clearly mention which  $Z'$  formula they adopted. As a few exceptions, the papers written by the developers of the LIOV code [67], [80], presented that they used their improved approximation formula based on one proposed by Sunde [74]. A frequency dependence of the line impedance [81] was also considered. Thus, these would have been implemented in the LIOV code.

#### **2.1.2.5 Recent topics of LEMP and TL-based calculation**

The recent LEMP studies mainly focus on 1) LEMP and lightning disturbances for underground cables [82]-[86], 2) LEMP above a stratified ground [87], and 3) LEMP and lightning induced overvoltages for non-vertical lightning [141]-[146]. The papers regarding the third topic will be reviewed later.

### **2.1.3 Numerical electromagnetic analysis (NEA) method**

Recently, several electromagnetic computation methods, for instance MoM [36], FEM [37], partial-element equivalent-circuit (PEEC) method [88], hybrid electromagnetic/circuit model (HEM) [89], and FDTD method [38] have been widely applied to lightning analysis. In the field of lightning induced overvoltages, MoM, FEM, and FDTD are mainly adopted.

#### **2.1.3.1 Method of moments (MoM)**

MoM is a general computational analysis method which is based on boundary integral equations. In the field of electrical engineering, the method has been applied to thin-wire structures, and an electric field radiated from the object is analyzed by considering the tangential component. The advantage of this method is the availability of both time- and frequency-domain analyses as well as a small computation cost [17].

The method has been adopted in a number of lightning studies including lightning surges on tall objects (e.g., [90], [91]), response of grounding electrodes (e.g., [92], [93]), LEMP (e.g., [93], [95]), and lightning induced overvoltages (e.g., [96], [97]). In recent lightning-induced overvoltage studies, Pokharel *et al.* [96] demonstrated lightning-induced voltage calculations by a MoM program called NEC-2 in 2003. The study investigated lightning induced voltages on a single conductor above a lossy earth caused by vertical lightning, and the results showed good agreement with measured results. In 2012, Janani *et al.* [97] demonstrated lightning-induced voltage calculations on three-phase lines including non-linear loads (arresters).

### **2.1.3.2 Finite-element method (FEM)**

FEM is another well-known computational analysis method which is based on differential equations in spatial elements. This method was first developed in the field of structural mechanics and applied to a wide range of research and engineering problems. To take advantage of its versatility, this method was recently applied lightning induced overvoltage calculations by Akbari, Paknahad, Sheshyekani *et al.* [98]-[105]. Commercial FEM software, “COMSOL Multiphysics”, was employed in these papers. The authors investigated effects of frequency dependent soil parameters, stratified grounds, and ocean-land mixed environments on lightning induced overvoltages.

It was presented in [98] and [99] that the frequency dependent soil mitigated the induced voltages when the earth conductivity (water content of soil in this study) was low. In [100], a stratified ground significantly affected the induced voltages when the thickness of the upper soil layer is less than 10 m and the earth resistivity is relatively low. In [101] and [102], the presence of a waterfront influenced horizontal electric field of LEMP. In addition, when the line became closer to the ocean, the induced voltages at the line midpoint were decreased while ones at the line terminations were increased. These effects were also investigated for buried cables in [103]-[105].

### **2.1.3.3 Finite-difference time-domain method (FDTD)**

FDTD is the most popular computational method for LEMP and lightning surge calculations. It is based on solving Maxwell’s equations in the time domain. Because of the advantages of relatively easy programming and capability of dealing with complex geometries, a number of publications

adopted this method. The recent topics of lightning study with FDTD are: 1) LEMP (e.g., [108], [109]), 2) lightning surges on towers (e.g., [110], [113]), 3) lightning surges on ground electrodes (e.g., [111], [112]), 4) lightning induced overvoltages (e.g., [113]-[121]), and 5) lightning disturbances on various equipment (wind turbines, photovoltaic arrays, buildings etc.) (e.g., [122]-[124]).

In recent lightning induced overvoltage studies, Baba *et al.* [113] investigated induced voltages on a line caused by lightning striking a 100 m-height grounded object in 2006. It was observed that induced voltage waveforms were largely affected by the object because an impedance mismatch between the lightning and the object generated reflection waves confined in the object. In 2008, Ren *et al.* [114] proposed a two-step analysis procedure for lightning induced overvoltages by 2D-FDTD and Agrawal coupling to calculate multi-wire systems. The advantage of this method is to deal with computationally expensive systems if it was modeled in one workspace. In 2012, Sumitani *et al.* [115] demonstrated an induced voltage calculation for a two-wire distribution system in one workspace with sub-gridding technique.

In 2014, Tatematsu *et al.* [117] presented a lightning induced overvoltage calculation on a three-wire system with a shield wire and arresters. Note that GPU computing acceleration was adopted in the calculation. Zhang *et al.* [119] studied an effect of horizontally stratified ground on lightning induced overvoltage and found that the voltage affected by the lower ground layer when the depth of the upper layer was less than 2 m. In 2015, Thang *et al.* [119] demonstrated an induced voltage calculation on a realistic multi-conductor system including a ground wire, arresters, and pole transformers. Transformers were represented by equivalent capacitors. In 2016 and 2017, Rizk *et al.* [120], [121] investigated the effect of earth resistivity on lightning induced overvoltage parametrically and validated Darveniza's correction (2.1) for the Rusck model. Also, the authors mentioned that the peak voltages became higher than the estimation by (2.1) in the higher earth-resistivity range.

## **2.2 Lightning induced overvoltages with non-vertical lightning**

Studies associated with non-vertical lightning, i.e. with inclined and tortuous lightning have been published since the 1970s [125]-[128]. However, the number of the papers was relatively limited.

From around the year 2000, when the LEMP calculation by antenna theory and by NEA methods had been developed, an increasing number of papers related to non-vertical lightning were published. Most of the studies can be classified into one or more of the following three groups: 1) lightning induced overvoltage by non-vertical lightning [126]-[135], 2) lightning induced overvoltage and LEMP with lightning tortuosity [125], [136]-[139], and 3) analytical and numerical representation of LEMP from inclined lightning [141]-[148]. Also, studies of non-uniform conductors and its application to lightning studies have been developed (e.g., [129]-[131]). In this section, the review will focus on the induced voltage studies in group 1) and 2) as well as the initial studies. The papers on LEMP in Group 2) and 3) will be briefly summarized.

### **2.2.1 Studies of non-vertical lightning between 1977-2000**

In 1977, Levine and Meneghini [125] investigated the effect of lightning tortuosity on LEMP by comparison between their calculation and a cloud-to-ground lightning flash observed at Kennedy Space Center. For the simulation, they used their own formulas for an EM field radiated from a current filament. The tortuous lightning channel was represented by superposition. A perfectly conducting earth was assumed. The calculated and measured electric field waveforms showed good agreement for the time scale of 100  $\mu$ s. They pointed out that the lightning tortuosity made the EM fields fluctuate and high-frequency-contained, which could not be obtained a vertical-lightning assumption. Although this study was not for lightning induced overvoltages but for LEMP, it demonstrated the importance of non-vertical lightning study.

In 1989, Sakakibara [126] published the first paper of a lightning induced overvoltage study for inclined lightning. As briefly mentioned above, his approach to calculate electric and magnetic fields was based on the Rusck model and the angle of the lightning channel was considered in the formulation. The analytical formulas for the EM fields were derived and Agrawal coupling [51] was applied to calculate the induced voltages on a distribution line. The results were validated by a mutual-induction experiment of two horizontal wires with different heights. He concluded that the lightning inclination along a distribution line induced a larger voltage on transmission lines. Note that the results of the inclination toward the line were not presented. This work was, even though based on several simplifying assumptions, quite significant because of being the first induced-voltage study and its experimental validation.

At a conference in 1994, Wu and Hsiao [127] presented an effect of inclined and non-vertical (zig-zag) lightning on lightning induced overvoltage. The formulation and details of the calculation parameters were not clearly presented in the paper. However, the formulas and calculation process look similar to Sakakibara's method. Several lightning-channel forms, e.g. inclination with 11.3°, 26.6°, and 45° along a line, and zig-zag with 2, 5, and 10 segments were compared. It was observed that some of the channels induced higher overvoltages than one caused by vertical lightning. It was pointed out that these results should be taken into account in lightning protection design.

Finally in 1996, Michishita *et al.* [128] performed a 1/20-scale lightning-induced voltage experiment for inclined lightning and compared with calculation results. In the experiment, a copper wire of 0.5 m-height and 15 m- and 25 m-length terminated by about 440  $\Omega$  resistors was hung on 2.5 m-interval wooden poles. The lightning channel was simulated by series of insulator poles with a 150 turns/m-wounded wire. The channel was connected to a pole of 16.7 m-distance and 9.2 m-height, in which the inclination angles to the ground were 81° at the bottom and 52° at the top. The propagation speed of the current was measured as 125 m/ $\mu$ s. In the numerical calculation, they used Sakakibara's approach and considered lossy earth by applying the Sommerfeld integral as well as earth return impedance. Several combinations of placements of the lightning channel, the line, and measuring points were tested. The observed voltages closely corresponded to the calculated results where the earth conductivity was assumed to be 0.03 S/m. Note that there was no comparison with vertical lightning. This publication is the first and only paper that lightning induced overvoltages by "inclined" lightning (not horizontal in Sakakibara's case) is clearly experimented and compared with calculations including the effect of the earth resistivity.

These initial contributions for non-vertical lightning study clearly illustrate the considerable effect of the lightning inclination and tortuosity which should be taken into account the lightning evaluation.

### **2.2.2 Induced voltages by non-vertical lightning**

After around a decade from Michishita's work, Matsubara and Sekioka [132] proposed a full-analytical solution for lightning induced overvoltages caused by inclined lightning. The assumptions in the formulation were the same as the Rusck model. It should be mentioned that the

solution was derived by assuming an infinite, lineally-rising current  $I = at$  to mitigate the formulation complexity. Thus, a superposition or convolution technique to represent an actual lightning-current waveform is required. They validated the formulation by comparing the results obtained by the proposed formulas with a finite-difference calculation by initially assumed differential equations for the formulation. It was made clear that the lightning inclination toward the line significantly increases the induced voltage. The authors also presented analytical approximate formulas to estimate the peak voltage and the time where the peak appears. The main part of the discussion focused on the error of the approximate formulas while no parametric study, for example in respect to the inclination angle, was demonstrated. Although the formulation assumed a perfectly conducting earth, proposed analytical solutions are quite useful in both research and engineering fields. This formula will be utilized to validate an FDTD model in this thesis.

At the ICPL in 2012 and 2013, N. Rameli *et al.* [133], [134] presented computed examples of lightning induced overvoltages on distribution lines caused by inclined lightning. This calculation was based on a TL method with a LEMP calculation for inclined lightning developed by the authors. However, the result looks somewhat questionable because the induced voltages decrease even if the lightning inclines toward the line, which is in opposition to previous research. Perhaps there were mistakes in the definition of angle or legends in the associated figures.

In 2015, Abouzeid *et al.* [135] demonstrated a lightning induced overvoltage calculation on multi-conductor transmission lines by a TL method. The calculation was based on their formulas for calculating electric and magnetic fields generated by inclined lightning. In addition, the formulas considered the Cooray-Rubinstein formula, Agrawal coupling, and transient ground impedance. Thus, almost all previous developments in the TL method were packaged in the calculation tool. In the induced voltage study, a transmission system with three-phase wires (PW) and two ground wires (GW) was assumed. The line heights were 19.1 m for the PW and 30 m for the GW. The author firstly demonstrated the effect of inclination on the induced voltage only with the horizontal PW above a perfectly conducting earth. Then, the inclination angle was fixed at 20° and effects of sag and GW were investigated. The decrease of the induced voltage by PW-sag and the shielding effect of the GW were clearly presented.



In these papers, the effect of lightning inclination on the induced overvoltage was demonstrated successfully by an analytical formula and several TL methods. However, the effect of the inclination was not comprehensively investigated and summarized. In addition, some of the papers contained questionable or opposing results. Therefore, the effect of the lightning inclination requires further thorough research to standardize the knowledge.

### **2.2.3 Lightning induced overvoltage and LEMP with lightning tortuosity**

In 2000, Lupò *et al.* [136] investigated an EM field generated from tortuous lightning. The field was calculated by a dipole approach and the effect of tortuosity and branch of the lightning were evaluated using a fractal parameter to represent the fluctuation of the field. The results showed that the fluctuation of the field increased up to a distance from the observation point of around 20 km.

In 2007, Song *et al.* [137] demonstrated that a series of two inclined lightning paths with different angles, i.e. “bent” lightning channels, increased lightning induced voltages in some cases, and an increase of the induced voltage by a lightning branch was presented.

In 2012, Andreotti *et al.* [137] simulated a real lightning channel and presented both a radiated EM field and its induced voltages on a single conductor at several locations. The calculation was performed using an analytical-based calculation called “CiLIV” (Circuit for Lightning Induced Voltage) developed by the authors in [46]. Although the formulation in [46] only considered vertical lightning, tortuous lightning in CiLIV was simulated by decomposing the lightning path into several segments and superposing the calculated results numerically. The author pointed out that channel tortuosity did not significantly affect the induced voltage in the study case, while the vertical-lightning assumption might lead to inaccurate results. He conducted a further study for six real-tortuous lightning paths in 2015 [139] and presented that the induced voltage deviated by 23 % on average from the results of vertical lightning.

These recent studies of tortuous and “real” lightning paths also supported the theory that lightning torsion and inclination affects the induced voltage. Although the lightning tortuosity did not significantly affect the peak value of the induced voltage in some cases, the increase in the high-frequency component of the radiated electric field was clearly observed. It may affect the induced

voltage under more realistic conditions, e.g. the inclusion of frequency dependence of soil and lines.

Considering the simulated line configurations in the above-mentioned papers, they considered only a single overhead line without any other components (poles, shield wires, groundings etc.). Thus, simulations including these components may be worth doing to clarify the responses of the components and support the results calculated by different methods. Also, the idea of “bent” lightning can be applied not only to the representation of lightning path in the air but also lightning-struck objects such as buildings, towers, and wind turbines. Because these objects have different surge impedances from the lightning path, it may affect the lightning induced overvoltage.

#### **2.2.4 LEMP study by non-vertical lightning**

In 2000, Lupò *et al.* [141] proposed an analytical expression to calculate electric and magnetic fields radiated from the lightning with arbitrary location and inclination. The motivation of this study was to calculate the field generated from both cloud-to-cloud and cloud-to-ground discharges. The formulation was done by Rusck-type modeling including perfectly conducting earth and by converting each coordinate of arbitrary lightning segments to vertical ones at origin. The calculated results at several measuring points were discussed carefully but not compared with any other calculations. Other analytical formulas and efficient calculation approaches based on dipole antenna theory were also proposed by Moini *et al.* [142] and M. Izadi *et al.* [143]-[144].

The characteristic of LEMP generated by non-vertical lightning have been investigated by: 1) Gomes *et al.* by an extension of dipole antenna theory in 2013 [145], 2) Nemamcha and Houabes by MoM in 2014 [146], 3) Abouzeid *et al.* by analytical calculation of LEMP in 2015 [147], and 4) Jiang by FDTD [148] in 2015, as well as Andreotti [138] in 2012 as mentioned above. In 1), the angle dependency of LEMP radiated from a bent lightning stroke was illustrated. In 2), the dependence of LEMP from a straight inclined channel was presented. In 3), the effect of a zig-zag lightning stroke (segmented by 2-5) was shown. In 4), LEMP from an inclined leader considering finite earth resistivity was investigated.

These LEMP studies also clearly demonstrate that non-vertical lightning gives non-negligible effects on LEMP and perhaps resultant induced voltage.

## 2.3 Conclusion

Recently, lightning induced overvoltages with non-vertical lightning have been widely discussed and several papers successfully demonstrated the differences in voltages caused by vertical and non-vertical lightning. The papers also stated that the differences should be taken into account for the induced-voltage evaluation. However, previous studies mainly focused on presenting only the differences. Therefore, the effects should be investigated and summarized parametrically and comprehensively considering several conditions such as lightning parameters, network configurations, earth conditions, groundings, and lightning-struck objects. For this purpose, FDTD will be adopted as a main evaluation method in the following chapters because of its flexibility in modeling and its ease of use.

## **CHAPTER 3      PRELIMINARY STUDY OF LIGHTNING INDUCED OVERVOLTAGES AND EARTH CURRENTS BY INCLINED LIGHTNING**

In this Chapter, a simple 3D-FDTD model circuit is built and the influences of inclined lightning on lightning induced voltages in a distribution line are investigated as a preliminary study. The distribution line is placed above a lossy ground in an orthogonal three-dimensional space. The induced voltage is calculated at the line center which is in front of the lightning channel base. The details of the FDTD modeling are described in Section 3.1. FDTD-computed results under various conditions of a lightning channel together with the return stroke velocity of the channel are presented, and the influences of the inclined lightning channel on the induced voltages are investigated in Section 3.2. Earth-surface current behavior influenced by the inclined lightning is discussed in Section 3.3. The findings of the investigations are summarized in Section 3.4.

### **3.1 Model circuit**

In FDTD modeling for lightning studies, the simplest representation of a lightning channel is the combination of a thin wire and a current source on the bottom of the channel as in Table 3.1. However, one problem with this representation is that the lightning current (return stroke) velocity, the average of which is generally assumed to be  $1 \times 10^8$  m/s [12], is not adjustable, i.e. it is fixed to the speed of light ( $3 \times 10^8$  m/s). Thus, this model is less flexible and expected to only be used for quick scanning investigations. Another model is that the channel is represented by a thin wire and inductances  $L$  in order to modify the return stroke velocity. The velocity can be roughly adjustable based on the value of the inductance, but there are three defects: (1) The lightning current waveform is distorted during its propagation due to the inductances, (2) When a fixed value of  $L$  is set, the return stroke velocity gradually varies in height because the channel capacitance between the channel and the earth varies in height, and therefore (3) Iterative trial is required to adjust the average velocity of the channel to the requested one. Thus, for lightning studies in FDTD, one better way to avoid these problems is to adopt the so-called traveling current source (TCS) model [56] for the lightning channel, of which current sources are connected in series to form the lightning path. Because an original current waveform can be set to each source, the current waveform does

not distort at all heights. In addition, the velocity can be easily adjusted by changing the excitation delay time for each current source. Because of these advantages, this project will adopt the TCS model in all investigations.

Table 3.1 Lightning channel modeling in FDTD

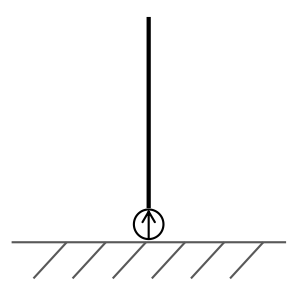
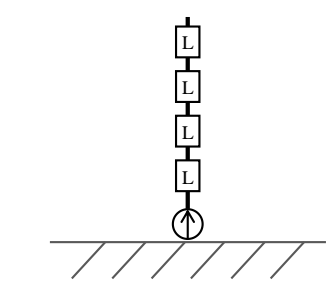
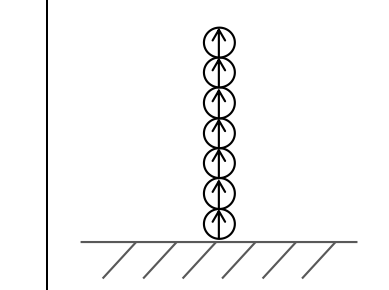
Model Circuit			
	Thin wire and current source	Thin wire and current source with inductance	Traveling current source (TCS) model
Modeling	Easy-to-model	Easy-to-model	Relatively easy-to-model
Lightning current and velocity	Almost no current distortion Only the light speed	Current distortion Adjustable but needs iterative trial.	No current distortion Easy-to-adjust

Figure 3.1 illustrates a model circuit for FDTD computations in this chapter. The current source array is aligned vertically and horizontally along the arbitrary inclined lightning path and the velocity is adjusted by the delay time of the excitation for each current source. The height of the lightning channel is set to 500 m, and two directions of the inclined channel are investigated: angle  $\theta$  on the  $yz$  plane for the inclination toward the line, and angle  $\varphi$  on the  $xz$  plane for the inclination along the line. The angle  $\theta$  and  $\varphi$  vary from  $+45^\circ$  to  $-90^\circ$  and  $0^\circ$  to  $+90^\circ$ , respectively. The angle of  $\pm 90^\circ$  is used for the confirmation of consistency. Also, two cases of return stroke velocity,  $\beta = 1.00$  and  $0.33$ , and two values of the wave front duration,  $T_f = 1.0$  and  $0.1 \mu\text{s}$  are adopted in this study. Note that  $\beta$  is the ratio of the return stroke velocity to the light speed, i.e.  $\beta = 1.00 = 3 \times 10^8 \text{ m/s}$  and  $\beta = 0.33 = 1 \times 10^8 \text{ m/s}$ . A single overhead line with a height of 10 m is placed 50 m away from the lightning base, which represents a 20-kV distribution line. In general, when the fast-rise return stroke current and low earth resistivity are assumed, the induced voltage becomes proportional to the line height and almost inversely proportional to the distance from the lightning base [34], [113].

Both ends of the line are connected to Liao's absorbing boundary of the working space of  $1060 \text{ m} \times 1060 \text{ m} \times 600 \text{ m}$ , which is composed of cubic cells with various sizes, ranging from  $1 \text{ m} \times 1 \text{ m} \times 1 \text{ m}$  to  $8 \text{ m} \times 8 \text{ m} \times 8 \text{ m}$ . The minimum grid size is adopted in the area including the lightning channel base and a measuring point ( $140 \text{ m} \times 140 \text{ m} \times 140 \text{ m}$ ). The measuring point of the induced voltage on the line is placed at the closest point to the lightning base. The earth depth is taken as  $100 \text{ m}$ , and the earth resistivity  $\rho_e$  is set to  $0 \text{ } \Omega\text{m}$  (perfectly conducting earth: PCE),  $100 \text{ } \Omega\text{m}$ , and  $2000 \text{ } \Omega\text{m}$ . A normalized value of current  $1 \text{ A}$  with  $T_f = 1.0$  and  $0.1 \text{ } \mu\text{s}$  shown in Figure 3.2, is adopted for each current source as a lightning return stroke current.

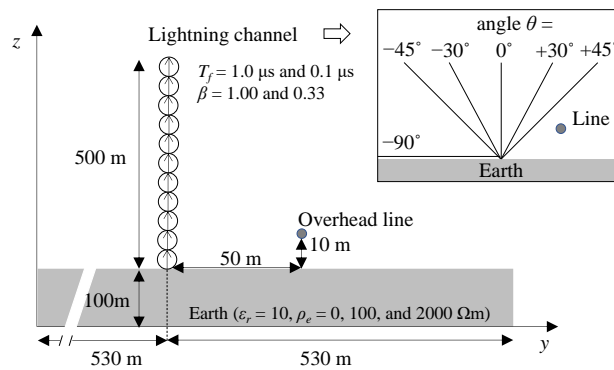
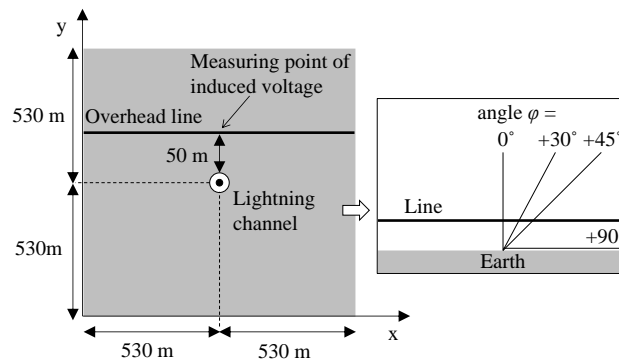
(a)  $yz$  plane(b)  $xy$  plane

Figure 3.1 FDTD experimental configuration: Lightning channel base is located at the center of the working space and the distance between the base and a  $10 \text{ m}$ -height overhead line is  $50 \text{ m}$ . Lightning inclination angle  $\theta$  and  $\phi$  vary from  $+45^\circ$  to  $-90^\circ$  and  $0^\circ$  to  $+90^\circ$ , respectively.

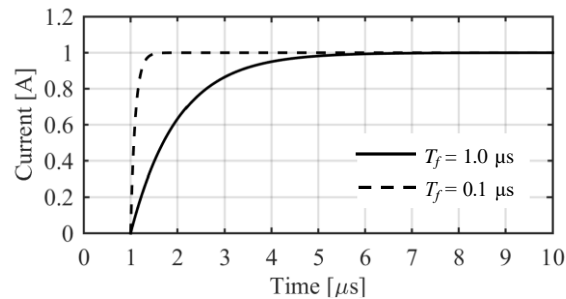


Figure 3.2 Return stroke current waveforms.

## 3.2 Lightning induced voltages by inclined lightning

### 3.2.1 Influence of angle $\theta$

Figure 3.3 shows induced voltage waveforms on the distribution line for various values of angle  $\theta$  with  $\varphi = 0^\circ$ .  $\beta$  is set to 1.00. In this case (a) is for the perfectly conducting earth, (b) is for earth resistivity  $\rho_e = 100 \Omega\text{m}$ , and (c) for  $\rho_e = 2000 \Omega\text{m}$ . It is clear that the inclined lightning of  $\theta = +45^\circ$ , i.e. the lightning channel being the nearest to the line, induces the highest voltage to the line. As the angle  $\theta$  increases, i.e. the channel becomes further to the line, the induced voltage decreases except the case of (c)  $\rho_e = 2000 \Omega\text{m}$  as shown in Figure 3.4. When  $\rho_e = 2000 \Omega\text{m}$ , the induced voltages in the cases of  $\theta = +30^\circ$  and  $0^\circ$  are higher than that in the case of  $\theta = +45^\circ$ .

It is observed in Figure 3.4 that the induced voltage becomes higher as the earth resistivity increases as is well known [44], [45]. Also, it should be noted that the rise time of the induced voltage becomes larger as  $\rho_e$  increases, and thus the induced voltage is sustained for much longer in the case of  $\rho_e = 2000 \Omega\text{m}$  than that in the case of  $\rho_e = 100 \Omega\text{m}$ .

In Figure 3.4, the induced voltage peak decreases monotonically as angle  $\theta$  varies from  $+45^\circ$  to  $-90^\circ$  for  $\rho_e = 0$  and  $100 \Omega\text{m}$ , while the largest peak appears at  $\theta = 0^\circ$  for  $\rho_e = 2000 \Omega\text{m}$ . The reason for this trend can be explained as the superposition of two components: 1) vertical vector potential in the same direction to the lightning channel and 2) traveling-wave voltage propagating along the line [34], [132]. The angle dependency is different in the components as can be explained by formulas in [132]. The details will be discussed in the next chapter. When  $\theta = -90^\circ$ , the lightning channel is placed above the earth surface by the height of 1 m, i.e. the channel is almost perpendicular to the distribution line, and thus the induced voltage is the smallest. For  $\rho_e = 0 \Omega\text{m}$ ,

the voltage is nearly zero, and increases to 5.5 V for  $\rho_e = 2000 \Omega\text{m}$ . By considering the fact that the channel is perpendicular to the line for  $\theta = -90^\circ$ , the induced voltage appears to be generated by the current flowing on the earth surface after the lightning hits the earth. The characteristic of the current will be discussed in Section 3.3 as the earth surface current.

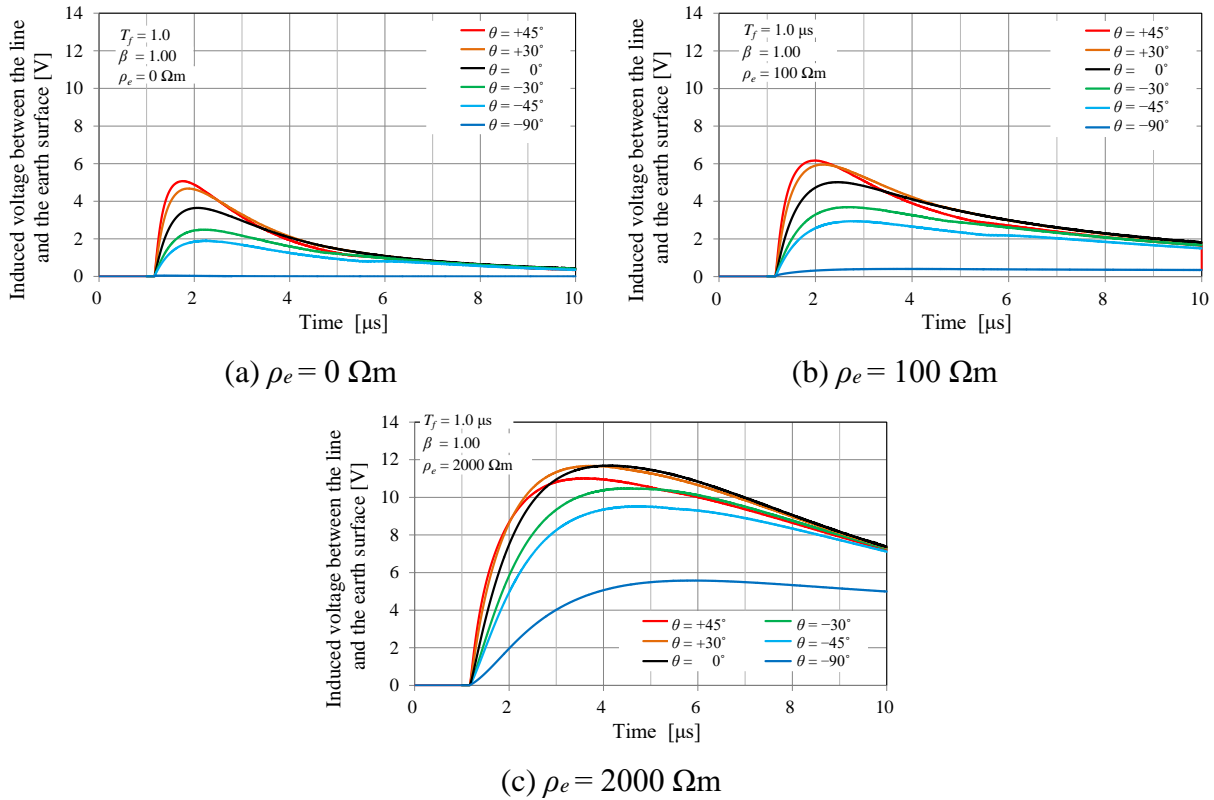


Figure 3.3 Induced voltages on the overhead line with the inclined lightning of angle  $\theta$  with  $\varphi = 0^\circ$ :  $\beta = 1.00$ ,  $T_f = 1.0 \mu\text{s}$ .

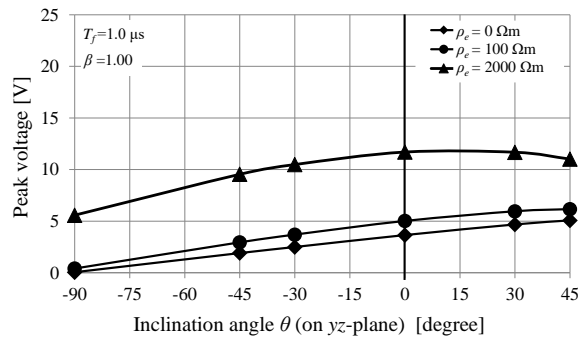


Figure 3.4 Influence of the inclination angle  $\theta$  with  $\varphi = 0^\circ$  on the peak induced voltages:  $\beta = 1.00$ ,  $T_f = 1.0 \mu\text{s}$ .



### 3.2.2 Influence of angle $\varphi$

Figure 3.5 shows induced voltage waveforms with various angle  $\varphi$  for  $\rho_e = 0, 100$  and  $2000 \Omega\text{m}$  when angle  $\theta = 0^\circ$ . Figure 3.6 shows the peak voltage as a function of the angle  $\varphi$ . The induced voltages become higher as  $\rho_e$  increases. The highest voltage is observed when  $\varphi = +45^\circ$  and the voltage decreases as  $\varphi$  becomes smaller except  $\varphi = +90^\circ$ . When  $\varphi = +90^\circ$ , the induced voltage becomes almost zero for  $\rho_e = 0 \Omega\text{m}$ , almost the same as that of  $\varphi = +45^\circ$  for  $\rho_e = 100 \Omega\text{m}$ , and much higher for  $\rho_e = 2000 \Omega\text{m}$ . The phenomena are estimated to be caused by the image current in the earth. When  $\varphi = +90^\circ$  ( $\theta = 0^\circ$ ), the lightning channel is placed 1-m above the earth surface, parallel to the line. The image current under the channel becomes large for  $\rho_e = 0 \Omega\text{m}$ , and it cancels almost all of the electromagnetic field generated from the lightning channel. Therefore, almost no voltage is induced on the line. On the other hand, the effect of the image current decreases for large  $\rho_e$ , and the electromagnetic field can reach the line and induce the voltage.

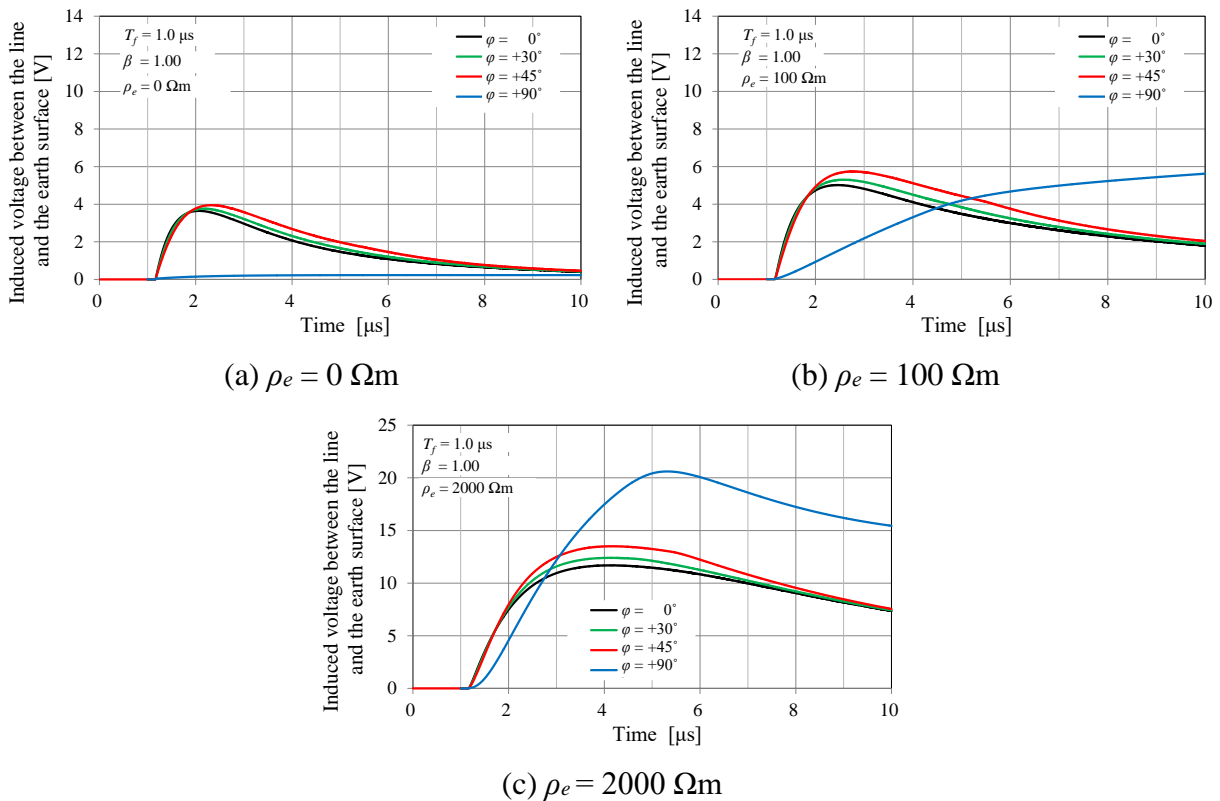


Figure 3.5 Induced voltages due to the inclined lightning for various angle  $\varphi$  with  $\theta = 0^\circ$ :  $\beta = 1.00$ ,  $T_f = 1.0 \mu\text{s}$ .

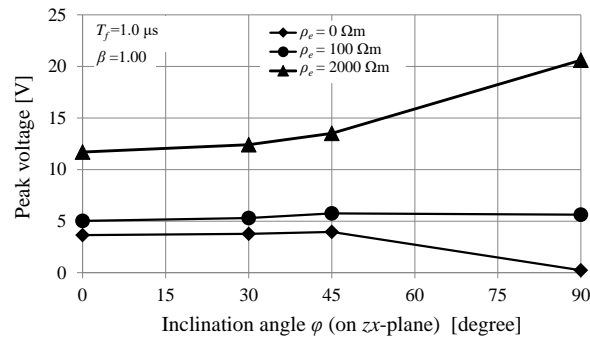


Figure 3.6 Influence of the inclination angle  $\varphi$  with  $\theta = 0^\circ$  on the peak induced voltages:  $\beta = 1.00$ ,  $T_f = 1.0 \mu\text{s}$ .

### 3.2.3 Influence of rise time $T_f$

Figure 3.7 shows a comparison of the results for  $T_f = 0.1 \mu\text{s}$  and  $1.0 \mu\text{s}$  at angle  $\theta = +45^\circ$  and  $\varphi = 0^\circ$ . The induced voltage peaks become higher and sharper for  $T_f = 0.1 \mu\text{s}$  than those for  $T_f = 1.0 \mu\text{s}$  as  $di/dt$  greater in the former.

In the case of large  $di/dt$ , i.e.  $T_f = 0.1 \mu\text{s}$ , the peak voltage is almost independent of the earth resistivity, while the decay time (wave tail duration) is significantly dependent on the resistivity. The greater the resistivity, the larger the decay time. In the case of  $T_f = 1.0 \mu\text{s}$ , both the peak voltage and decay time become larger as the earth resistivity becomes greater.

The relation between the peak voltage and angle  $\theta$  (with  $\varphi = 0^\circ$ ) for  $T_f = 0.1 \mu\text{s}$  in Figure 3.8 (a) is similar to that for  $T_f = 1.0 \mu\text{s}$ . The peak voltage increases as angle  $\theta$  decreases. The increase ratio of the voltage according to angle  $\theta$  is larger than those for  $T_f = 1.0 \mu\text{s}$ , indicating that the induced voltage is more sensitive to the angle for shorter  $T_f$ . Note that an induced voltage is generally proportional to the time derivative of the inducing current, i.e. inversely proportional to  $T_f$ . However, the lightning induced voltage, which is caused by the superposition of the electromagnetic field, does not simply increase.

Figure 3.8 (b) shows the influence of the angle  $\varphi$  (with  $\theta = 0^\circ$ ) on the induced voltage for  $T_f = 1.0$  and  $0.1 \mu\text{s}$ . It is observed for  $\rho_e = 0 \Omega\text{m}$  that the peak voltage for  $T_f = 1.0 \mu\text{s}$  becomes largest at  $\varphi = +45^\circ$  while that for  $T_f = 0.1 \mu\text{s}$  decreases monotonically as  $\varphi$  increases. This trend can be explained by the different behavior of the vector potential and traveling voltage as already explained in

Section 3.2.1, and can be reproduced by the formulas in [132]. The same trend is observed for  $\rho_e = 100 \Omega\text{m}$ . For  $\rho_e = 2000 \Omega\text{m}$ , the voltages for both  $T_f$  increases monotonically as  $\varphi$  increases.

In Figure 3.8 (b), the peak voltage is higher for  $T_f = 0.1 \mu\text{s}$  as expected, but the voltage increase from  $T_f = 1.0$  to  $0.1 \mu\text{s}$  is not proportional to the ratio of  $T_f$ , even at  $\varphi = +90^\circ$ . Using a very simple approximation, for  $\varphi = +90^\circ$  with  $\beta = 1.00$  ( $3 \times 10^8 \text{ m/s}$ ) and  $T_f = 1.0 \mu\text{s}$ , the induction is contributed by the length of 300 m. For  $T_f = 0.1 \mu\text{s}$ , the length becomes only 30 m. It is estimated that the difference of the length cancels the effect of  $di/dt$  and results in a minor change of the voltage between  $T_f = 1.0$  and  $0.1 \mu\text{s}$  at  $\varphi = +90^\circ$ .

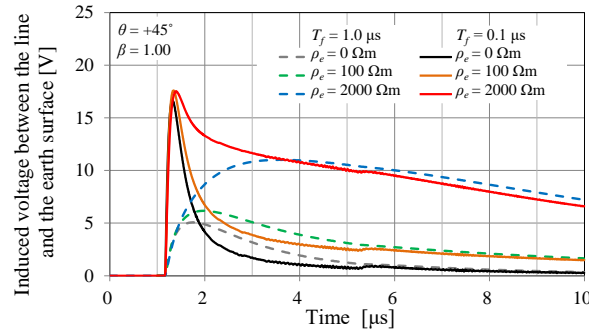
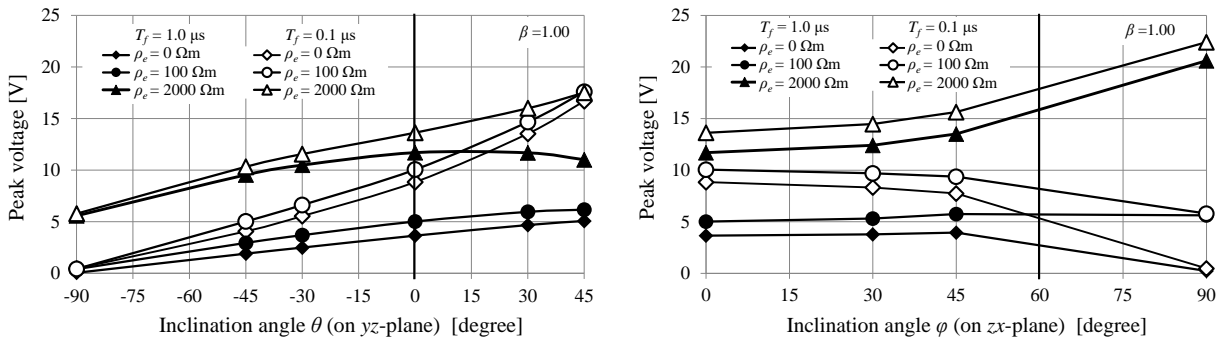


Figure 3.7 Comparisons of the induced voltage waveforms between  $T_f=1.0 \mu\text{s}$  and  $0.1 \mu\text{s}$ :  $\beta = 1.00$ ,  $\theta = +45^\circ$ ,  $\varphi = 0^\circ$ .



(a) Peak voltage versus angle  $\theta$  with  $\varphi = 0^\circ$

(b) Peak voltage versus angle  $\varphi$  with  $\theta = 0^\circ$

Figure 3.8 Comparison of the influence of the lightning inclination on the peak voltages between  $T_f=1.0$ :  $\beta = 1.00$ ,  $\theta = +45^\circ$ .

### 3.2.4 Influence of return stroke velocity $\beta$

Figure 3.9 shows the peak induced voltages for  $\beta = 0.33$  (return stroke velocity =  $1 \times 10^8$  m/s). Nearly the same trend as in Figure 3.8 (a) for  $\beta = 1.00$  is observed. It is confirmed that the influence of the lightning inclination on the induced voltage is not sensitive to the return stroke velocity. Thus, in the following chapters in this thesis, the velocity will be set to  $1 \times 10^8$  m/s in computations.

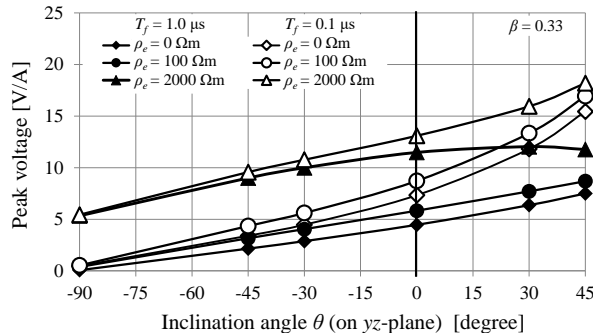


Figure 3.9 Influence of the lightning inclination angle  $\theta$  with  $\varphi = 0^\circ$  on the peak voltages between  $T_f = 1.0 \mu\text{s}$  and  $0.1 \mu\text{s}$ :  $\beta = 0.33$ .

### 3.3 Earth surface current by inclined lightning

The distribution and the influence of the earth current are investigated by using the same models in the previous study. Figure 3.10 shows the earth surface current density right under the overhead line (at the distance of 50 m from the lightning channel base) when the lightning of  $\beta = 1.00$  strikes the earth for: (a)  $\rho_e = 0 \Omega\text{m}$ , (b)  $\rho_e = 100 \Omega\text{m}$ , and (c)  $\rho_e = 2000 \Omega\text{m}$ . Note that the direction of the current flow from the overhead line toward the lightning base is considered as positive. It is observed in Figure 3.10 (a) to (c) that the earth surface current for  $T_f = 0.1 \mu\text{s}$  is larger than that for  $T_f = 1.0 \mu\text{s}$  as is easily understood. Also, the current is larger for  $\theta = +45^\circ$  than that for  $\theta = 0^\circ$  (vertical channel), because the lightning channel is near to the line for  $\theta = +45^\circ$ . A comparison of Figure 3.10 (a) to (c) illustrates clearly that the earth surface current is largest in the case of  $\rho_e = 0 \Omega\text{m}$ , and smallest in the case of  $\rho_e = 2000 \Omega\text{m}$ . When time becomes greater than  $6 \mu\text{s}$  for the lossy earth shown in Figure 3.10 (b) and (c), the current for  $\theta = +45^\circ$  converges to that for  $\theta = 0^\circ$ , i.e. no significant difference of the currents between the cases for  $\theta = +45^\circ$  and  $0^\circ$  is observed. This fact indicates that the influence of the inclined channel becomes less for the lossy earth as time passes,

as is easily estimated. Also, it is observed in Figure 3.10 (b) and (c) that the current decay time for  $T_f = 0.1 \mu\text{s}$  is faster for  $\rho_e = 2000 \Omega\text{m}$  than that for  $\rho_e = 100 \Omega\text{m}$ . This can be explained by the higher damping due to the larger resistance for  $\rho_e = 2000 \Omega\text{m}$  than that for  $\rho_e = 100 \Omega\text{m}$ .

Figure 3.11 shows the peak values of the earth surface current density. Note that solid black and gray lines indicate the currents that are assumed to be distributed evenly in the circular and hemispherical surface, respectively, i.e. when the FDTD cell size of 1 m in depth is considered, the values are:

$$I_{\text{circular dist.}} = \frac{1 \text{ [A]}}{(2\pi r \text{ [m]} \times 1 \text{ [m]})} = \frac{1}{2\pi r} \text{ [A/m}^2\text{]} \quad (3.1)$$

$$I_{\text{hemispherical dist.}} = \frac{1}{2\pi r^2} \text{ [A/m}^2\text{]} \quad (3.2)$$

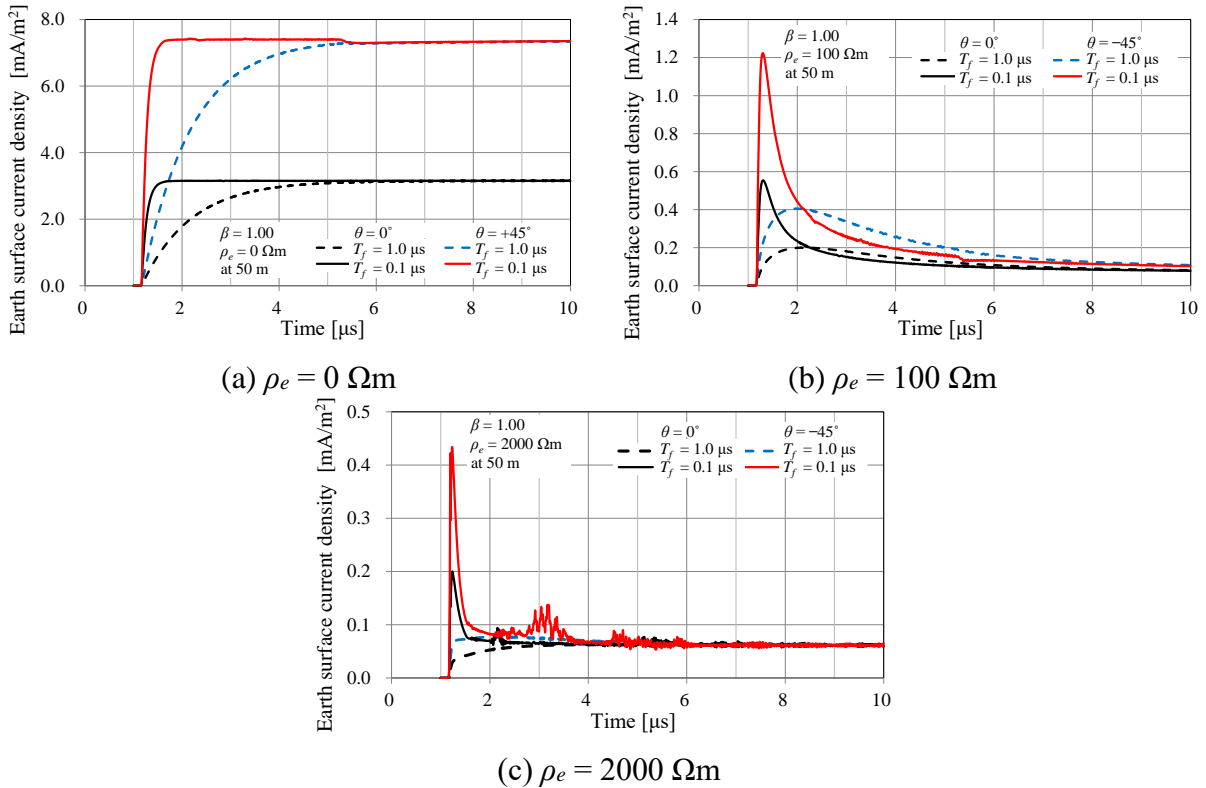


Figure 3.10 Earth-surface current-density waveforms in the earth of  $\rho_e = 0, 100, \text{ and } 2000 \Omega\text{m}$  for  $\theta = 0^\circ$  and  $+45^\circ$  with  $\varphi = 0^\circ$ :  $\beta = 1.00$ .

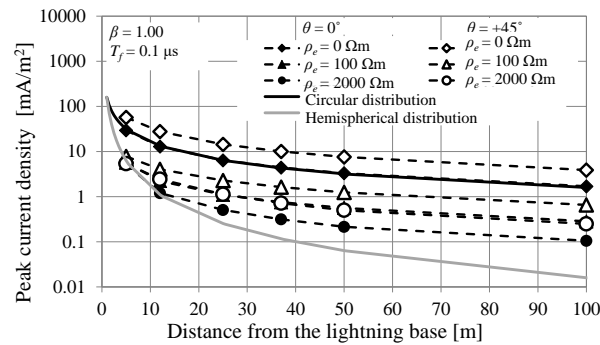
(a)  $T_f = 1.0 \mu\text{s}$ (b)  $T_f = 0.1 \mu\text{s}$ 

Figure 3.11 Peak values of the earth-surface current density caused by the lightning inclined at  $\theta = 0^\circ$  and  $+45^\circ$  with  $\varphi = 0^\circ$ :  $\beta = 1.00$ .

Figure 3.12 shows an example of the horizontal differential voltage between the earth surface under the measuring point of the overhead line and the surface of 50 m behind in the y-direction. Note that in the case of  $\rho_e = 0 \Omega\text{m}$ , there is no differential voltage between the points. The ground potential significantly decreases due to the voltage drop of the surface current, and the influence of angle  $\theta$  is clearly observed. The peak value of the differential voltage is illustrated in Figure 3.13. As expected, the voltage decreases noticeably in the case of higher resistivity  $\rho_e = 2000 \Omega\text{m}$  and shorter  $T_f = 0.1 \mu\text{s}$ . The earth voltage decreases when the lightning strikes the lossy earth.

There are few measurements and computer simulations of the earth surface current [6], [149], [150]. In a measured result, it is observed that the current is inversely proportional to the square of the distance from the source (impulse generator) to the measured position. For example,  $5 \text{ mA/m}^2$  at the distance of 5 m was measured when 1 A with  $T_f = 1.0 \mu\text{s}$  was applied to the source electrode. The FDTD simulation result agrees with the measured one, although the result is not shown here.

The above results clearly show that an inclined lightning channel affects the earth surface current and differential voltage on the earth. It is known that a lightning current injected to the earth near a distribution line flows into the line through the groundings, and occasionally causes breakdown and malfunction of electrical and control equipment due to induced overvoltage and ground potential rise (GPR) [6], [29], [151]. The results in this Chapter also suggest that the inclined channel can affect the overvoltage and GPR when a distribution line with groundings is considered.

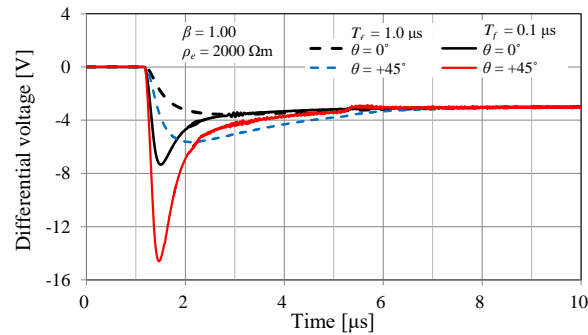


Figure 3.12 Horizontal differential voltages between the earth surface under the measuring point of the overhead line and the surface of 50 m behind in the  $y$ -direction:  $\beta = 1.00$ ,  $\rho_e = 2000 \Omega\text{m}$ ,  $\varphi = 0^\circ$ .

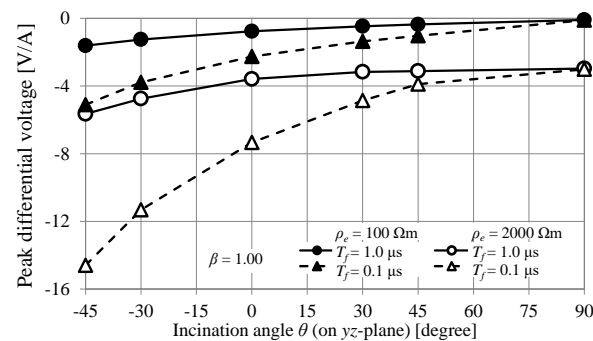


Figure 3.13 Peak differential voltages between the earth surface under the measuring point of the overhead line and the surface of 50 m behind in the  $y$ -direction:  $\beta = 1.00$ ,  $\varphi = 0^\circ$ .

### 3.4 Concluding remarks

Lightning induced voltages on a distribution line have been investigated by FDTD computations when inclined lightning channels and a lossy earth are assumed. From the investigations, the following concluding remarks can be made.

- (1) The inclined lightning channel (angle  $\theta$  and  $\varphi$  being non-zero) results in an induced voltage significantly different, either larger or smaller, than that due to a vertical lightning channel. The inclined channel also affects the earth surface current which could cause a larger earth potential drop in the horizontal direction.

- (2) For angles  $\theta$  and  $\varphi$  except  $+90^\circ$ , the induced voltage increases with increasing earth resistivity.
- (3) The induced voltage due to the inclined lightning channel becomes larger for  $T_f = 0.1 \mu\text{s}$  than that for  $T_f = 1.0 \mu\text{s}$  as is expected. The influence of angle  $\theta$  on the induced voltage increases as  $T_f$  becomes shorter.
- (4) For  $\beta$  (ratio of the return stroke velocity to the light speed) = 1.00 and 0.33, the inclined channel shows similar characteristics.

According to the preliminary study in this chapter, it is demonstrated that non-vertical lightning significantly influences both the induced voltage and the earth current behavior. Therefore, further investigations will be performed in the following chapters.



## **CHAPTER 4      LIGHTNING INDUCED OVERVOLTAGES CAUSED BY INCLINED LIGHTNING**

In this Chapter, lightning induced overvoltages due to inclined lightning are investigated with more practical conditions by referring to published standards and papers. An FDTD method is adopted to make model circuits for a single conductor line and a multi-phase line (three-phase conductors with a shield wire, utility poles, groundings, and arresters). The investigation includes, in addition to the studies in the previous chapter, 1) comparisons of FDTD results with those calculated using an analytical formula [132], 2) voltage profiles along the line, 3) several lightning distances from the line, and 4) induced voltages in a practical three-phase line with a shield wire, utility poles, groundings, and arresters.

In Section 4.1, an FDTD model of the inclined lightning for a single-conductor overhead line is validated in comparison with an analytical formula [132] and a TL-based method [66]-[71]. Then, influences of the inclined lightning on the peak induced voltage and voltage profile along the overhead line are investigated by the FDTD for various lightning distances and lightning current waveforms above both perfectly conducting and lossy earth. In Section 4.2, the induced voltages by the inclined lightning in the three-phase line are investigated. Concluding remarks are summarized in Section 4.3

### **4.1 Lightning induced voltage in a single-conductor line by inclined lightning**

#### **4.1.1 Models**

##### **4.1.1.1 FDTD model circuit**

Figure 4.1 illustrates an FDTD model circuit for inclined lightning. A lightning channel of 3 km-height is placed at the center of a working space and two directions of the lightning inclination are investigated: angle  $\theta$  on the  $yz$  plane for the inclination toward the line and angle  $\varphi$  on the  $xz$  plane for the inclination along the line. The angles  $\theta$  and  $\varphi$  vary from  $-45^\circ$  to  $+45^\circ$  and  $0^\circ$  to  $+45^\circ$ , respectively. The channel is represented by a series of small current sources known as a traveling-

current-source model [56]. The sources are aligned vertically and horizontally along the inclined lightning path. Lightning current waveforms calculated by the Heidler function are set to the sources.

$$I(t) = \frac{I_0}{\eta} \frac{(t/\tau_1)^n}{1+(t/\tau_1)^n} e^{(-t/\tau_2)} \quad (4.1)$$

The current amplitude  $I_0$  is assumed to be 50 kA, which is one of the standard values for first and subsequent strokes in IEC Std. 62305 [14]. Three different waveforms of  $t_{d10-90}/t_h = 0.25/100$ ,  $1/200$  and  $5.5/200$   $\mu\text{s}$  are investigated in this study ( $t_{d10-90}$  is a wave-front duration time of which the lightning current rises from 10 to 90 %.  $t_h$  is a decay time from peak to half [12]-[16]). The first two waveforms are standard first and subsequent strokes presented in the IEC standard with parameters for (4.1). The third one is similar to the median rise-time (5.63  $\mu\text{s}$ ) of the stroke presented in IEEE Std. 1410 [12]. The parameters for (1) are  $n = 10$ ,  $\eta = 0.932$ ,  $\tau_1 = 10.5$   $\mu\text{s}$ ,  $\tau_2 = 273$   $\mu\text{s}$ . Figure 4.2 shows the calculated current waveforms. The return stroke velocity is assumed to be  $1 \times 10^8$  m/s. Earth resistivity  $\rho_e$  is assumed to be zero (perfectly conducting), 100, and 1000  $\Omega\text{m}$  with relative earth permittivity  $\epsilon_r = 10$ . A single-conductor overhead line of 10 m height ( $h = 10$  m) is placed at distances of  $d = 50$ , 100, and 1000 m away from the lightning channel base. Lightning induced voltages at several measuring points on the line are computed by the FDTD.

Note that according to a shielding distance evaluation for distribution lines in IEEE Std. 1410 [12],  $y_{min}$  (the distance at which the lightning may become a direct stroke to the line) becomes 72.5 m when  $h = 10$  m and  $I_0 = 50$  kA. However, this study assumes the lightning being indirect even when  $h = 10$  m and  $I_0 = 50$  kA for easy comparison.  $y_{min}$  becomes 50 m when  $h = 10$  m and  $I_0 = 24$  kA, where the lightning may be an indirect stroke. The induced voltage becomes simply 24/50 times if there are no nonlinear components, such as arresters.

The FDTD working space of  $12 \text{ km} \times 7.3 \text{ km} \times 3.1 \text{ km}$  is composed of several cell lengths between 1.25 m and 25 m. The cell composition is varied according to the lightning current waveforms and the line distances. For example, the minimum cell size of 1.25 m is used for 0.25/100  $\mu\text{s}$  with  $d = 50$  m to suppress numerical fluctuation due to the quick-changing current and resulting induced voltage. For 5.5/200  $\mu\text{s}$ , the minimum size of 5 m is adopted. The working space is covered by

Liao's absorbing boundary [107]. One FDTD computation for  $40 \mu\text{s}$  needs about 4 to 16 hours using a desktop computer, Core i7 2.8 GHz with 16-GB dual channel memory.

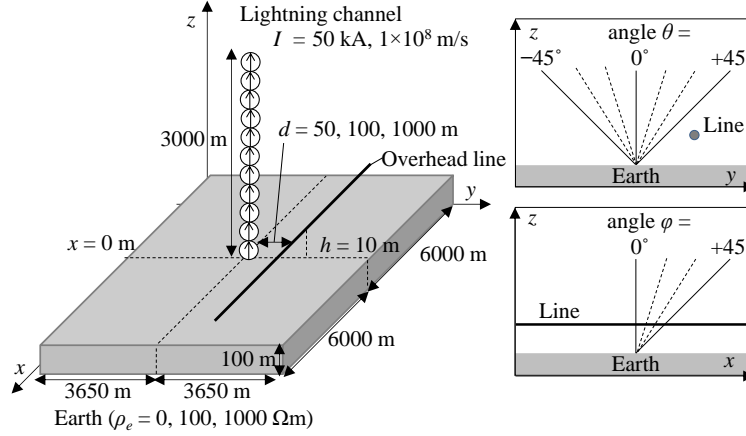


Figure 4.1 Model circuit.

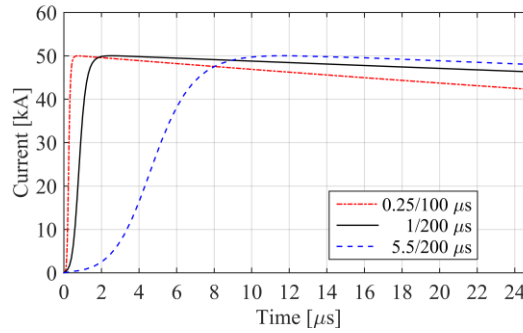


Figure 4.2 Return-stroke current waveforms.

#### 4.1.1.2 Analytical formula

Matsubara and Sekioka derived an analytical formula of the induced voltage for arbitrary inclined lightning [132]. The formula is employed to validate the FDTD model in this study. From the theoretical view point, a lightning induced voltage  $U$  at a position  $x$  on a single-conductor overhead line above a perfectly conducting earth, can be obtained by a summation of traveling voltages ( $V_{s1}$  and  $V_{s2}$ ) and a vector-potential contribution ( $e_m$ ) as follows [132].

$$U = V_{s1} + V_{s2} + e_m \quad (4.2)$$

$$V_{s1}(x, t) = \frac{1}{2} \int_0^t \frac{\partial}{\partial \tau} [e_s(\zeta, \tau) - v_0 A_{ix}(\zeta, \tau)]_{\zeta=x-v_0(t-\tau)} d\tau \quad (4.3)$$

$$V_{s2}(x, t) = \frac{1}{2} \int_0^t \frac{\partial}{\partial \tau} [e_s(\zeta, \tau) + v_0 A_{ix}(\zeta, \tau)]_{\zeta=x+v_0(t-\tau)} d\tau \quad (4.4)$$

$$e_s(x, t) = \int_0^h \left( \frac{\partial V_i}{\partial z} \right)_{z=0} dz \quad (4.5)$$

$$e_m(x, t) = \int_0^h \left( \frac{\partial A_{iz}}{\partial t} \right)_{z=0} dz \quad (4.6)$$

where  $U$  is the total induced voltage,  $V_{s1}$  and  $V_{s2}$  are traveling-wave voltages from the left side ( $-\infty$  to  $x$ ) and from the right side ( $+\infty$  to  $x$ ), respectively,  $e_s$  is an induced voltage by a scalar potential  $V_i$ ,  $A_{ix}$  is a horizontal vector potential, and  $e_m$  is an induced voltage by a vertical vector potential  $A_{iz}$ .  $v_0$  is the light speed and  $h$  is the line height. Influences of the lightning inclination on the total voltage  $U$  and the components ( $V_{s1}$ ,  $V_{s2}$ , and  $e_m$ ) will be discussed later.

#### 4.1.1.3 Transmission-line (TL) based method

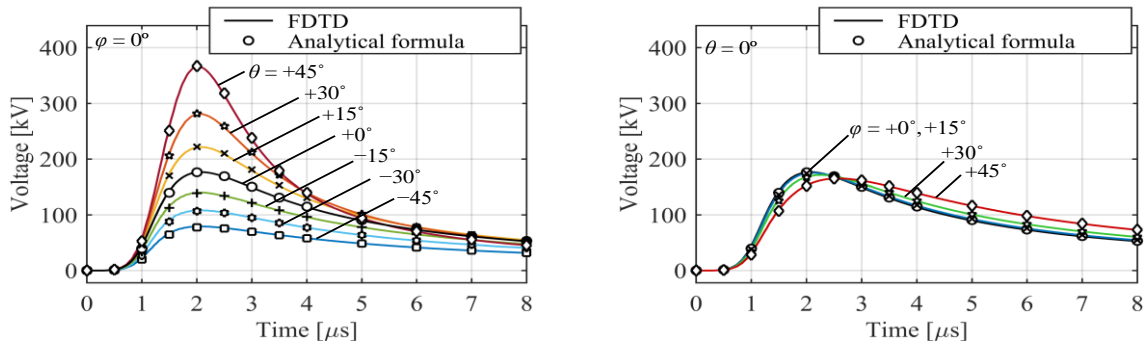
Because Matsubara-Sekioka formula cannot deal with a lossy earth, another approach, a TL-based method (EMTP LIOV ToolBox [66]-[71]), is also employed to validate the FDTD model in this study. In the TL method, the effect of the lossy earth is implemented using the Cooray-Rubinstein formula which modifies the horizontal electric field radiated from lightning to a line [62], [67]. For details, please refer to [62], [66]-[71]. The basics of the method are also introduced in IEEE Std. 1410 [12].

### 4.1.2 Lightning induced voltages caused by inclined lightning above a perfectly conducting earth

Figure 4.3 shows induced voltages by inclined lightning at  $x = 0$  m (in front of the lightning channel base) in the single-conductor line. The voltages calculated by FDTD and the analytical formula [132] are presented. The simulation parameters are:  $t_{d10-90}/t_h = 1/200 \mu\text{s}$ ,  $d = 50$  m, and  $\rho_e = 0 \Omega\text{m}$ .

The FDTD results for both angles  $\theta$  and  $\varphi$  agree very well with those obtained by the analytical formula. It indicates the inclined lightning is satisfactorily modeled in the FDTD.

In Figure 4.3 (a), the induced voltage increases significantly as  $\theta$  increases, and the voltage at  $\theta = +45^\circ$  reaches about 2.1 p.u. (365/176 kV) of that by vertical lightning ( $\theta = 0^\circ$ ). On the other hand, the voltage amplitude is not largely influenced by the angle  $\varphi$  in Figure 4.3 (b) although the wave-tail of  $\varphi = +45^\circ$  is sustained slightly longer. These trends have been observed in the previous chapter. The influence of the inclined lightning on the induced voltage is also clearly observed when a standard lightning current waveform of  $1/200 \mu\text{s}$  is assumed.



(a) Inclined angle  $\theta$  ( $\varphi = 0^\circ$ ).

(b) Inclined angle  $\varphi$  ( $\theta = 0^\circ$ ).

Figure 4.3 Lightning induced voltages on a single-conductor overhead line caused by inclined lightning:  $1/200 \mu\text{s}$ ,  $x = 0 \text{ m}$ ,  $d = 100 \text{ m}$ ,  $\rho_e = 0 \Omega\text{m}$ , comparison with an analytical formula [132].

To understand the mechanism, the total induced voltage  $U$  and its components  $V_{s1}$ ,  $V_{s2}$  and  $e_m$  are investigated by the analytical formulas (4.2) to (4.6). Figure 4.4 shows the voltages for  $\theta = 0^\circ$  and  $\pm 45^\circ$ , and  $\varphi = +45^\circ$ . In Figure 4.4 (a) for the vertical lightning ( $\theta = 0^\circ$ ,  $\varphi = 0^\circ$ ), the amplitude of the traveling-wave voltage ( $V_{s1}+V_{s2}$ ) is nearly doubled compared with  $e_m$ . Note that  $V_{s1}$  becomes equal to  $V_{s2}$  in this case because the lightning channel is symmetric to the voltage measuring point at  $x = 0 \text{ m}$  on the line. Thus, it can be said  $V_{s1}$ ,  $V_{s2}$ , and  $e_m$  give almost the same contribution to  $U$ .

When the lightning is inclined towards the line ( $\theta = +45^\circ$ ), in Figure 4.4 (b), both  $(V_{s1}+V_{s2})$  and  $e_m$  increase because of shorter distance to the line. However, the increase ratio of  $(V_{s1}+V_{s2})$  is larger than that of  $e_m$ , i.e. the former increases to 2.4 p.u. (286/117 kV) while the latter increases to 1.3

p.u. (91/72 kV) at their peaks compared with the vertical case. Similarly, when  $\theta = -45^\circ$  in Figure 4.4 (c), the both components decrease and the decrease ratio of  $(V_{s1}+V_{s2})$  is greater than that of  $e_m$  (0.39 p.u. = 78/117 kV and 0.53 p.u. = 39/72 kV, respectively). These results indicate that the traveling-wave voltage component  $(V_{s1}+V_{s2})$  is more sensitive to the lightning inclination.

In Figure 4.4 (d), for the inclined lightning along the line ( $\varphi = +45^\circ$ ), although the total voltage  $U$  appears not greatly influenced by the inclination compared to Figure 4.4 (a), the traveling voltage from the right side  $V_{s2}$  increases while the voltage from the left side  $V_{s1}$  and  $e_m$  decrease. This is because 1) the inclined lightning maintains a closer position to the right side of the line and 2) both  $x$  and  $z$  components of the vector potential  $A_i$  in equations (4.3), (4.4), and (4.6) are varied due to the inclination.

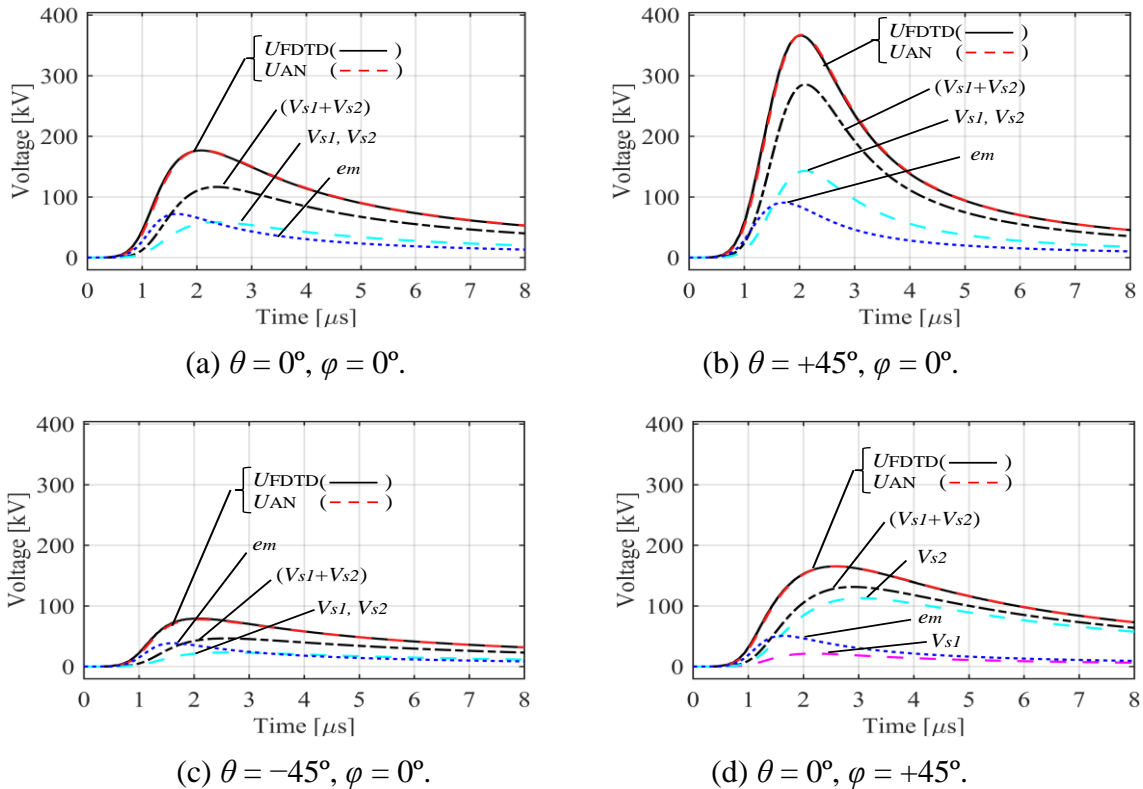
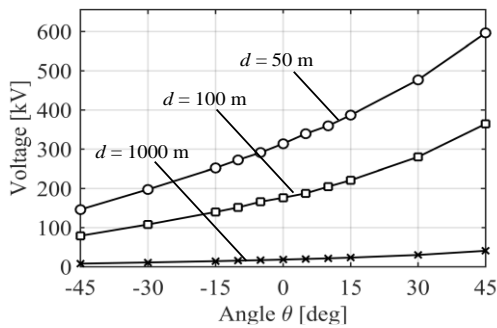
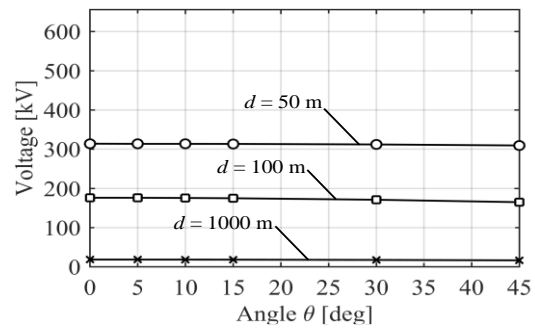


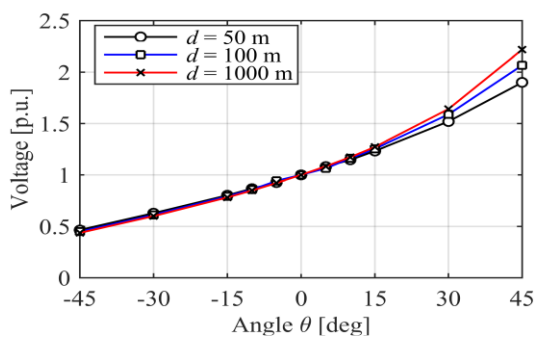
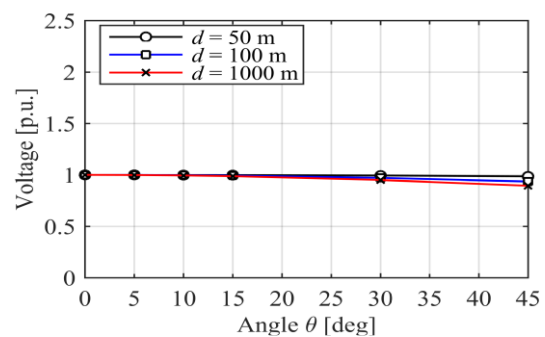
Figure 4.4 Influence of lightning inclination on voltage components of the induced voltage calculated by an analytical formula [132]:  $x = 0$  m,  $1/200 \mu\text{s}$ ,  $d = 100$  m,  $\rho_e = 0 \Omega\text{m}$ .  $U_{FDTD}$  is computed with FDTD and the others are computed with the analytical formula.

When the lightning is vertical, the vector potential  $A_i$  has only the vertical component  $A_{iz}$  since the potential has the same direction as the lightning current. For the inclined lightning of  $\varphi = +45^\circ$ , the vertical component  $A_{iz}$  and resulting  $e_m$  decrease to  $1/\sqrt{2}$  of those for the vertical lightning. In addition, the horizontal component  $A_{ix}$  appears and contributes to generating the traveling voltages in (4.3) and (4.4).  $A_{ix}$  makes the potential on the right side of the line higher than that on the left side, which increases  $V_{s2}$  and decreases  $V_{s1}$ .

Figure 4.5 summarizes peaks of the induced voltages at  $x = 0$  m for  $d = 50, 100$  and  $1000$  m as a function of angles  $\theta$  and  $\varphi$ . In Figure 4.5 (a-1) for  $\theta$ , it is clearly shown that the peak voltage increases as  $\theta$  increases. This trend can be observed for all of the distances. In Figure 4.5 (a-2), almost no significant change on the voltages is observed for the angle  $\varphi$ .

(a-1) Inclined angle  $\theta$  ( $\varphi = 0^\circ$ ).(a-2) Inclined angle  $\varphi$  ( $\theta = 0^\circ$ ).

(a) Peak voltage in kV.

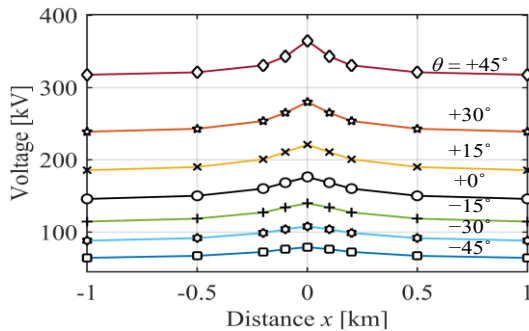
(b-1) Inclined angle  $\theta$  ( $\varphi = 0^\circ$ ).(b-2) Inclined angle  $\varphi$  ( $\theta = 0^\circ$ ).

(b) Peak voltage in p.u.

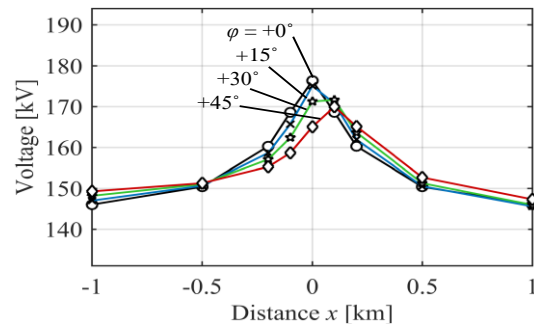
Figure 4.5 Peak induced voltages at  $x = 0$  as a function of the angles  $\theta$  and  $\varphi$  computed by FDTD:  $1/200 \mu\text{s}$ ,  $d = 50, 100$ , and  $1000$  m,  $\rho_e = 0 \Omega\text{m}$ .

The change ratios of the voltages (p.u.) to the vertical cases are also summarized in Figure 4.5 (b). There is no remarkable difference among the three distances for both the angles  $\theta$  and  $\varphi$  except  $\theta = +45^\circ$ . At  $\theta = +45^\circ$ , the increase ratio for  $d = 50$  m becomes smaller than those for  $d = 100$  and 1000 m.

Figure 4.6 shows examples of the peak voltage profiles along the line for  $d = 100$  m. The profiles become symmetric for the angle  $\theta$  in Figure 4.6 (a) while it becomes asymmetric for the angle  $\varphi$  in Figure 4.6 (b). The peak voltages become stable after  $x = 1$  km because only the traveling voltage induced at around the line center reaches there by lossless propagation. For  $\varphi = +45^\circ$ , the maximum voltage appears at  $x = +100$  m, and the voltages on the left side become slightly larger than those on the right side because the traveling voltage from the right to the left ( $V_{s2}$ ) increases due to the lightning inclination as explained above.



(a) Inclined angle  $\theta$  ( $\varphi = 0^\circ$ ).



(b) Inclined angle  $\varphi$  ( $\theta = 0^\circ$ ).

Figure 4.6 Peak voltage profiles along the line for the various angles  $\theta$  and  $\varphi$  computed by FDTD:  $1/200 \mu\text{s}$ ,  $d = 100$  m,  $\rho_e = 0 \Omega\text{m}$ .

### 4.1.3 Influence of earth resistivity on induced voltage

Figure 4.7 shows lightning induced voltages at  $x = 0$  m for the earth resistivity of  $\rho_e = 100$  and  $1000 \Omega\text{m}$ . The other parameters are the same as in the previous case. Firstly, the FDTD results for the vertical lightning agree well with those obtained by the TL method [71]. The induced voltage increases when the earth resistivity increases as is well known [44], [45], [120], [121]. However, the influences of the angles  $\theta$  and  $\varphi$  on the induced voltage are similar to the results of  $\rho_e = 0 \Omega\text{m}$  shown in Figure 4.3.



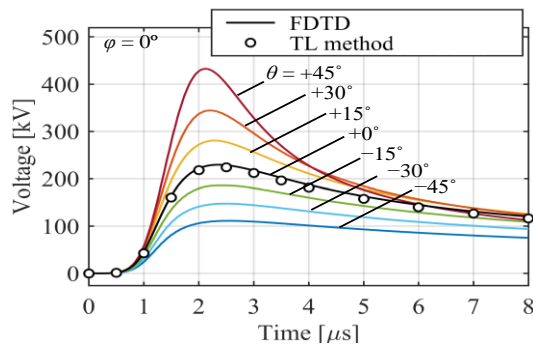
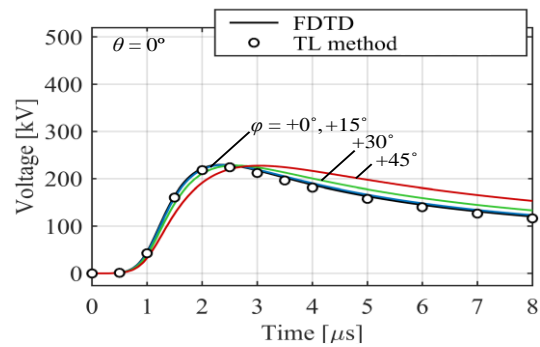
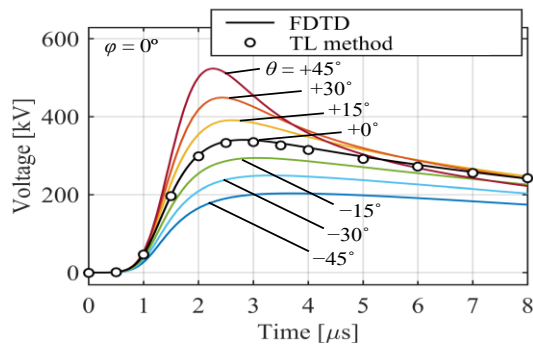
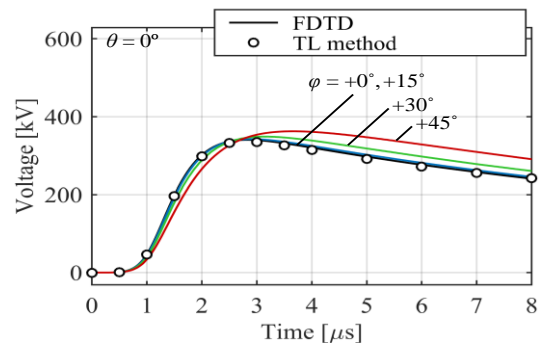
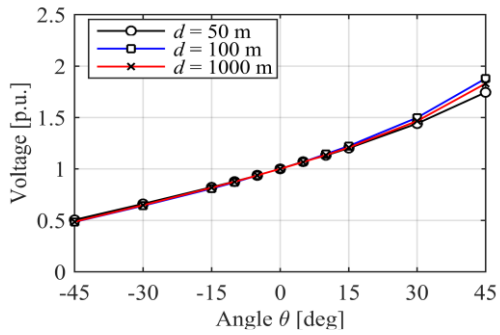
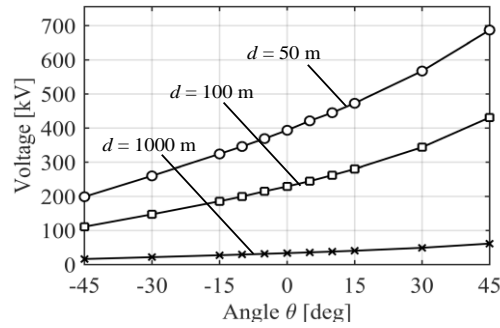
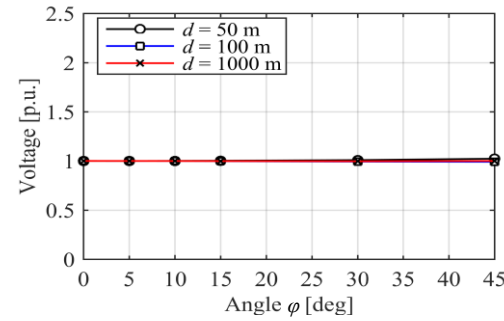
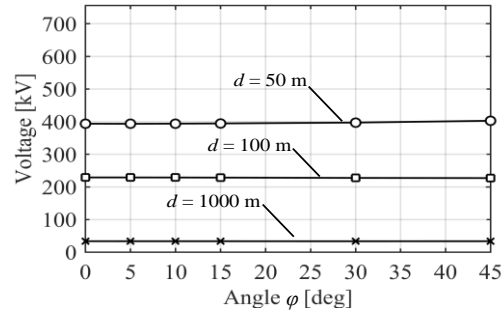
(a-1) Inclined angle  $\theta$  ( $\varphi = 0^\circ$ ).(a-2) Inclined angle  $\varphi$  ( $\theta = 0^\circ$ ).(a)  $\rho_e = 100 \Omega\text{m}$ (b-1) Inclined angle  $\theta$  ( $\varphi = 0^\circ$ ).(b-2) Inclined angle  $\varphi$  ( $\theta = 0^\circ$ ).(b)  $\rho_e = 1000 \Omega\text{m}$ 

Figure 4.7 Lightning induced voltages on a single-conductor line above a lossy earth caused by inclined lightning:  $1/200 \mu\text{s}$ ,  $x = 0 \text{ m}$ ,  $d = 100 \text{ m}$ , in comparison with a TL method [71] for vertical lightning.

Figure 4.8 summarizes peak values of the induced voltages at  $x = 0 \text{ m}$  for  $d = 50, 100$  and  $1000 \text{ m}$  as functions of the angle  $\theta$  and  $\varphi$ . A similar trend to the case of  $\rho_e = 0 \Omega\text{m}$  is observed. However, in the case of the angle  $\theta$ , the increase ratio at  $\theta = +45^\circ$  becomes smaller as the earth resistivity becomes higher, which means that the influence of lightning inclination becomes less significant at higher earth resistivity. In contrast to the angle  $\theta$ , there are almost no significant changes due to the angle  $\varphi$  in  $\rho_e = 100$  and  $1000 \Omega\text{m}$ , similar to the results shown in Figure 4.5 (b-2).

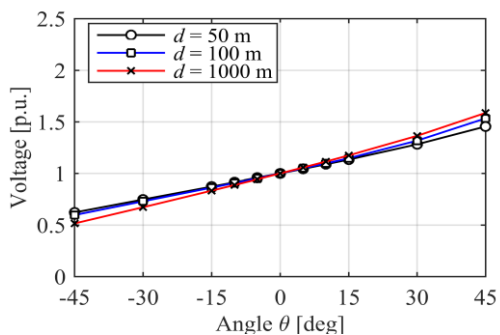
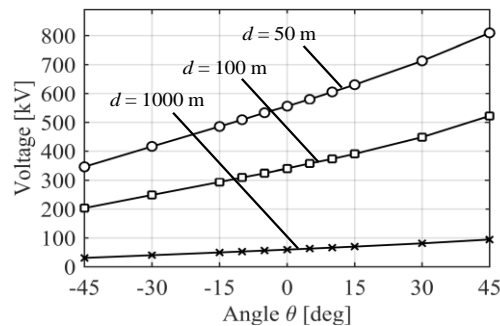


(a-1) Inclined angle  $\theta$  ( $\varphi = 0^\circ$ ).

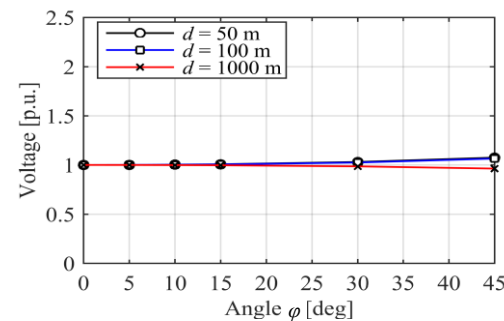
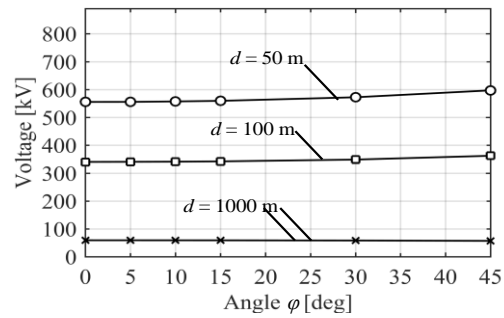


(a-2) Inclined angle  $\varphi$  ( $\theta = 0^\circ$ ).

(a)  $\rho_e = 100 \Omega\text{m}$



(b-1) Inclined angle  $\theta$  ( $\varphi = 0^\circ$ ).



(b-2) Inclined angle  $\varphi$  ( $\theta = 0^\circ$ ).

(b)  $\rho_e = 1000 \Omega\text{m}$

Figure 4.8 Peak voltages at  $x = 0$  m for the lossy earth as functions of the angle  $\theta$  and  $\varphi$  computed by the FDTD:  $1/200 \mu\text{s}$ ,  $d = 100$  m.

Figure 4.9 shows peak voltage profiles along the line for  $\rho_e = 100$  and  $1000 \Omega\text{m}$  with  $d = 100$  m. Because the traveling-wave voltages on the line are attenuated during the propagation due to the lossy earth, the peak voltages decrease as the distance  $x$  becomes further from the line center. The decrease is more obvious at higher values of earth resistivity.

Summarizing the above observations, the induced voltages caused by inclined lightning above lossy earth clearly increase as for perfectly conducting earth. The influence of the lightning inclination for the lossy earth shows a similar trend to that for perfectly conducting earth. However, the increase ratio of the voltage to the vertical lightning decreases when the earth resistivity increases.

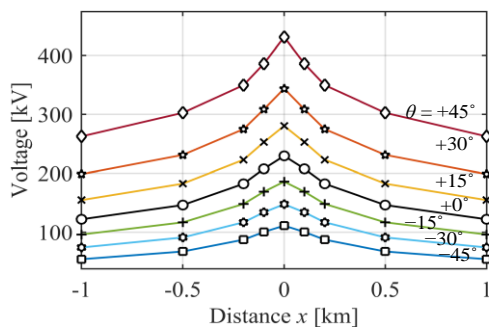
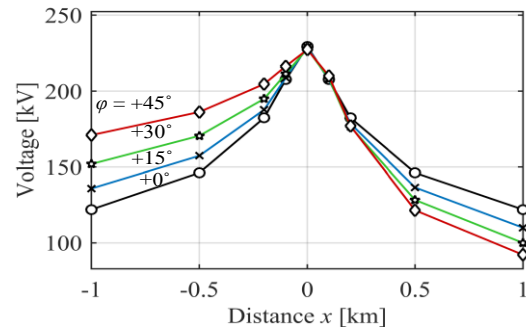
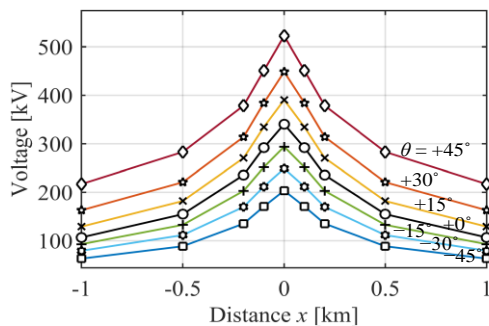
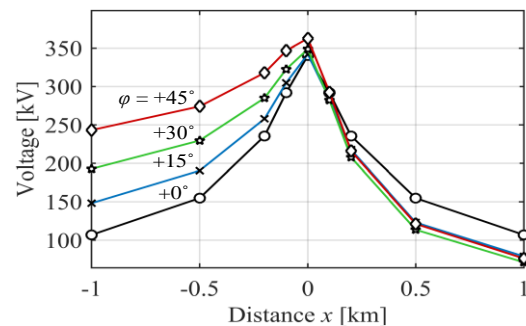
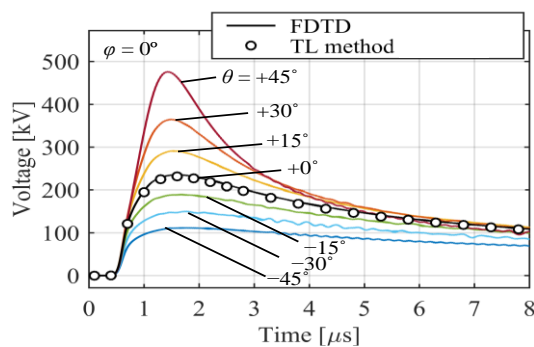
(a-1) Inclined angle  $\theta$  ( $\varphi = 0^\circ$ ).(a-2) Inclined angle  $\varphi$  ( $\theta = 0^\circ$ ).(a)  $\rho_e = 100 \Omega\text{m}$ (b-1) Inclined angle  $\theta$  ( $\varphi = 0^\circ$ ).(b-2) Inclined angle  $\varphi$  ( $\theta = 0^\circ$ ).(b)  $\rho_e = 1000 \Omega\text{m}$ 

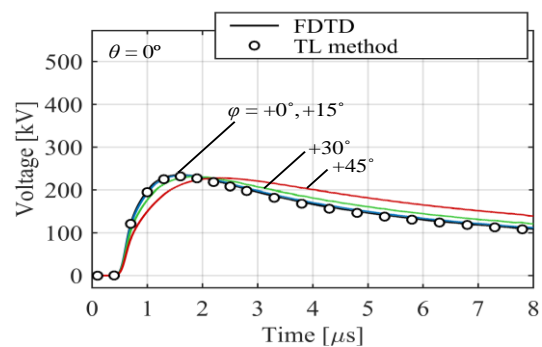
Figure 4.9 Peak voltage profiles along the line above the lossy earth for the various angles  $\theta$  and  $\varphi$  computed by the FDTD:  $1/200 \mu\text{s}$ ,  $d = 100$  m.

#### 4.1.4 Influence of lightning current waveforms on the induced voltage

Figure 4.10 shows induced voltages at  $x = 0$  for the lightning current waveforms of 0.25/100 and 5.5/200  $\mu\text{s}$ . Note that the time duration in the figure is extended to 40  $\mu\text{s}$  for the latter case. The line distance  $d$  is taken as 100 m and the earth resistivity  $\rho_e$  is set to 100  $\Omega\text{m}$ . The FDTD results agree well with those obtained using the TL method. Higher voltages are observed with the 0.25/100- $\mu\text{s}$  current because of greater  $di/dt$ .

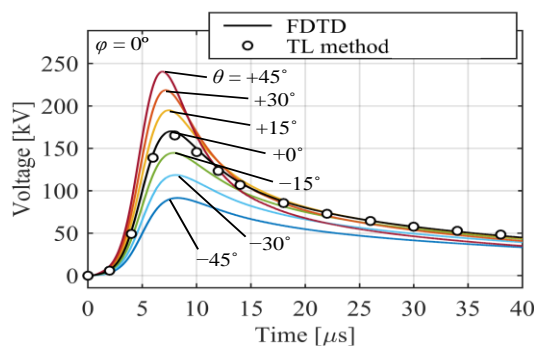


(a-1) Inclined angle  $\theta$  ( $\varphi = 0^\circ$ ).

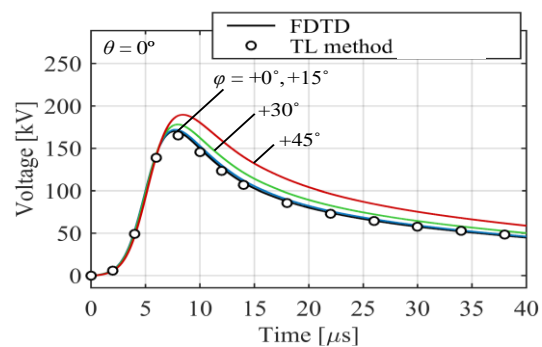


(a-2) Inclined angle  $\varphi$  ( $\theta = 0^\circ$ ).

(a) 0.25/100  $\mu\text{s}$ .



(b-1) Inclined angle  $\theta$  ( $\varphi = 0^\circ$ ).



(b-2) Inclined angle  $\varphi$  ( $\theta = 0^\circ$ ).

(b) 5.5/200  $\mu\text{s}$ .

Figure 4.10 Lightning induced voltages by current waveforms of 0.25/100 and 5.5/200  $\mu\text{s}$ :  $x = 0$  m,  $d = 100$  m,  $\rho_e = 100 \Omega\text{m}$ , in comparison with a TL method [71] for vertical lightning.

Figure 4.11 shows peak voltage ratios as a function of the angle  $\theta$ . For the waveform of 0.25/100  $\mu\text{s}$  in Figure 4.11 (a), the trends among the distances show only minor differences. The ratios at  $\theta = +45^\circ$  for  $\rho_e = 100$  and 1000  $\Omega\text{m}$  become higher than those for 1/200  $\mu\text{s}$  shown in Figure 4.8 (a-2) and (b-2). On the other hand, for 5.5/200  $\mu\text{s}$ , the peak voltage becomes dependent on the distance as shown in Figure 4.11 (b). The ratio decreases as the lightning becomes closer to the line. The peak voltage profiles along the line are similar to those in Figure 4.9 although they are not presented.

It is clearly shown by the above observations that the influence of lightning inclination becomes significant with faster rise time of the lightning current.

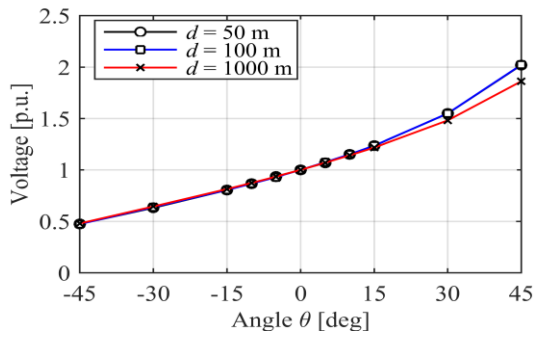
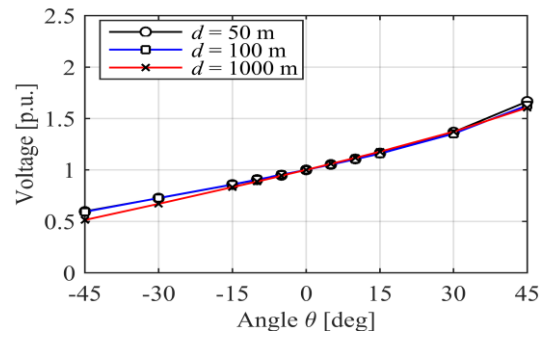
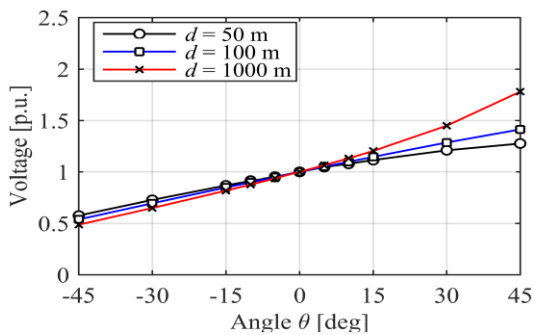
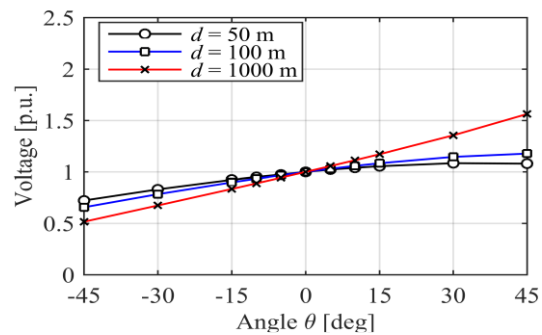
(a-1)  $\rho_e = 100 \Omega\text{m}$ .(a-2)  $\rho_e = 1000 \Omega\text{m}$ .(a) 0.25/100  $\mu\text{s}$ .(b-1)  $\rho_e = 100 \Omega\text{m}$ .(b-2)  $\rho_e = 1000 \Omega\text{m}$ .(b) 5.5/200  $\mu\text{s}$ .

Figure 4.11 Peak voltage ratios for lightning current waveforms of 0.25/100 and 5.5/200  $\mu\text{s}$  as a function of angle  $\theta$  computed by the FDTD:  $x = 0$  m.

### 4.1.5 Mean value of the induced voltage by inclined lightning

When the inclined lightning is considered, the increase ratio of the peak voltage by the inclination does not show a linear trend as in Figure 4.5, Figure 4.8, and Figure 4.11. This indicates that the mean values of the voltages may be different from the values evaluated by the vertical lightning. To check the mean value of induced voltage by inclined lightning, the following procedures are applied to the FDTD results: 1) the peak voltage trends as a function of the angles  $\theta$  and  $\varphi$  are re-summarized, i.e. some of the peak voltages for the angle  $\varphi$  are taken at  $x = +100$  m instead of  $x = 0$  m, 2) the new trends are fitted by 5th order polynomial functions, 3) arithmetic means of the induced voltages within  $\theta = \pm 45^\circ$  and  $\varphi = \pm 45^\circ$  are calculated respectively based on the polynomial functions. As a very simple hypothesis, the inclined angles are assumed to be equiprobable in the evaluation.

Table 4.1 shows the calculated mean values in kV and in p.u. to the voltage of the vertical lightning when  $d = 100$  m. The mean values are different from those by vertical lightning, as is expected. For the angle  $\theta$ , the mean values become greater than those by vertical lightning when the rise-time of the lightning current is faster and the earth resistivity is lower. The difference reaches 7 % for  $0.25/100 \mu\text{s}$  and  $\rho_e = 100 \Omega\text{m}$ . On the other hand, the mean values for the angle  $\varphi$  become greater when the rise-time is slower, and the earth resistivity is higher. However, the changes are relatively smaller than those of the angle  $\theta$ .

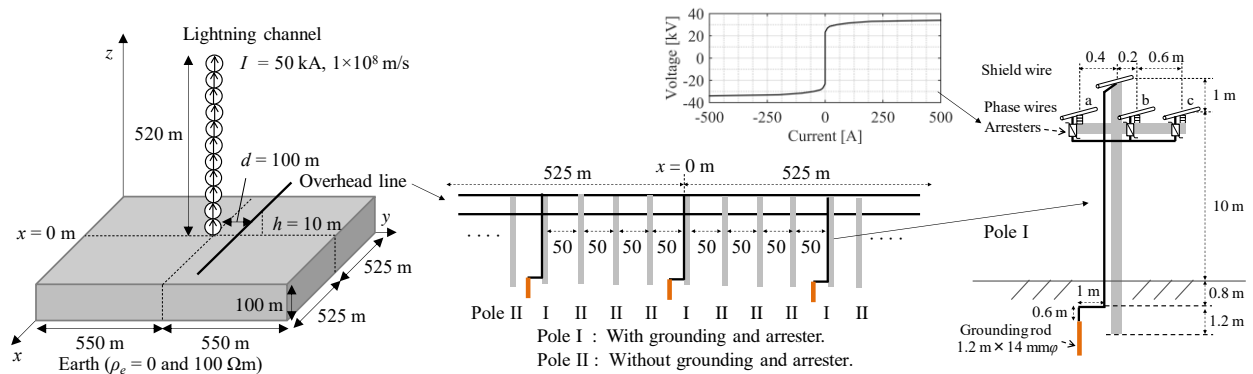
Table 4.1 Peak voltages and mean values.

$d = 100$		Angle $\theta$				Angle $\varphi$			
$t_{d10-90}/t_h$	$\rho_e \Omega\text{m}$	-45	0	+45	Mean		$\pm 45$	Mean	
		kV	kV	kV	kV	p.u.	kV	kV	p.u.
0.25/100	0	82	186	412	204	1.10	175	181	0.98
	100	112	235	476	253	1.07	228	232	0.99
	1000	202	341	556	352	1.03	360	347	1.02
1/200	0	79	176	365	190	1.08	170	173	0.98
	100	111	229	431	242	1.06	227	228	1.00
	1000	204	340	522	347	1.02	362	347	1.02
5.5/200	0	55	112	178	114	1.01	122	116	1.03
	100	92	170	241	169	0.99	190	176	1.04
	1000	188	287	338	279	0.97	325	299	1.04

## 4.2 Lightning induced voltage in a three-phase distribution line by inclined lightning

### 4.2.1 FDTD model circuit

Figure 4.12 illustrates an FDTD model circuit for a multi-phase distribution line with utility poles, a shield wire with groundings, and arresters. Three phase wires with a height of 10 m and a separation distance of 0.6 m between the phases are supported by insulators of  $100 \text{ M}\Omega$  on the poles at intervals of 50 m. A shield wire is placed 1 m above the phase wires between phases a and b, and the shield wire is connected to a 1.2 m-length grounding rod through a ground lead with intervals of 200 m at the poles. The grounding resistance is estimated to be  $30 \text{ }\Omega$  per grounding by an FDTD analysis where a stepwise current of 1 A is applied, and the resistance becomes stable within  $0.2 \text{ }\mu\text{s}$ . Arresters are installed at the same poles with the groundings. The arrester discharge voltage is 33 kV as illustrated in Figure 4.12. The poles with/without the groundings and arresters are called Pole-I and Pole-II, respectively. The lightning current is assumed  $1/200 \text{ }\mu\text{s}$  with a return stroke velocity of  $1 \times 10^8 \text{ m/s}$ . The earth resistivity  $\rho_e$  is set to 0 and  $100 \text{ }\Omega\text{m}$  with a relative permittivity  $\epsilon_r = 10$ . The line distance  $d$  is fixed to 100 m. The working space is resized to  $1.05 \text{ km} \times 1.1 \text{ km} \times 0.62 \text{ km}$  with the minimum cell size of 0.2 m to model the pole structure. One FDTD computation for  $8 \text{ }\mu\text{s}$  needs approximately 8 hours on the same computer as that mentioned in Section 4.1.



(a) FDTD model circuit. (b) Line and pole configuration. (c) Pole structure and components.

Figure 4.12 FDTD model circuit of a multi-phase distribution line.

By using the new model, induced voltages in a single-phase (S) overhead line are compared to those in the multi-phase (M) overhead lines with some combinations of the poles (P), the shield wire with the groundings (G), and the arresters (A). Note that the phase-b wire in the M line is at the same position as the phase wire in the S line.

Figure 4.13 shows induced voltages at  $x = 0$  m on the lines for the vertical lightning. Phase-b voltages are presented for M lines. Comparing the results of S, SP, and MP lines, the poles and the multi-phase wires make no significant difference to the voltage. The voltage in the MPG line is decreased to about 70 % by the shield wire. In the MPGA line, the arresters suppress the peak voltages to 45 kV for  $\rho_e = 0$  and 57 kV for  $100 \Omega\text{m}$ , respectively.

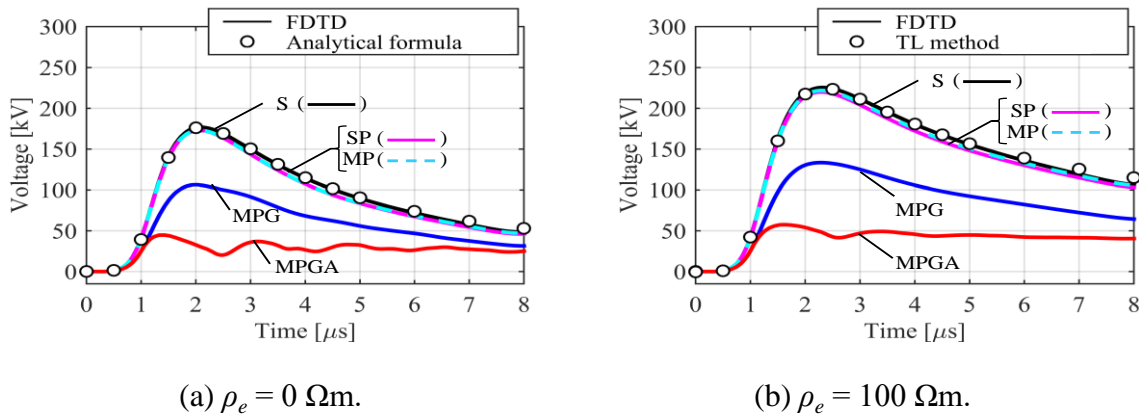


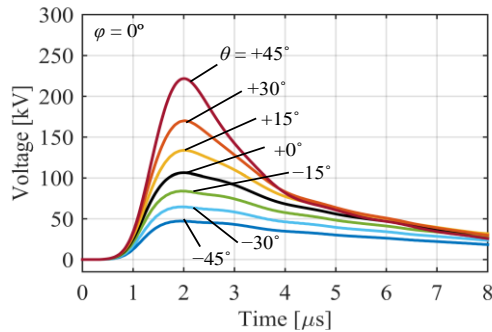
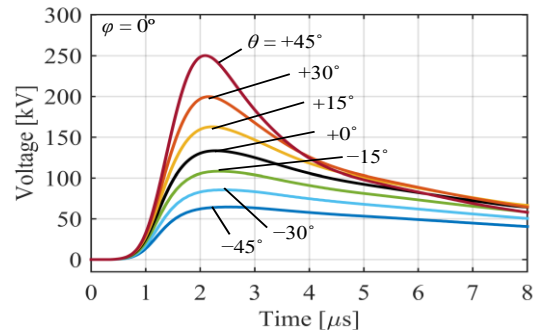
Figure 4.13 Lightning induced voltages at  $x = 0$  m by the vertical lightning with various line configurations: single-phase (S) and multi-phase (M) overhead lines with utility poles (P), a shield wire with groundings (G), and arresters (A):  $1/200 \mu\text{s}$ ,  $d = 100$  m, in comparison with analytical formula[132] and the TL method [71] for the cases of (S).

## 4.2.2 Induced voltages due to inclined lightning

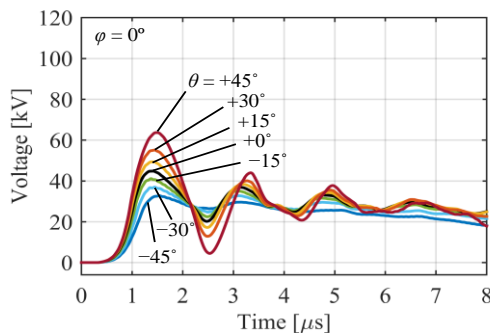
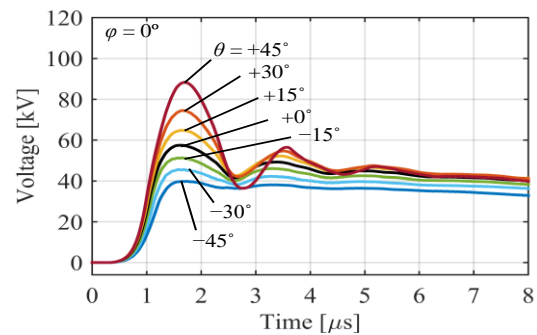
Figure 4.14 shows the influences of lightning-inclined angle  $\theta$  on the induced voltages at  $x = 0$  m in MPG and MPGA lines computed by the FDTD. In the MPG line, a trend similar to the single overhead line in Section 4.1 is observed: the voltage increases as the angle  $\theta$  increases. In the MPGA line, the voltage at  $\theta = +45^\circ$  rises from 57 kV to 88 kV in the initial transient, i.e. the



arresters cannot suppress the transient voltage to the same level as that for the vertical lightning. However, the voltage at  $8 \mu\text{s}$  converges to a value almost identical to the vertical one.

(a-1)  $\rho_e = 0 \Omega\text{m}$ .(a-2)  $\rho_e = 100 \Omega\text{m}$ .

(a) Multi-phase line with poles and a shield wire with groundings (MPG).

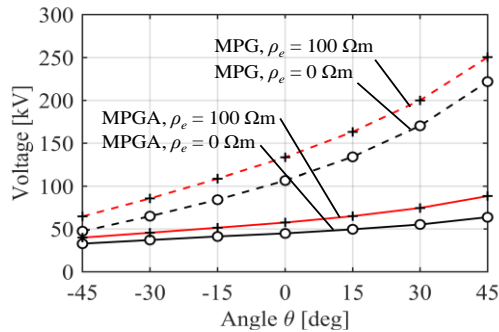
(b-1)  $\rho_e = 0 \Omega\text{m}$ .(b-2)  $\rho_e = 100 \Omega\text{m}$ .

(b) Multi-phase line with poles, a shield wire with groundings, and arresters (MPGA).

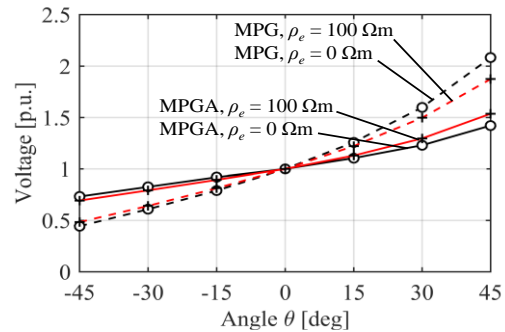
Figure 4.14 Lightning induced voltages at  $x = 0 \text{ m}$  on the phase-b wire of MPG and MPGA lines due to the incline lightning:  $1/200 \mu\text{s}$ ,  $d = 100 \text{ m}$ .

Figure 4.15 summarizes peak voltages in MPG and MPGA lines as a function of the angle  $\theta$ . In Figure 4.15 (b), the p.u. trends of MPG line for  $\rho_e = 0$  and  $100 \Omega\text{m}$  show almost the same trends as those in Figure 4.5 (b-1) and Figure 4.8 (a-2). The voltage increases to 1.8–2.1 p.u. at  $\theta = +45^\circ$ . On the other hand, the p.u. trends of MPGA line only increases to 1.4–1.5 p.u., indicating that the

arresters operate correctly to suppress the higher voltage due to inclined lightning. However, the influence of the lightning inclination is still clearly observed on the line.



(a) Induced voltage in kV.



(b) Induced voltage in p.u.

Figure 4.15 Peak voltages at  $x = 0$  m in MPG and MPGA lines as a function of the angle  $\theta$ :  $1/200$   $\mu$ s,  $d = 100$  m.

### 4.3 Concluding remarks

This chapter investigated the influences of inclined lightning on induced voltages in distribution lines by FDTD when single-phase and multi-phase lines with a shield wire, poles, groundings, and arresters are considered. The FDTD models in this study are validated with calculated results obtained using an analytical formula and a TL-based method, and the following conclusions can be drawn based on the FDTD results.

- (1) The induced voltages are significantly influenced by inclined lightning, especially by the inclination toward the line (angle  $\theta$ ). The peak voltages at  $\theta = +45^\circ$  reach 1.5 to 2.1 p.u. of those for the vertical lightning when a lightning current waveform of  $1/200$   $\mu$ s is assumed.
- (2) Lightning inclination along the line (angle  $\varphi$ ) causes only minor differences to the peak voltage. However, it makes the voltage profile along the line asymmetric.
- (3) The increase ratio of peak voltages by the angle  $\theta$  increases with decreasing earth resistivity and the rise-time of the lightning current becomes shorter.

- (4) For the angle  $\theta$ , the mean value of the induced voltage by the inclined lightning is estimated to be greater than the voltage caused by the vertical lightning when the rise-time of the lightning current is faster and the earth resistivity is lower.
- (5) When the three-phase line with the shield wire is assumed, the increase ratio of the voltage by the angle  $\theta$  shows similar trends to that for the single-phase line. The influence of the angle  $\theta$  is clearly observed even when the arresters are installed on the line. However, the arresters decrease both the induced voltages and the increase ratio of the voltages caused by the angle  $\theta$ .

The influences of the non-vertical lightning on lightning induced overvoltages are investigated under various conditions and summarized. The knowledge obtained in this chapter clearly indicates that the influences should be considered for an accurate evaluation of lightning induced overvoltages.

## **CHAPTER 5      LIGHTNING INDUCED OVERVOLTAGES CAUSED BY NON-VERTICAL LIGHTNING**

In this Chapter, lightning induced voltages on an overhead line are investigated considering “bent” and “computationally-generated” non-vertical lightning channels by using a finite-difference time-domain (FDTD) method.

As already explained in Chapter 2, recent developments of the analytical formulas [132] and the transmission-line based approach [126]-[128], [133]-[140] reveal some influences of non-vertical lightning on the induced voltages above a perfectly conducting earth. In [138], influences of lightning tortuosity on the voltages are investigated using a reconstructed lightning channel from a photo, and it is demonstrated that lightning channel geometry in low altitude is more significant for the induced voltage. The influences of non-vertical lightning above both a perfectly conducting earth and a lossy earth have been investigated in detail in Chapter 3 and Chapter 4 in this thesis. However, in the investigations, the lightning channel is assumed simply inclined, i.e. the path is straight and tilted with a fixed angle. Considering the knowledge presented in [138], a further study should be performed for the influence of lightning channel geometry especially in low altitude.

In Section 5.1, lightning induced voltages in a distribution line caused by bent lightning with various bent heights are investigated by the FDTD. Further, the effects of earth resistivity, lightning distance to the line, and lightning current waveforms are investigated. In Section 5.2, line voltages induced by computationally-generated channels are compared with those by simply inclined channels, to evaluate the influence of channel non-uniformity on the voltages. Section 5.3 summarizes the findings obtained from the investigations in this Chapter.

### **5.1 Induced voltages by bent lightning channels**

#### **5.1.1 FDTD model circuit**

Figure 5.1 illustrates an FDTD model circuit. A lightning channel of 800-m height is placed at the center of a working space and in front of a single-conductor overhead line. The channel has various

geometries described by channel types (Cases A and B) and bent heights ( $h_A$  and  $h_B$ ) with bent angles ( $\theta$  and  $\varphi$ ) as depicted in Figure 5.1 (b) and (c). Case A indicates a combination of lower-vertical and upper-inclined lightning channels with various connecting heights of  $h_A$ . Case B uses the opposite combinations of Case A with the bent height of  $h_B$ . The bent angle  $\theta$  is for the inclination toward the line, and the angle  $\varphi$  is for the inclination along the line as illustrated in Figure 5.1 (b). The angles  $\theta$  and  $\varphi$  vary between  $-45^\circ$  and  $+45^\circ$  and  $0^\circ$  and  $+45^\circ$ , respectively. The channels are represented by a series of small current sources known as a traveling-current-source (TCS) model [56], of which the current sources are aligned vertically and horizontally along the lightning paths. The Heidler function is used to calculate lightning current waveforms for the sources.

$$I(t) = \frac{I_0}{\eta} \frac{(t/\tau_1)^n}{1+(t/\tau_1)^n} e^{-(t/\tau_2)} \quad (5.1)$$

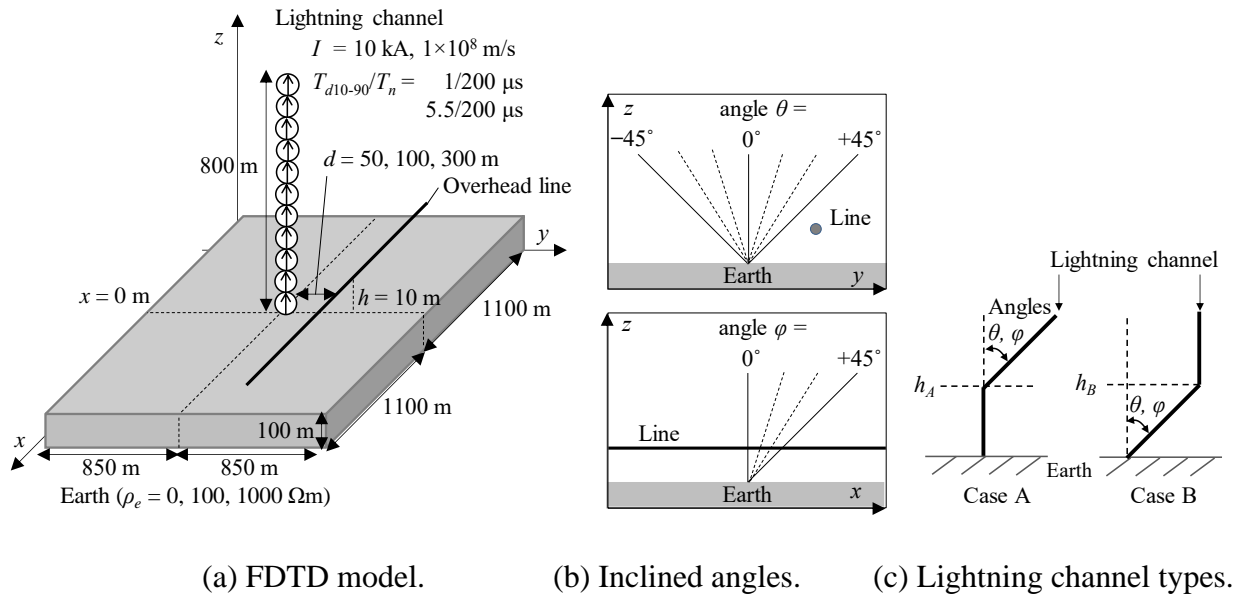


Figure 5.1 Model circuit.

The current amplitude  $I_0$  is assumed to be 10 kA. Two different waveforms of  $t_{d10-90}/t_n = 1/200 \mu\text{s}$  and  $5.5/200 \mu\text{s}$  are investigated in this Chapter as shown in Figure 5.2. The return stroke velocity is taken to be  $1 \times 10^8 \text{ m/s}$ . Earth resistivity  $\rho_e$  is set to 0 (perfectly conducting), 100, and 1000  $\Omega\text{m}$  with relative permittivity of  $\epsilon_r = 10$ . The overhead line of 10-m-height is placed at distances  $d = 50$  to 300 m away from the lightning channel base. A voltage measuring point is set at the center of

the line (in front of the lightning channel base). The FDTD working space of  $2200 \text{ m} \times 1700 \text{ m} \times 900 \text{ m}$  is composed of 2-, 4-, and 8-m cell lengths. The minimum length is applied to a region including the lightning channel base and voltage measuring point. The working space is covered by Liao's absorbing boundary to suppress unintended reflections from the boundaries [107].

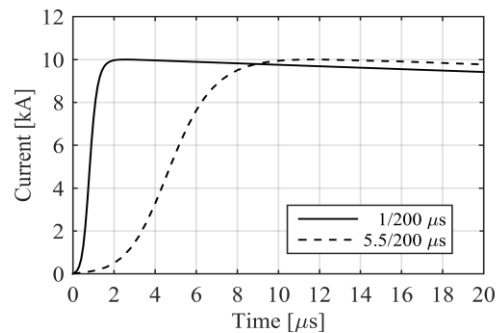


Figure 5.2 Return stroke current.

## 5.1.2 Induced voltages by bent lightning

### 5.1.2.1 Case A above a perfectly conducting earth: angle $\theta$

Figure 5.3 shows lightning induced voltages in Case A for the angle  $\theta$  where the lightning rises vertically at first and then inclined toward the line at height  $h_A$ . The lightning channel base is placed 50-m away from the line and the earth resistivity is set to  $0 \Omega\text{m}$ . The bent height  $h_A$  is varied from 0 m to 100 m. In Figure 5.3 (a), when  $h_A = 0 \text{ m}$ , the lightning channel is assumed simply inclined on the earth surface with the angle  $\theta$ . It is clear in the figure that the induced voltages are significantly influenced by the inclined angle, as already reported in Chapter 4. The voltage for  $\theta = +45^\circ$  reaches about 200 % of that for  $\theta = 0^\circ$  (vertical lightning). The change is also confirmed in comparison with results calculated by an analytical formula for the inclined lightning [132].

However, as observed in Figure 5.3 (b) to (d), the influence of the lightning inclination rapidly decreases as  $h_A$  increases. The peak voltage for  $\theta = +45^\circ$  decreases about 15 % even when only 10 m of the vertical part ( $h_A = 10 \text{ m}$ , same as the line height) is considered. The influence of the angle  $\theta$  on the peak voltages becomes very minor when  $h_A = 50 \text{ m}$ , and the peak voltages converge when  $h_A = 100 \text{ m}$ . These results indicate that the peak voltage is mainly influenced by the lightning

channel geometry under 100-m altitude, at least when severe conditions of a  $1/200\text{-}\mu\text{s}$  waveform and a lightning distance  $d$  of 50 m are assumed.

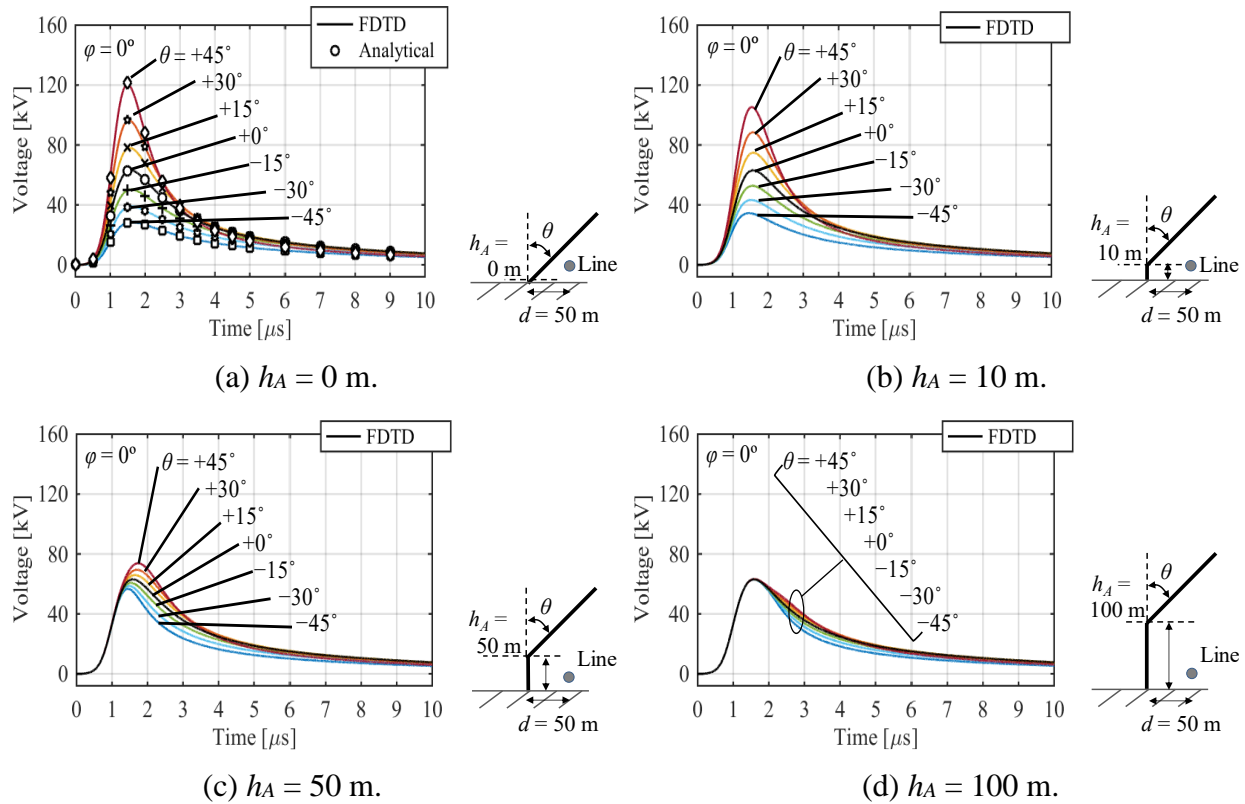


Figure 5.3 Lightning induced voltages on a single-conductor overhead line by bent lightning with various bent heights and inclined angles  $\theta$ : Case A,  $1/200\text{ }\mu\text{s}$ ,  $\rho_e = 0\text{ }\Omega\text{m}$ ,  $d = 50$  m,  $\varphi = 0^\circ$ .

### 5.1.2.2 Case B above a perfectly conducting earth: angle $\theta$

Figure 5.4 shows lightning induced voltages in Case B for the angle  $\theta$  where the lightning is firstly inclined toward the line and then bent back to the vertical position at a height  $h_B$ . The remainder of the parameters are the same as those in the previous section. Note that results for  $h_B = 0$  m are not presented in Figure 5.4 because they are the same as those obtained for the vertical lightning. When  $h_B = 10$  m, only the inclination of 10-m height is considered, the induced voltage starts to vary according to the inclined angle. The voltages for  $h_B = 50$  and 100 m become almost the same as

those by the inclined lightning in Figure 5.3 (a). These results also support the importance of the lightning channel geometry under 100-m altitude.

The influence of  $h_B$  is more noticeable than that of  $h_A$  because the lightning channels in Case B become closer to the line than those in Case A when  $h_A = h_B$ . However, both Cases A and B clearly demonstrate the importance of the lightning channel geometry in low altitude. Thus, only Case A is investigated after Section 5.1.2.4.

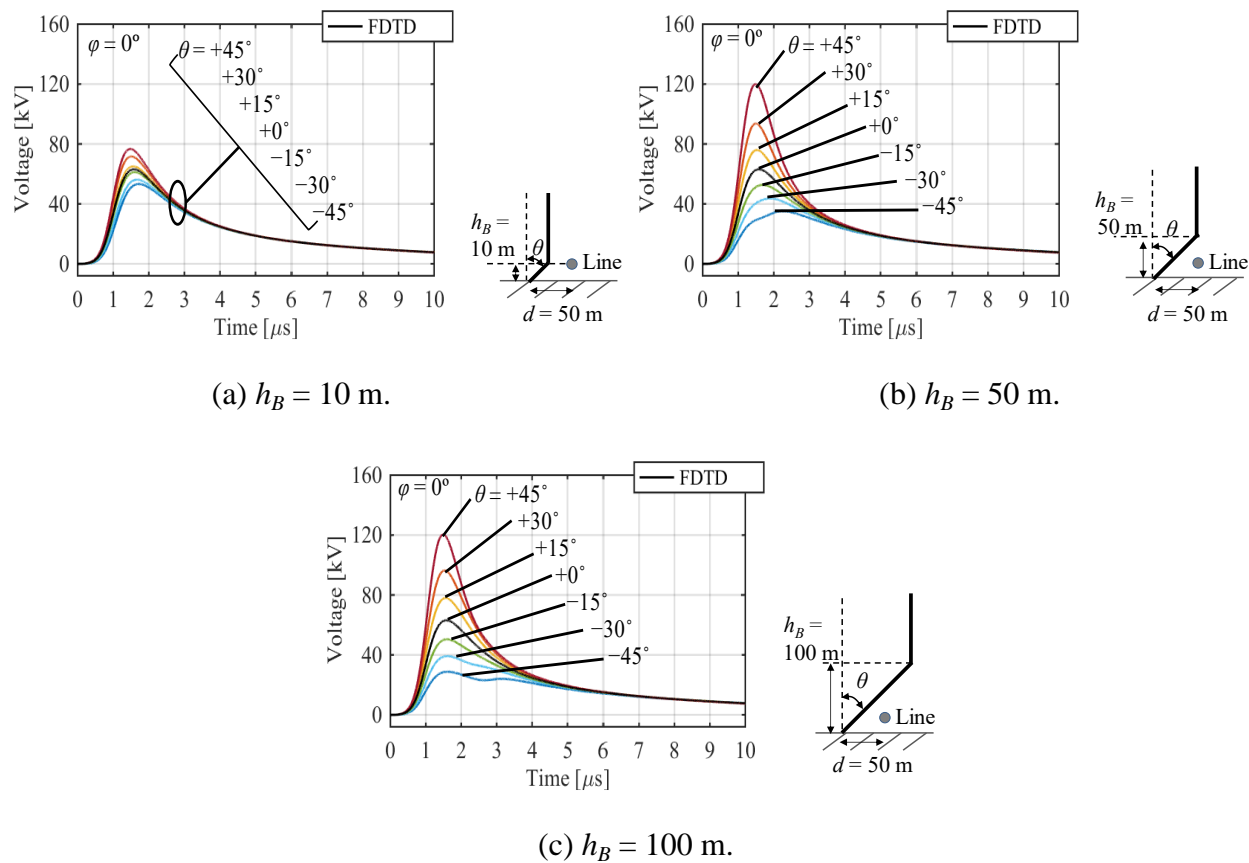


Figure 5.4 Lightning induced voltages on a single-conductor overhead line by bent lightning with various bent heights and inclined angles  $\theta$ : Case B,  $1/200 \mu\text{s}$ ,  $\rho_e = 0 \Omega\text{m}$ ,  $d = 50$  m,  $\varphi = 0^\circ$ .

### 5.1.2.3 Case A/B above a perfectly conducting earth: angle $\varphi$

Figure 5.5 shows lightning induced voltages in Cases A and B for the angle  $\varphi$  where the lightning is inclined along the line. In contrast to the angle  $\theta$ , the influence of the angle  $\varphi$  on the induced voltages is very minor even when  $h_A = 0$  m and  $h_B = 100$  m. These results indicate that considering



only the inclination toward the line (angle  $\theta$ ) is sufficient to investigate the influence of non-vertical lightning on the induced voltage, at least for the voltage measured at the line center in this study.

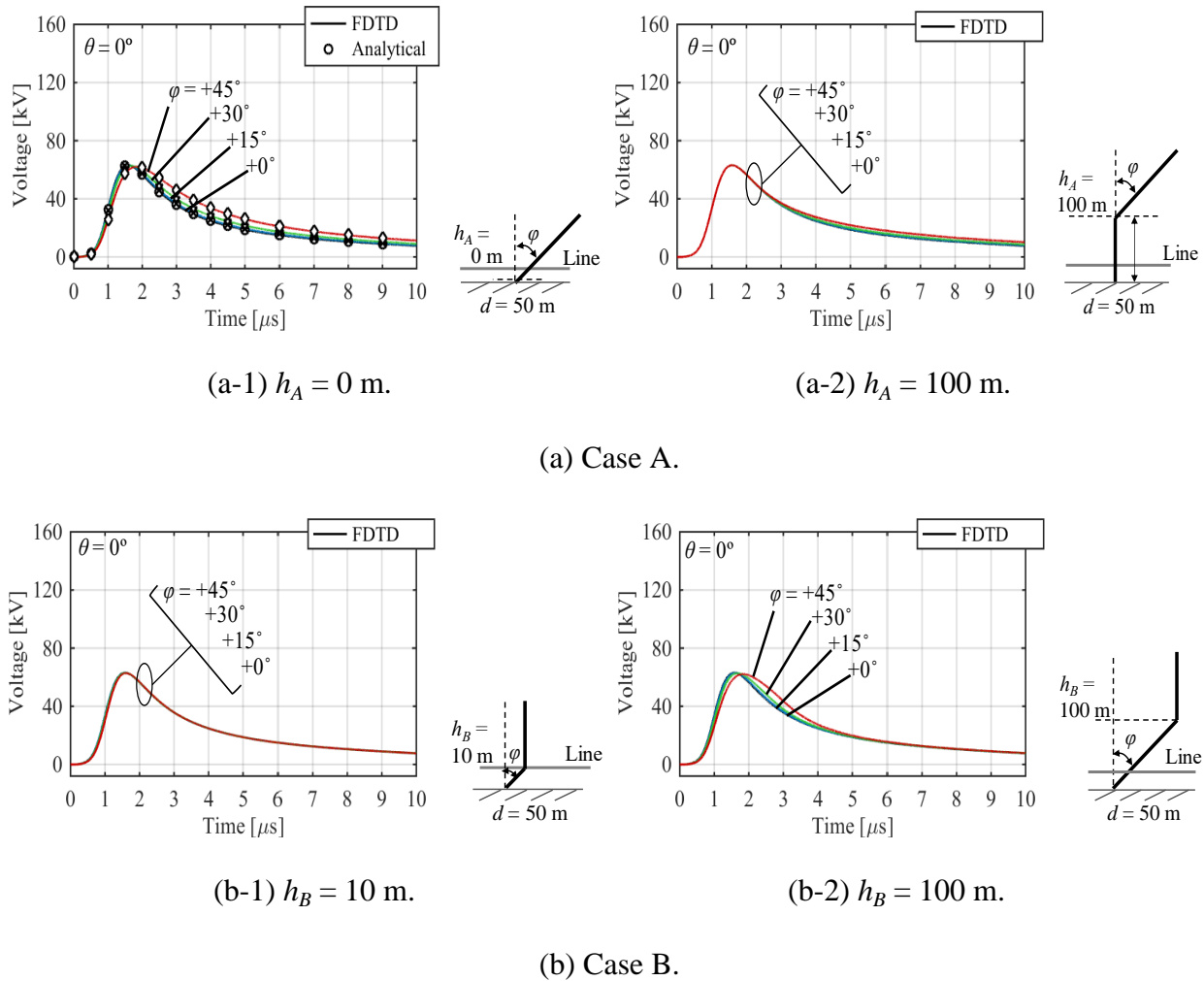


Figure 5.5 Lightning induced voltages on a single-conductor overhead line by bent lightning with various bent heights and inclined angles  $\varphi$ : Cases A and B,  $1/200 \mu\text{s}$ ,  $\rho_e = 0 \Omega\text{m}$ ,  $d = 50$  m,  $\theta = 0^\circ$ .

#### 5.1.2.4 Effect of earth resistivity

It is well-known that the induced voltage waveform is dependent on the earth resistivity (e.g., [44], [120]). The peak voltage becomes higher and the waveform becomes slightly wider as the resistivity increases. It may affect the dominant lightning-channel height to induce the peak voltage.

Figure 5.6 shows induced voltages in Case A for the angle  $\theta$  when the earth resistivity  $\rho_e$  is  $1000 \Omega\text{m}$ . The voltages increase because of the high resistivity. However, the influence of the bent height  $h_A$  is similar to the results of  $\rho_e = 0 \Omega\text{m}$  in Figure 5.3. The lightning channel geometry under 100-m altitude is still dominant for the peak voltage when the lossy earth is assumed.

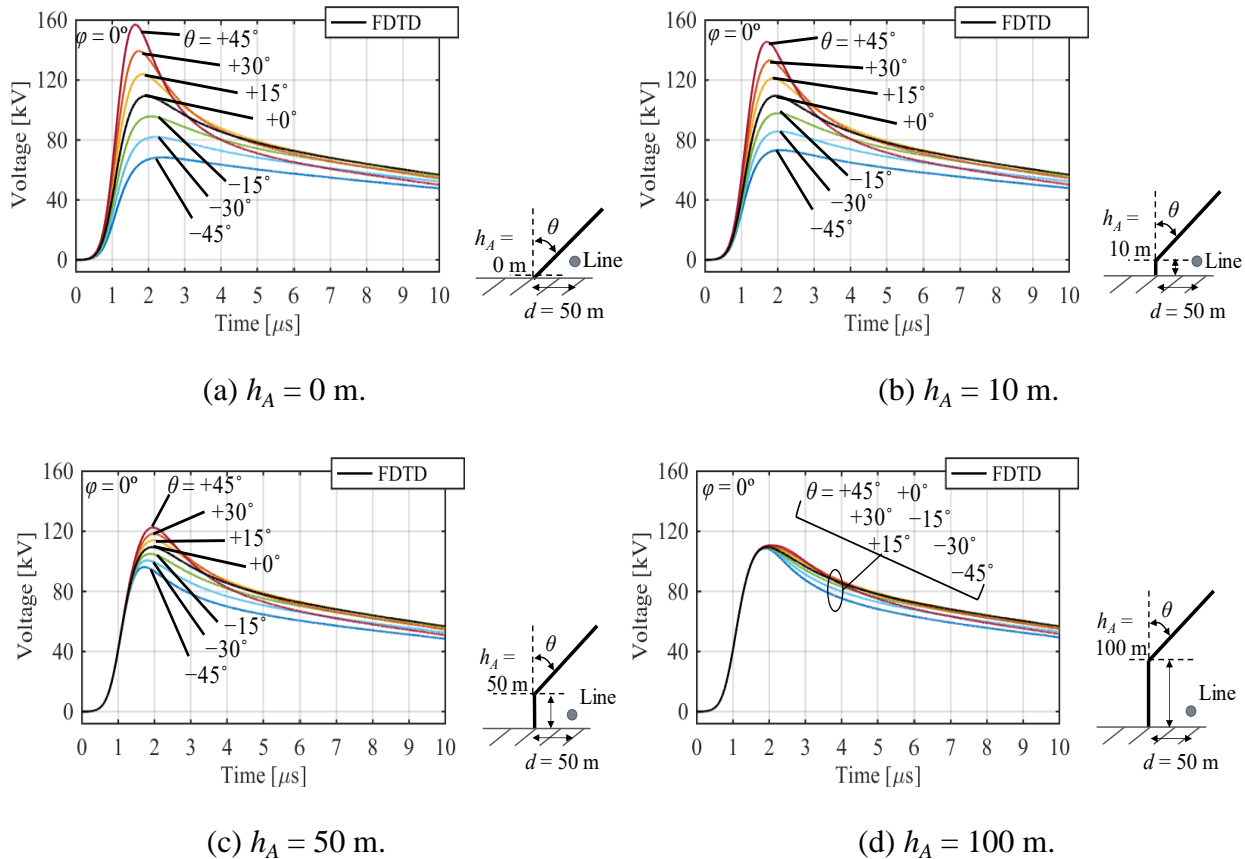
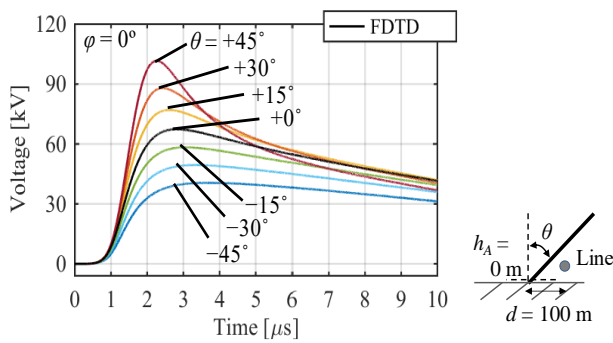
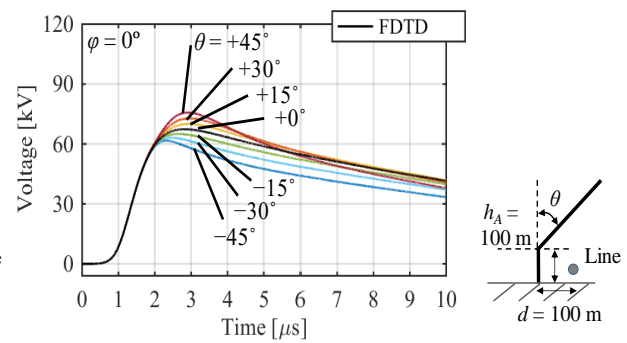
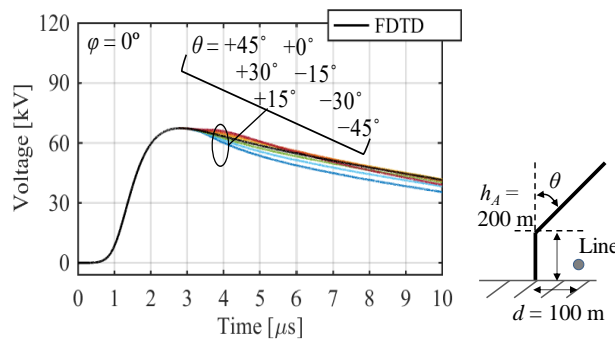


Figure 5.6 Lightning induced voltages on a single-conductor overhead line by bent lightning with various bent heights and inclined angles  $\theta$ : Case A,  $1/200 \mu\text{s}$ ,  $\rho_e = 1000 \Omega\text{m}$ ,  $d = 50 \text{ m}$ ,  $\varphi = 0^\circ$ .

### 5.1.2.5 Effect of lightning distance to the line

Figure 5.7 shows induced voltages in Case A for the angle  $\theta$  when the lightning becomes farther from the line ( $d = 100$  and  $300 \text{ m}$ ). The voltages decrease and the decay time increases compared to values obtained for  $d = 50 \text{ m}$  as is well understood. In addition, the voltages still differ from each

other when  $h_A = 100$  m. This means that the lightning channel geometry of over 100-m altitude is still significant for the peak voltage. The dominant height is estimated to be approximately 200 m for  $d = 100$  m and approximately 500 m for  $d = 300$  m because of their peak voltage position. The delay time from the voltage rise to the peak is approximately  $2 \mu\text{s}$  for  $d = 100$  m, and the time is equal to 200 m when the return stroke velocity is  $1 \times 10^8$  m/s. The delay time of  $5 \mu\text{s}$  for  $d = 300$  m corresponds to 500 m. The estimation can be confirmed with Figure 5.7 (a-3) and (b-3).

(a-1)  $h_A = 0$  m.(a-2)  $h_A = 100$  m.(a-3)  $h_A = 200$  m.(a)  $d = 100$  m

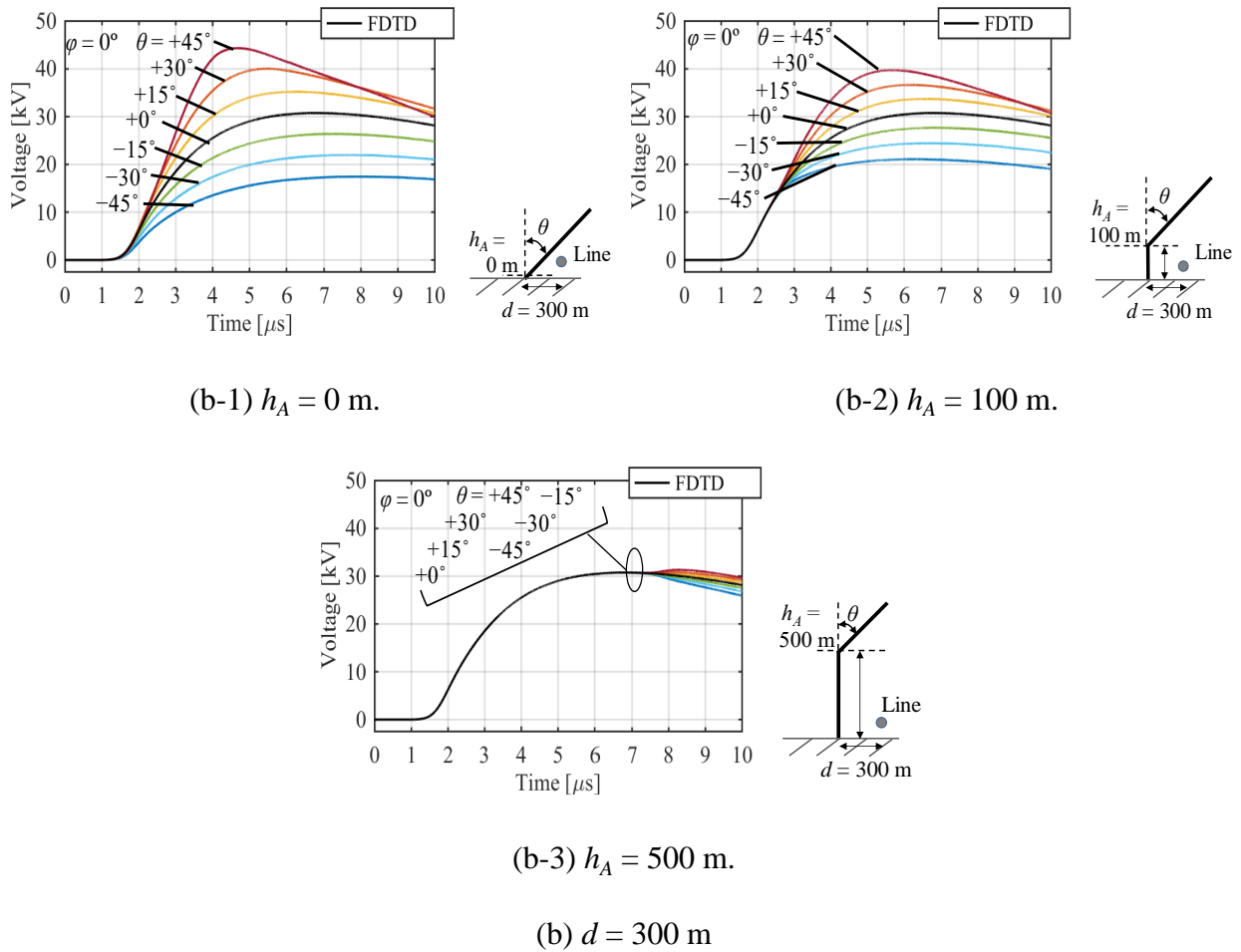


Figure 5.7 Lightning induced voltages on a single-conductor overhead line by bent lightning with various bent heights and inclined angles  $\theta$ : Case A,  $1/200 \mu\text{s}$ ,  $\rho_e = 1000 \Omega\text{m}$ ,  $d = 100$  and  $300$  m,  $\varphi = 0^\circ$ .

These results indicate that to evaluate the induced voltage with large  $d$ , the lightning channel geometry of higher altitude increases in its influence and should be considered in an induced-voltage evaluation. However, the peak voltage is decreased since  $d$  is large, and the evaluation itself becomes less significant.

### 5.1.2.6 Effect of return-stroke current waveform

Figure 5.8 shows induced voltages in Case A for the angle  $\theta$  when the return stroke current of  $5.5/200 \mu\text{s}$  is applied. Note that the time duration is extended to  $20 \mu\text{s}$  in the figure. The peak voltages still differ from each other when  $h_A = 100 \text{ m}$ , indicating the dominant height becomes higher than  $100 \text{ m}$  similarly to large  $d$ . The peak voltages finally converge when  $h_A = 500 \text{ m}$ .

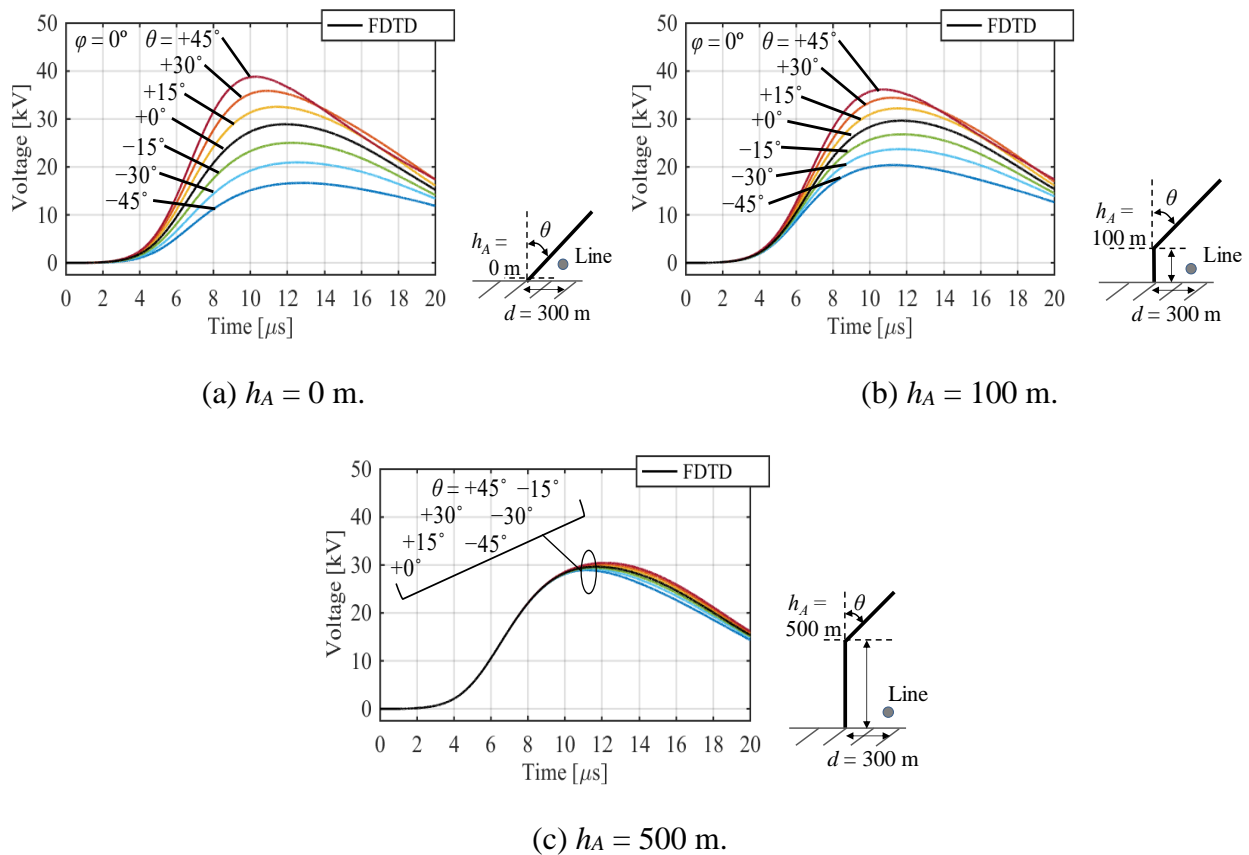


Figure 5.8 Lightning induced voltages on a single-conductor overhead line by bent lightning with various bent heights and inclined angles  $\theta$ : Case A,  $5.5/200 \mu\text{s}$ ,  $\rho_e = 1000 \Omega\text{m}$ ,  $d = 300 \text{ m}$ ,  $\varphi = 0^\circ$ .

## 5.2 Voltages by non-vertical lightning-like channel

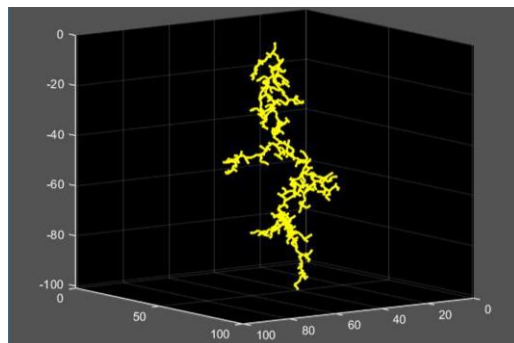
### 5.2.1 Computationally generated lightning-like channel

Many lightning photos have been taken and investigated in published papers (e.g., [44], [120]). Further, some papers investigate lightning induced voltages by using real or rocket-triggered lightning geometries in three-dimensional space which are reconstructed from photographs [138]-[140]. However, one difficulty is that lightning observations and experiments are expensive, and thus the information of the 3D lightning geometry is quite limited.

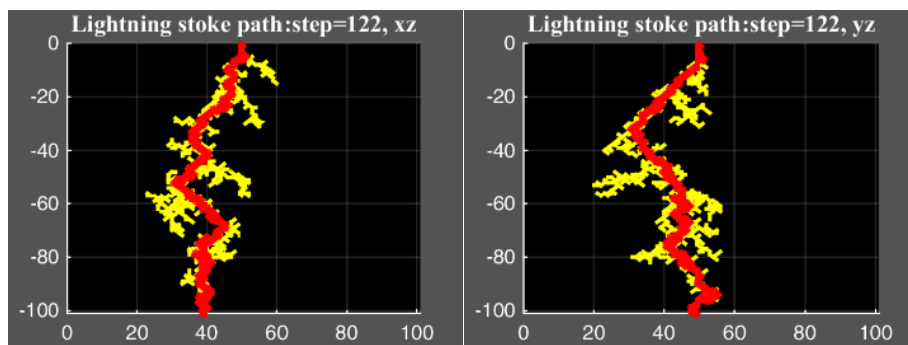
Another method to obtain the 3D lightning geometry is a probabilistic calculation based on an electric potential distribution [155], [156]. The similarity of the computed lightning channel to the real lightning channel is evaluated by fractal dimension. Even though the computed channel is not “lightning” but a “lightning-like” channel, it can represent the non-uniformity of the lightning channel geometry.

In this section, lightning leader paths (cloud to ground) are computationally generated by a probabilistic calculation and the return stroke path is exploited after the leader attaches to the ground. Then, the return stroke path is imported to FDTD computation to investigate the induced voltage.

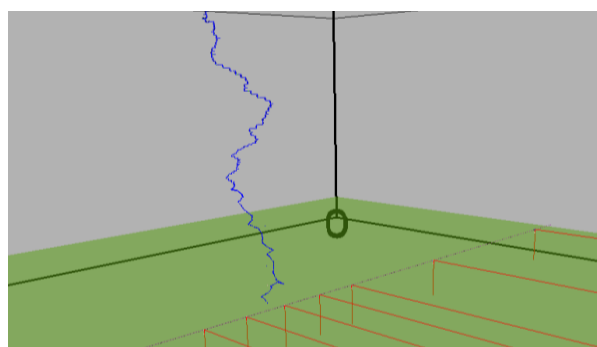
Figure 5.9 shows an example of the lightning channel generation. A working space of  $1000\text{ m} \times 1000\text{ m} \times 1000\text{ m}$  is composed of 10-m cubic cells. An initial electric-potential difference between the top and bottom boundaries (cloud and ground) is assumed, resulting in an electric field strength that has the same value at all the cells in the initial stage. Then, the lightning leader starts to grow from the center of the top boundary. The next cell, to which the leader progresses, is calculated probabilistically by the electric field strength around the leader path. After the leader grows into the next cell, the electric potential distribution and electric field strength are re-calculated. The procedure is performed iteratively until the leader attaches to the ground. The details of the probabilistic calculation are presented in [155], [156].



(a) Three-dimensional image (height = 1000 m).



(b)  $xz$  and  $yz$  plane images (height = 1000 m).



(c) Implementation in FDTD computation.

Figure 5.9 A lightning path generated by a probabilistic calculation based on an electric potential distribution [155], [156]. Yellow lines show lightning leaders which progress from cloud to ground, and a red line indicates a return stroke path after the leader attaches to the ground.

## 5.2.2 Induced voltage

Figure 5.10 shows a comparison of voltages induced by 1) the computationally-generated and 2) simply-inclined channels with different earth resistivity. The latter channel is same as  $h_A = 0$  m in Case A. Average angles of 1) in low altitude (between 0- and 100-m heights) are set to the inclined angles  $\theta$  and  $\varphi$  of 2), i.e.  $\theta = 11.5^\circ$  and  $\varphi = 0.5^\circ$  for the channel in Figure 5.9. The current waveform of  $1/200 \mu\text{s}$  and distance of  $d = 50$  m are adopted.

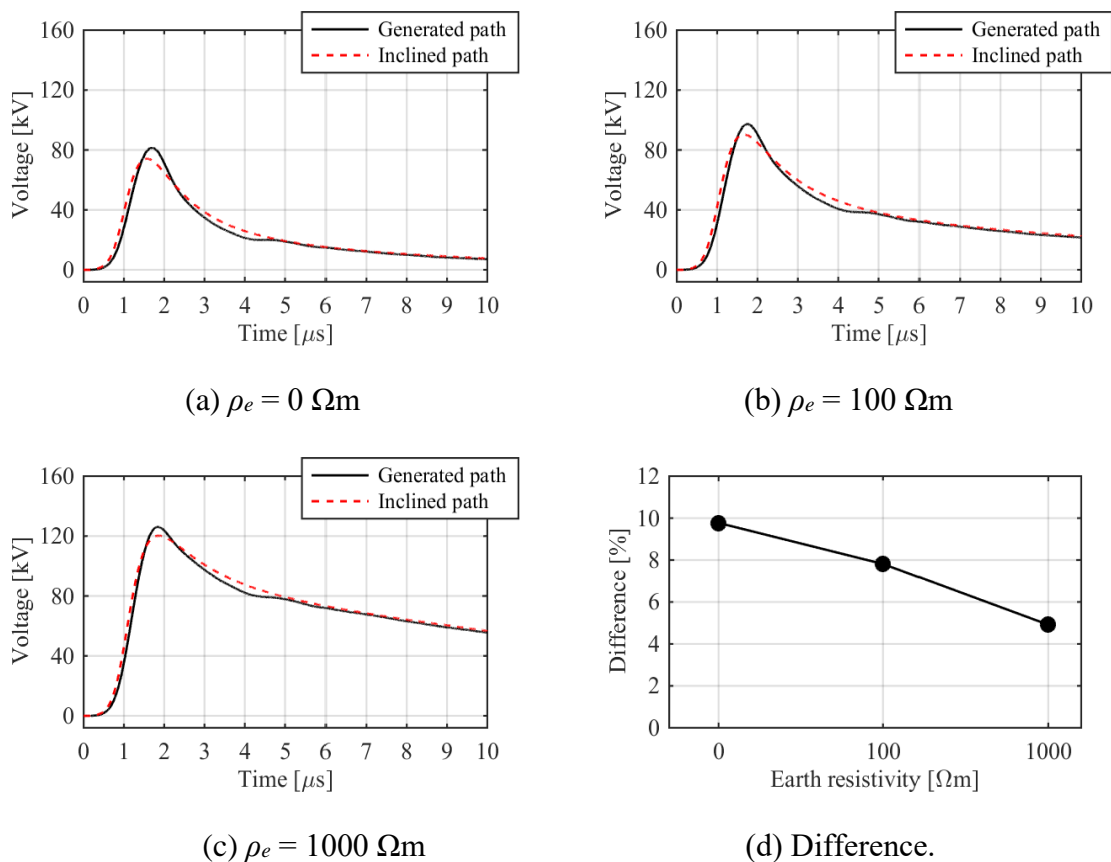


Figure 5.10 Lightning induced voltages on a single-conductor overhead line by 1) the computationally-generated and 2) simply-inclined lightning channels:  $1/200 \mu\text{s}$ ,  $d = 50$  m, inclined angles  $\theta = 11.5^\circ$ , and  $\varphi = 0.5^\circ$ .

In Figure 5.10 the voltages obtained by the generated channel agree well with those obtained by the inclined channels. The zig-zag channel geometry in the generated path does not significantly



affect the entire voltage waveform for all values of the earth resistivity. The difference of the peak voltages between the generated and inclined channels is less than 10 %, and it decreases as the earth resistivity increases. These results indicate that a realistic non-vertical lightning channel can be represented by a simply-inclined lightning path. The approximation becomes more reasonable with higher earth resistivity.

### 5.2.3 Incident electric field to the distribution line

To ensure the results of the induced voltage, electric fields radiated from the lightning channel to the line are also investigated. The incident electric field, especially the  $x$ -component (direction along the line), contributes to generate traveling voltages on the line which result in the induced voltage. Figure 5.11 shows examples of the incident electric field ( $x$ -component) when  $\rho_e = 100$  and  $1000 \Omega\text{m}$  at the line height. The fields are measured at  $x = +50$  m (50-m distance from the line center) because the  $x$ -component is nearly zero at  $x = 0$  m. In Figure 5.11, the electric field of the generated path shows fluctuations due to the zig-zag lightning path. It is clear that the field is influenced by the zig-zag lightning geometry. However, the influence becomes minor in the resultant induced voltage as observed in Figure 5.10, because the induced voltage is produced by the superposition of the traveling-wave voltages which are generated at every position on the line by the incident field. The superposition makes the resultant induced voltage waveform smoother.

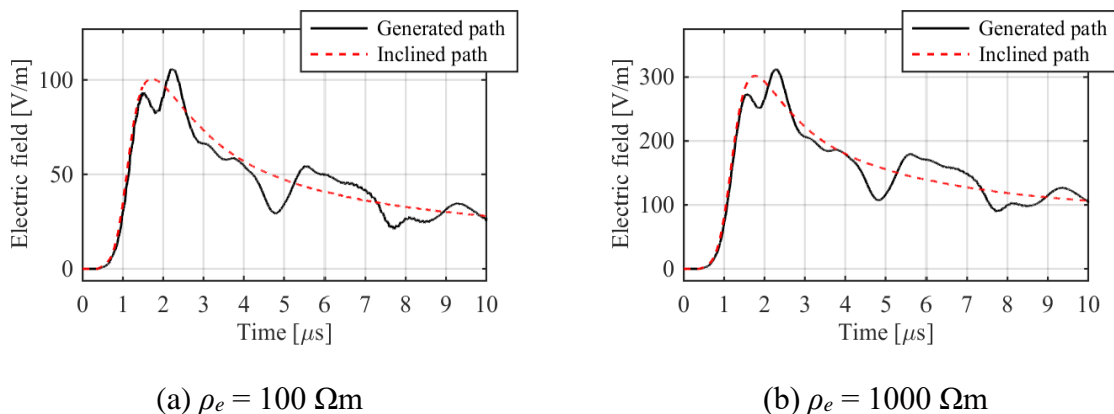


Figure 5.11 Incident electric field at  $h = 10$  m (the line height) and  $x = 50$  m (50-m distant from the line center) generated by 1) the computationally-generated and 2) simply-inclined lightning channels:  $1/200 \mu\text{s}$ ,  $d = 50$  m, inclined angles  $\theta = 11.5^\circ$ , and  $\varphi = 0.5^\circ$ .

### 5.3 Concluding remarks

The influences of non-vertical lightning on lightning-induced overvoltages have been investigated by FDTD computations by assuming “bent” and “computationally-generated” lightning channels. The following conclusions can be made:

- (1) The lightning channel geometry with an altitude below 100 m is dominant for the peak voltage evaluation when a severe condition of  $t_{d10-90}/t_n = 1/200 \mu\text{s}$ ,  $d = 50 \text{ m}$ , and  $\rho_e = 1000 \Omega\text{m}$  is assumed.
- (2) When the distance  $d$  becomes larger and rise time  $t_{d10-90}$  becomes slower, the induced voltage duration becomes larger and the dominant channel height becomes higher.
- (3) For a condition of  $1/200 \mu\text{s}$  and  $d = 50 \text{ m}$ , a realistic non-vertical lightning channel can be represented by a simple model of inclined lightning with average inclined angles below 100-m altitude.
- (4) The differences in peak voltages between the generated and inclined channels is less than 10 %, and decrease with increasing earth resistivity.

The importance of lightning channel geometry in low altitude is clearly demonstrated in this Chapter. In addition, the third remark endorses that the knowledge obtained in Chapter 3 and Chapter 4, where simply-inclined lightning is assumed in the investigations, can be used to represent realistic non-vertical lightning.

## CHAPTER 6      FUNDAMENTAL EARTH CURRENT BEHAVIOR AND RESULTING GROUND POTENTIAL RISE

There are a number of studies on lightning overvoltages due to lightning on transmission lines, distribution lines, and earth surface near the lines, because of the insulation design and coordination of the power transmission and distribution systems [12]-[17]. Also, many publications have investigated a ground potential rise (GPR) related to step and foot voltages for human safety [157]-[161]. When lightning strikes the earth surface near distribution lines, induced voltages to the phase wires have been a primary concern. Few papers have investigated distribution-line pole voltages generated by the GPR at the pole foot [6], [29] and the lightning current flowing into the pole through its grounding.

The study in this chapter focuses on revealing fundamental behavior of the lightning current flows into the earth. Distributions of the earth currents (density  $J$ ) and GPRs as a function of distance “ $r$ ” from the lightning channel base and depth “ $d$ ” from the earth surface, with a conducting pole with a grounding structure, are investigated. Measured results of the earth currents and GPRs [162] are presented, and FDTD computation results are compared with the measured results to validate the accuracy of the FDTD in Section 6.1. Distribution of the earth currents and GPRs due to lightning to the earth surface and to a vertical conductor are calculated by the FDTD, and the characteristics of the current and GPRs as functions of  $r$  and  $d$  are investigated in Section 6.2. When lightning strikes near a distribution line, a lightning current flowing into the grounding structure of a distribution pole is also calculated by the FDTD, and the effect of the earth currents and GPRs on the overall currents and voltages on the distribution line is investigated in Section 6.3. Concluding remarks are summarized in Section 6.4.

Note that a vertical lightning channel is modeled in the FDTD in Section 6.2 and 6.3 to consider its influence on the earth current behavior.

## 6.1 Experiment for impulse current applied to grounding electrode

### 6.1.1 Test circuit

#### 6.1.1.1 Experiment

In [162], results of experiments on the transient grounding resistance for tower footings conducted at the CRIEPI Akagi Testing Center are presented. A unique aspect of the experiments is that earth currents and voltages (GPRs) in the ground are measured as well as those of the tower-foot grounding electrode. It is observed that the current and GPR distributions/waveforms around the electrode are clearly influenced by the electrode structure.

Figure 6.1 (a) illustrates the test circuit to measure earth current density  $J$  and GPRs as a function of the distance  $(x, y, z)$  from a grounding electrode  $(x = 0, y = 0, z = 0 \text{ m})$  to which an impulse current in Figure 6.1 (b) is applied. The symbol “ $z$ ” indicates the depth from the earth surface. The electrode of 15 mm-radius and 30 m-length is inserted into a boring hole of 48 mm-radius, and the hole is filled with concrete to represent a steel-reinforced concrete structure. The impulse current generator (IG) is positioned at  $(x = 0, y = -200, z = 0 \text{ m})$  and is connected to the grounding electrode through a current lead wire at a height of  $h = 1.5 \text{ m}$  with a matching resistance of  $600 \Omega$ . GPR measuring circuits are also terminated by  $600 \Omega$ . The earth currents are measured at  $(x, y) = (2, 2 \text{ m}), (5, 5 \text{ m}),$  and  $(10, 10 \text{ m})$  at a depth of  $z = 0.5, 1.0,$  and  $1.5 \text{ m}$ .

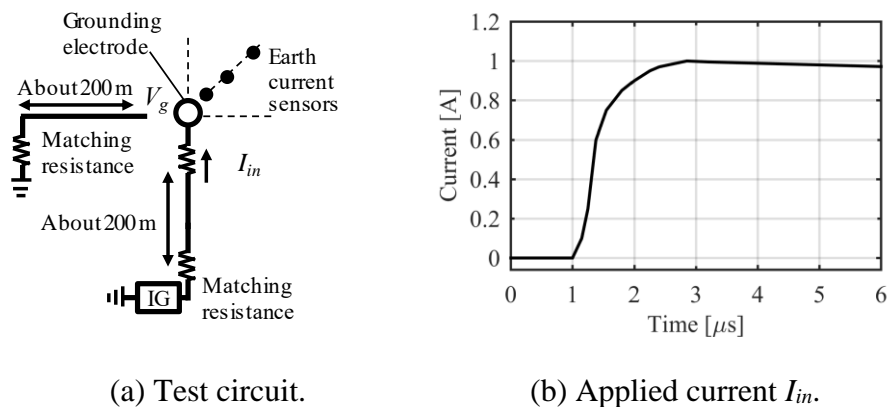


Figure 6.1 Test circuit of earth current and GPR measurements for a 30 m-length grounding electrode.

Earth current sensors (current transformers) are connected to oscilloscopes through matched-impedance amplifiers. The specifications of measuring devices are explained in [162]. Results of a soil boring test near the test yard indicate that the earth is, as an example, composed of the following three layers: (1)  $z = 0$  to 2.5 m, earth resistivity  $\rho_e = 100$  to 200  $\Omega\text{m}$ , (2)  $z = 2.5$  to 18 m,  $\rho_e = 1500$  to 1800  $\Omega\text{m}$ , and (3)  $z = 18$  to 40 m,  $\rho_e = 200$  to 500  $\Omega\text{m}$  [162].

### 6.1.1.2 FDTD modeling

Figure 6.2 illustrates the FDTD model circuit used to represent the experimental circuit [162]. The FDTD working space of  $300\text{ m} \times 300\text{ m} \times 110\text{ m}$  is composed of several cell lengths between 50 mm and 2 m. The minimum cell size is applied to a region of  $30\text{ m} \times 30\text{ m} \times 3\text{ m}$  including the current injecting point and all the earth-current measuring points. The measuring points at  $z = 0.5$ , 1.0, and 1.5 m are set at the distance of  $r = 2.8\text{ m}$ , 7.1 m, and 14.1 m in the  $y$ -direction from the injecting point, which represent the positions  $(x, y) = (2, 2\text{ m})$ ,  $(5, 5\text{ m})$ , and  $(10, 10\text{ m})$  in the test. The reason for converting  $(x, y)$  to  $(0, y)$  in the FDTD is to simplify the current/GPR computations by avoiding the Pythagorean Theorem calculation. The grounding electrode is modeled by a 15 mm-radius and 30 m-length rod covered by a dielectric (concrete,  $\rho = 100\text{ }\Omega\text{m}$ ). The dielectric has a square cross-section of  $100\text{ mm} \times 100\text{ mm}$  because the diameter of the concrete (boring hole) exceeds the minimum cell length of 50 mm. The working space is covered by Liao's absorbing boundary [107].

The earth depth is taken as 100 m. The earth structure is assumed as follows: (1) depth  $z = 0$  to 2.5 m, earth resistivity  $\rho_e = 150\text{ }\Omega\text{m}$ , (2)  $z = 2.5$  to 18 m,  $\rho_e = 1800\text{ }\Omega\text{m}$ , and (3)  $z = 18$  to 100 m,  $\rho_e = 100\text{ }\Omega\text{m}$ . The resistivity in the last layer is lower than the measured result but shows better agreement in a steady-state grounding-impedance measurement (8.4  $\Omega$  by FDTD and 7.9  $\Omega$  in [162]). The earth relative permittivity  $\epsilon_r$  is assumed to be 10. One FDTD computation for 6  $\mu\text{s}$  needs about 24 hours on a desktop computer, Core i7 2.8 GHz with 16 GB dual-channel memory. The required RAM is 4.8 GB for the computation. The calculation is optimized for multi-processing.

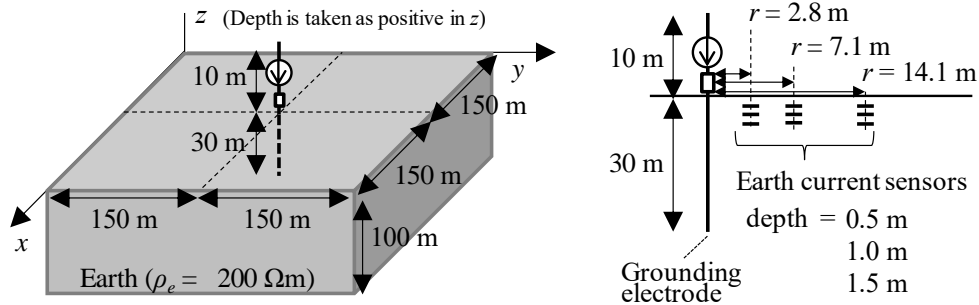


Figure 6.2 FDTD model circuit for earth current and GPR measurements.

### 6.1.2 Test and FDTD results

Figure 6.3 shows measured and FDTD computed earth currents ( $z = 1$  m) and GPRs. The FDTD results (solid lines) show a reasonable agreement with the measured results (dotted lines). Although the waveforms for  $z = 0.5$  and  $1.5$  m are not presented, they show nearly the same results to those in Figure 6.3.

One difference between the measured and FDTD results is the initial sharp peaks in the measured currents, which are not observed in the GPR waveforms. In general, electric field  $E$  in the earth and earth current density  $J$  have the following relation.

$$E = \rho_e J \quad (6.1)$$

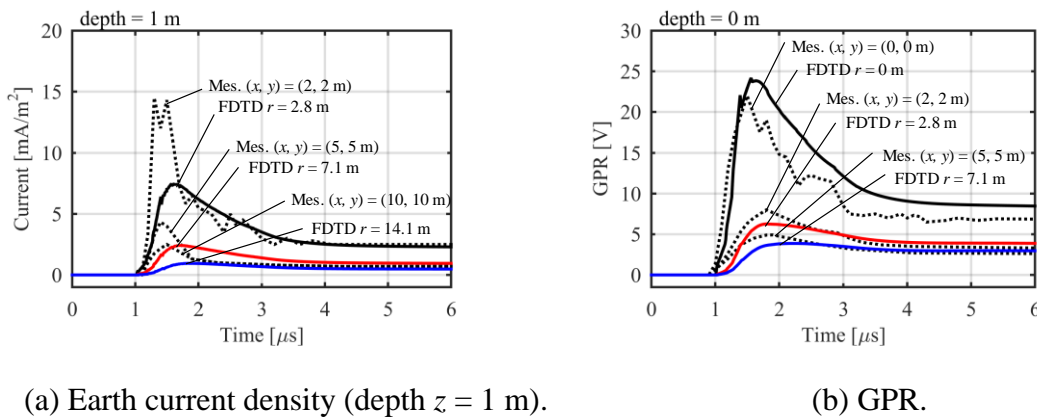
where  $J$  is earth current density [ $A/m^2$ ],  $E$  is electric field strength [ $V/m$ ], and  $\rho_e$  is earth resistivity (or current path resistivity) [ $\Omega m$ ].

Because GPR is obtained by the integral of  $E$ , the current and GPR waveforms are expected to be similar to those shown in the FDTD results if the current path resistivity is constant.

One possible cause of the difference is an error in the current measurement. Although impedance matching is considered, unintended reflection might occur in the circuit. Another possibility is that the measured current peaks involve a phenomenon with a transient lower-resistivity current path, for example, a transient current leakage from the injecting point through the concrete top-surface

to the earth. After  $2 \mu\text{s}$ , where the phenomena would become negligible, the FDTD current wave-tails agree well with the measured results in terms of the decays and steady-state values. If the earth current simply flows and distributes cylindrically from the electrode, considering the three earth layers, the steady-state current  $J$  is estimated to become 2.6, 1.0, and  $0.51 \text{ mA/m}^2$  for  $r = 2.8, 7.1,$  and  $14.1 \text{ m}$ , respectively. The results are in good agreement with the measured/FDTD results in Figure 6.3.

The above observation indicates that the FDTD can be used to calculate the earth currents and GPRs due to lightning, at least when the current path resistivity is assumed constant.



(a) Earth current density (depth  $z = 1 \text{ m}$ ).

(b) GPR.

Figure 6.3 Measured and FDTD computed results of earth currents and GPRs. Dotted lines show measured results in the test [22] and solid lines show FDTD computed results.

## 6.2 FDTD Computation for earth current and GPR

### 6.2.1 FDTD model circuit for the current and GPR computation

Figure 6.4 illustrates an FDTD model circuit for computing earth current density  $J$  and GPRs. A lightning channel of 400 m-height is placed at the center of a working space, of which the channel is represented by a series of small current sources known as a traveling-current-source model [56]. A normalized current of  $-1 \text{ A}$  (direction of injecting to the earth) with the waveform of  $t_{d10-90}/t_h = 1/80 \mu\text{s}$  is assumed. The return stroke velocity  $\beta$  (ratio to the light speed) is set to 0.33. The bottom

of the lightning channel is connected directly to the earth surface in Case A, and to a 10 m-height conducting pole with the grounding electrode of length “ $L$ ” in Case B. The radii of the electrode and the pole are 48 mm. The electrode length “ $L$ ” is varied from 0 to 30 m. Note that soil ionization is not considered in this study. The earth depth is taken as 100 m in the FDTD model circuit. The earth resistivity  $\rho_e$  is set to  $100 \Omega\text{m}$  with the relative permittivity  $\epsilon_r = 10$ . Earth current density  $J$  and GPR at various points from the lightning base to 30 m in both distance and depth are computed by FDTD. The direction of the earth current flowing from the lightning base to the boundary of the working space is considered as positive.

The FDTD working space of  $300 \text{ m} \times 300 \text{ m} \times 500 \text{ m}$  is composed of cells with 1, 2, and 4 m-length. The minimum cell size is applied to a region of  $70 \text{ m} \times 70 \text{ m} \times 100 \text{ m}$  including the lightning base and all the current/GPR measuring points. Note that GPRs of grid points (for example.  $r = 0, 1, 2 \dots$ ) and average currents between a grid point and the next adjacent (for example.  $r \approx 0.5, 1.5, 2.5 \dots$  for  $r = 0, 1, 2 \dots$ ) are used because of the nature of the FDTD [38]. Because current behavior near the earth surface and the resultant GPR are significant for equipment and structures on the ground, currents of the horizontal ( $y$ ) component are presented in figures in this section. The current of the  $x$  component is the same as the  $y$  component due to symmetry. The current of the  $z$  component is omitted in the figures. The working space is covered by Liao’s absorbing boundary. One FDTD computation needs 0.5 GB RAM and 30 minutes using the computer described in Section 6.1.

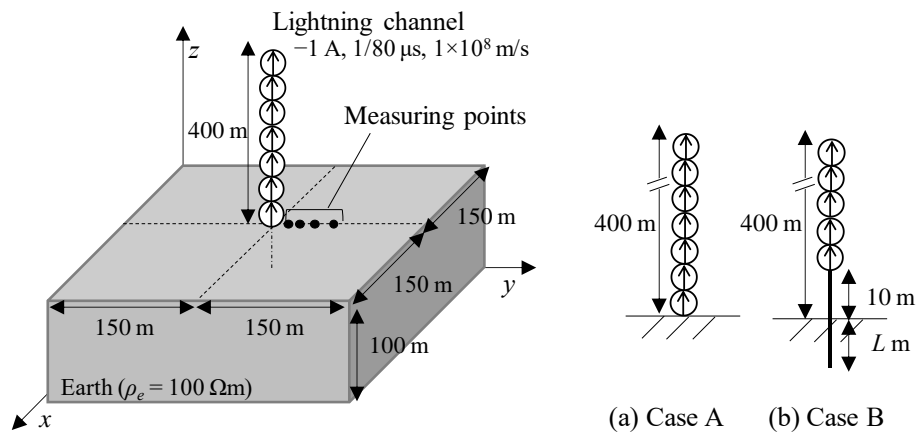


Figure 6.4 Model circuit for FDTD computation.



## 6.2.2 Difference between lightning to earth and conducting pole

Figure 6.5 shows FDTD computed results of earth-surface current density  $J$  at distance  $r$  from the lightning channel base for Cases A and B with  $L = 0$ . The red solid line shows the case of lightning to the earth surface (Case A) and the black dashed line is the case of lightning to a conducting pole (Case B:  $L = 0$ ). No significant difference is observed between the two cases.

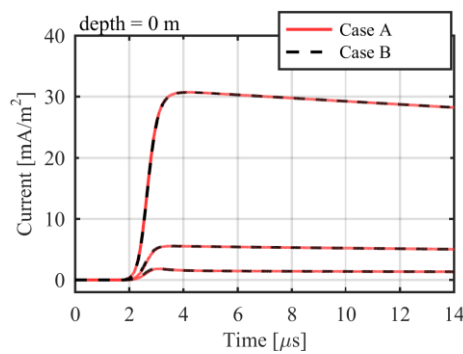


Figure 6.5 Earth-surface current density due to lightning to a ground and to a pole:  $L = 0$  m, current of y component.

Figure 6.6 shows GPRs for Cases A and B. As in Figure 6.5, no difference is observed. Thus, it is concluded that a lightning strike to a vertical conductor with no grounding electrode (Case B:  $L = 0$ ) can be represented by a direct strike to the earth surface (Case A). Note that this is only applicable when the conducting pole on the ground is short. If the pole is long, current/voltage reflections on the pole would occur and influences the current/GPR waveforms.

Electric field strength  $E$  [V/m] is also computed by FDTD, but  $E$  is proportional to current density  $J$  as in (6.1). For example,

$$\rho_e = 100 \Omega\text{m}: J = 30 \text{ mA/m}^2 \text{ at } r = 2 \text{ m}, E = 3 \text{ V/m}$$

The waveform of  $E$  is the same as that of  $J$  shown in Figure 6.5.

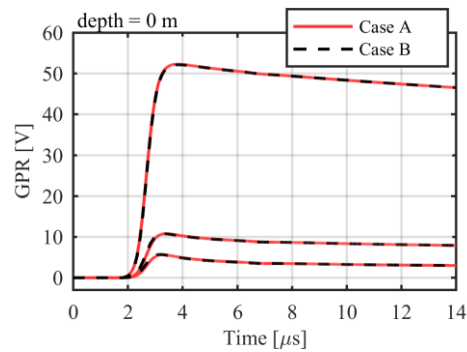
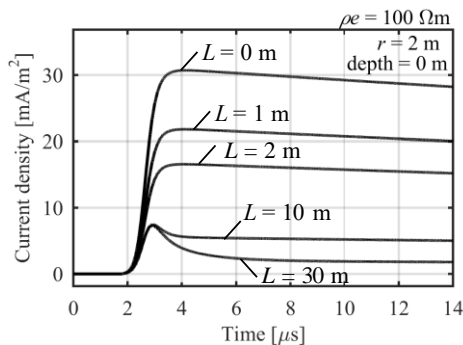


Figure 6.6 GPR at the earth surface due to lightning to a ground and to a pole:  $L = 0$  m.

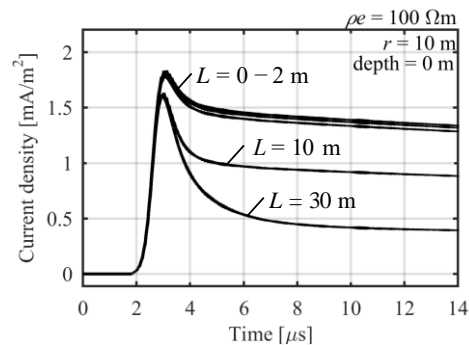
### 6.2.3 Influence of grounding electrode on earth current

Figure 6.7 shows the earth-surface current density  $J(x = 0, y = r, z = 0 \text{ m})$  at positions  $r = 2$  and  $10$  m for the grounding electrode length of  $L = 0, 1, 2, 10$  and  $30$  m. Figure 6.8 shows the peak values of the current density (y component) as a function of electrode length “ $L$ ”. Figure 6.8 (a) is the case for depth  $d = 0$  m and (b) is for  $d = 10$  m.

It is observed in Figure 6.7 (a) for  $r = 2$  m and  $d = 0$  m (earth surface) that  $J = 30.7 \text{ mA/m}^2$  flows out from the lightning channel onto the earth surface for  $L = 0$ , while  $21.8 \text{ mA/m}^2$  flows out with  $L = 1$  m, and only  $7.4 \text{ mA/m}^2$  for  $L = 10$  to  $30$  m. In the vicinity of the electrode ( $r = 2$  m), a large current density appears on the earth surface when the electrode is short, as is easily understood. However, the electrode length makes no significant difference to the peak current densities when  $r$  is  $10$  m or greater as can be observed in Figure 6.7 (b).



(a)  $r = 2$  m.



(b)  $r = 10$  m.

Figure 6.7 Current density  $J$  for various electrode lengths  $L$ : current of y component.

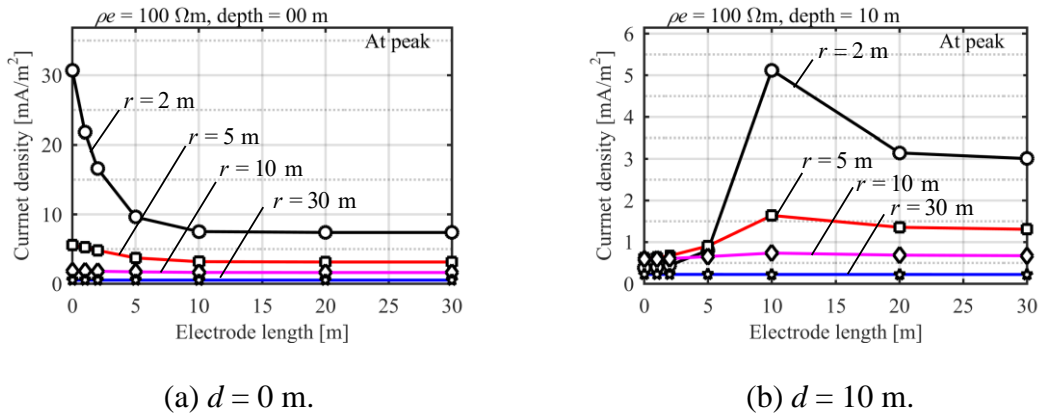


Figure 6.8 Peak earth current density as a function of electrode length  $L$ : current of  $y$  component.

The above characteristics of the earth current density  $J$  can be explained physically in the following manner. Since the earth is assumed to be homogeneous, a lightning current injected into the earth in Case A can be assumed to be distributed hemispherically in the earth. Then, the current density is approximated by the following equation [157], [158].

$$J_{hes} = I_0 / 2\pi R^2 \quad : \text{Case A} \quad (6.2)$$

where  $R^2 = r^2 + d^2$ ,  $r$  is horizontal distance [m],  $d$  is depth [m].

When lightning strikes a vertical conductor with a grounding electrode of length  $L$  (Case B), the equipotential electric field in the earth near the electrode becomes cylindrical, and thus the current density in the earth can be approximated in the following form [157], [158].

$$J_{cyl} = I_0 / 2\pi r L \quad : \text{Case B} \quad (6.3)$$

The above formulas give the following current density corresponding to Figure 6.8 with the lightning current of 1 A (step function).

Case A: formula (6.2)

$$d = 0 \text{ m}: \quad r = 2, 2.5, 5, 10 \text{ m} \Rightarrow J = 39.8, 25.5, 6.4, 1.7 \text{ mA/m}^2$$

Case B: formula (6.3)

$$L = 5 \text{ m}: \quad r = 2, 2.5, 5, 10 \text{ m} \Rightarrow J = 15.9, 12.7, 6.4, 3.2 \text{ mA/m}^2$$

$$L = 10 \text{ m}: \quad r = 2, 2.5, 5, 10 \text{ m} \Rightarrow J = 8.0, 6.4, 3.2, 1.6 \text{ mA/m}^2$$

The hemispherical electrode formula shows reasonable agreement with the FDTD results for Case A in Figure 6.8 (a). The formula for a cylindrical case, (6.3), gives a reasonable result in comparison with Figure 6.8 (a) for Case B, i.e.  $L \neq 0$  when  $L$  is equal to and greater than 5 m. When  $L$  is smaller than 5 m, the electric field within the earth cannot be uniform, and thus (6.3) is not applicable. It should be recalled that the formulas are intended for steady state assuming uniform electric field distribution in the earth.

Figure 6.8 (b) at the depth  $d = 10$  m shows an increasing characteristic of the peak current density up to  $L = 10$  m except  $r = 30$  m, contrary to the decreasing characteristic in Figure 6.8 (a) at the earth surface ( $d = 0$ ). When  $L$  is shorter than  $d = 10$  m, the current density in  $d = 10$  m becomes small because only the current injected near the earth surface flows into the depth. When  $L$  is equal to or greater than  $d = 10$  m, the current directly reaches the depth along the electrode and then flows into the earth according to (6.3). Thus, the current density suddenly increases at the critical depth “ $d = L$ ”, especially for a region near the electrode. The density then decreases for  $d < L$  because the injecting current density from the electrode into the earth decreases for longer  $L$  according to (6.3).

#### 6.2.4 Influence of grounding electrode on GPR

Figure 6.9 shows transient GPR waveforms at (a)  $r = 0$  and (b) 10 m. Figure 6.10 summarizes the peak GPR values as a function of electrode length “ $L$ ”. It is observed in Figure 6.9 (a) that GPR = 52 V at  $r = 0$  for  $L = 0$  (no grounding electrode) decreases to 34 V for  $L = 1$  m, and about 13 V for  $L = 10$  and 30 m. The observation indicates that the GPR due to lightning to the earth is much higher than that due to the lightning to a vertical conductor with a grounding electrode. If the electrode length is greater than 2 m, the GPR is decreased to less than a half as observed in Figure 6.9 (a) at  $r = 0$ . However, the GPR converges when  $L \geq 10$  m. This phenomenon corresponds to the so-called effective length of a horizontal grounding electrode which defines the electrode length giving a nearly minimum grounding resistance [158], [163]-[165]. Note that the GPR in Case B in Figure 6.9 (a) and Figure 6.10 (a) is the same as the grounding resistance of the vertical electrode for the lightning current peak being 1 A.

One interesting point is that the initial GPR peaks at  $r = 0$  m differ among  $L = 0$  to 10 m in Figure 6.9 (a) while they show convergence at  $r = 10$  m in Figure 6.9 (b). This means that even the GPR at the lightning striking point is significantly decreased by the grounding electrode of  $L = 0$  to 10 m, the GPR around the striking point is not effectively suppressed by the grounding, at least when a vertical electrode is assumed. This phenomenon could be explained by direct electromagnetic-field coupling between the lightning channel and earth, which will be discussed later.

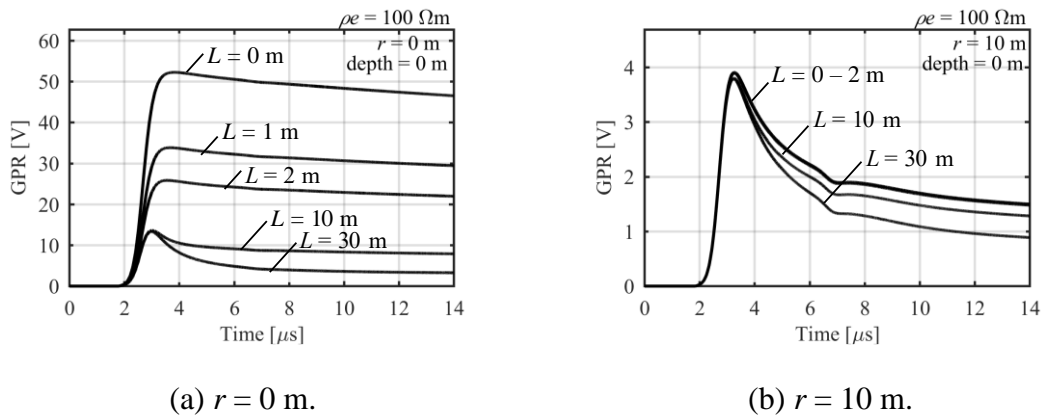


Figure 6.9 GPR waveforms with various electrode lengths  $L$ .

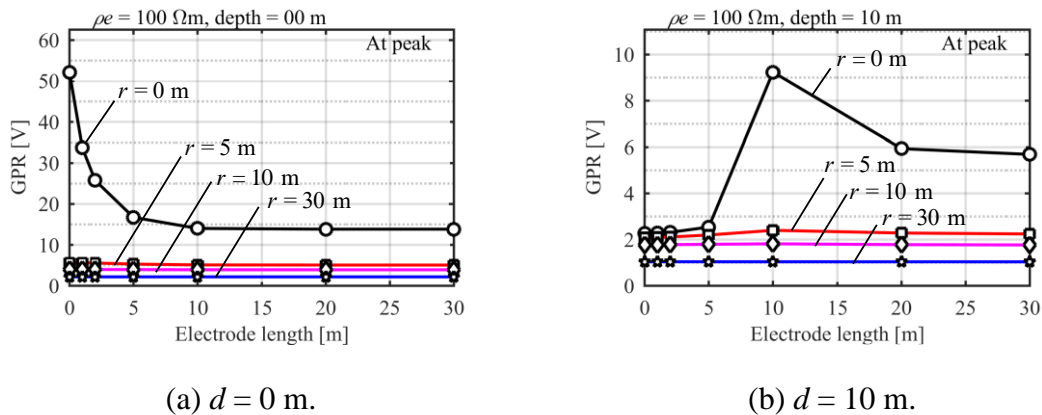


Figure 6.10 GPR peak values as a function of electrode length  $L$ .

Summarizing the results of the earth current and GPR, it is confirmed that the current is distributed hemispherically or cylindrically within the earth, as is easily understood based on electromagnetic theory. The FDTD computed results also clearly demonstrate the “effective length” phenomenon due to the conductor inductance. The effect of the grounding electrode on decreasing the GPR is only applicable on and near the grounding electrode (lightning striking point). In addition, in comparison with Figure 6.7 to Figure 6.10, the earth current and GPR show similar trends. Thus, observing either one of the current or GPR would be sufficient to investigate their characteristics.

## 6.2.5 Distribution of earth currents and GPR

### 6.2.5.1 Distance “ $r$ ” from lightning channel base

In this section, the results of the earth current are re-summarized as functions of the distance  $r$  from the lightning channel base and the earth depth  $d$  to confirm their distribution. The GPR results are not presented but confirmed to show a similar trend.

Figure 6.11 shows the peak current density  $J$  as a function of distance  $r$ . (a) is for Case A (lightning to the earth surface) and (b) to (d) are for Case B (lightning to a vertical conductor with a vertical grounding electrode of length  $L = 5, 10, \text{ and } 30 \text{ m}$ ). The dotted line in Figure 6.11 is calculated by the analytical formula of  $I_{hes}$  in (6.2), and the dashed line is the result of  $I_{cyl}$  in (6.3). It is observed in Figure 6.11 (a) that  $I_{hes}$  in (6.2) agrees well with the FDTD computed results at  $d = 0$ , as discussed in the previous sections. The lightning to the earth surface can be represented by the current applied to a hemisphere electrode as per the approach adopted by Sunde [158].  $I_{cyl}$  in (6.3) agrees with the FDTD results at  $d = 0$  for  $L = 10 \text{ m}$ . When  $r$  becomes large, no significant difference is observed in (a)-(d) because the influence of the electrode length becomes minor and the current distribution becomes  $I_{hes}$  in (6.2).

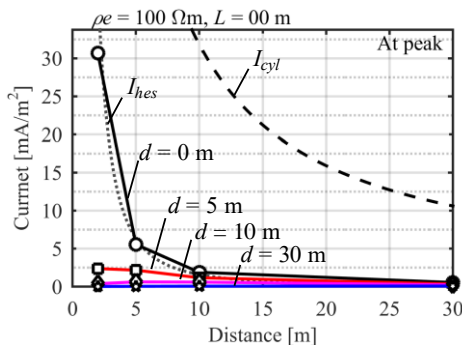
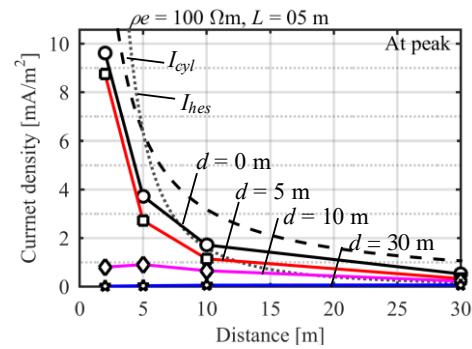
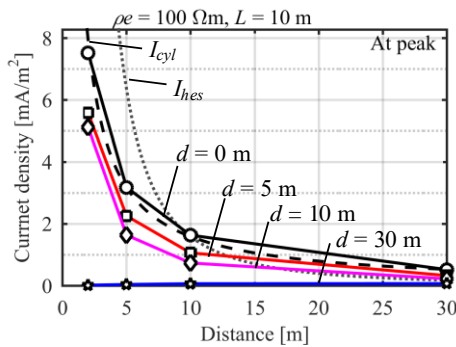
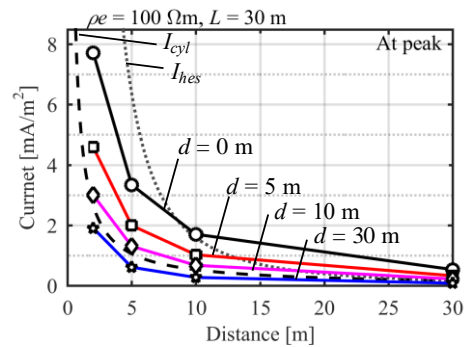
Case A ( $L = 0\text{ m}$ ).(b) Case B:  $L = 5\text{ m}$ .(c) Case B:  $L = 10\text{ m}$ .(d) Case B:  $L = 30\text{ m}$ .

Figure 6.11 Current density peaks as a function of distance  $r$  from the source: current of  $y$  component.

### 6.2.5.2 Depth “ $d$ ” from earth surface

Figure 6.12 shows the peak values of the earth current density  $J$  as a function of depth  $d$ . (a) is for Case A, and (b) to (d) are for Case B with  $L = 5, 10, 30\text{ m}$ . In Case A, Figure 6.12 (a), the current decreases as depth  $d$  increases, roughly proportional to “ $1/d$ ” to “ $1/d^2$ ”, similarly to those in Figure 6.11 (a). In Case B, Figure 6.12 (b), the existence of a vertical grounding rod of length  $L$  influences the current, because a large portion of the lightning current flows into the electrode rather than into the soil, in contrast to Case A. For example, in Figure 6.12 (b), the current at  $r = 2$  keeps its value for the depth up to  $d = 5\text{ m}$  because of the electrode length being  $L = 5\text{ m}$ . At the depth greater than  $d = 5\text{ m}$ , the current decreases rapidly for  $d$  greater than  $L$ . For  $r \geq 5\text{ m}$ , the current shows a smooth decreasing characteristic as a function of  $d$ , and no significant difference of the current for various  $L$  is observed.

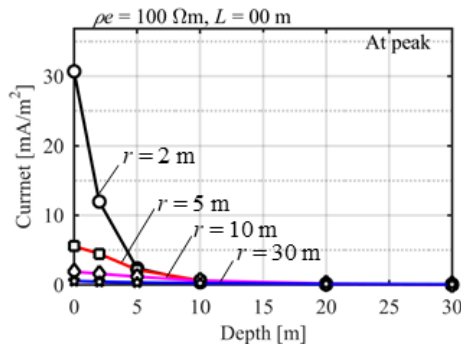
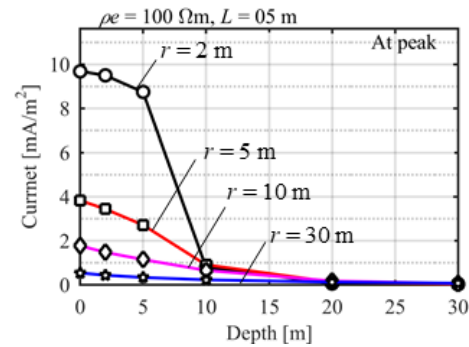
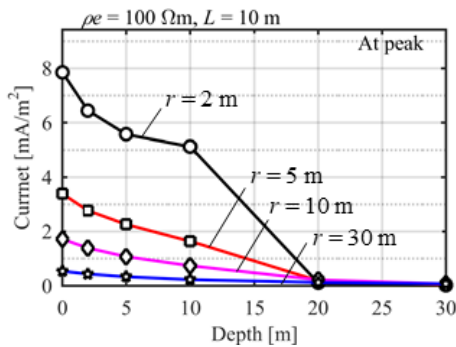
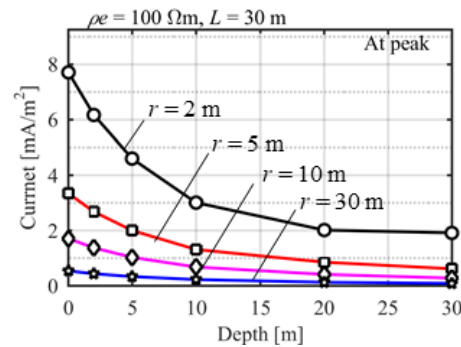
Case A ( $L = 0$  m).(b) Case B:  $L = 5$  m.(c) Case B:  $L = 10$  m.(d) Case B:  $L = 30$  m.

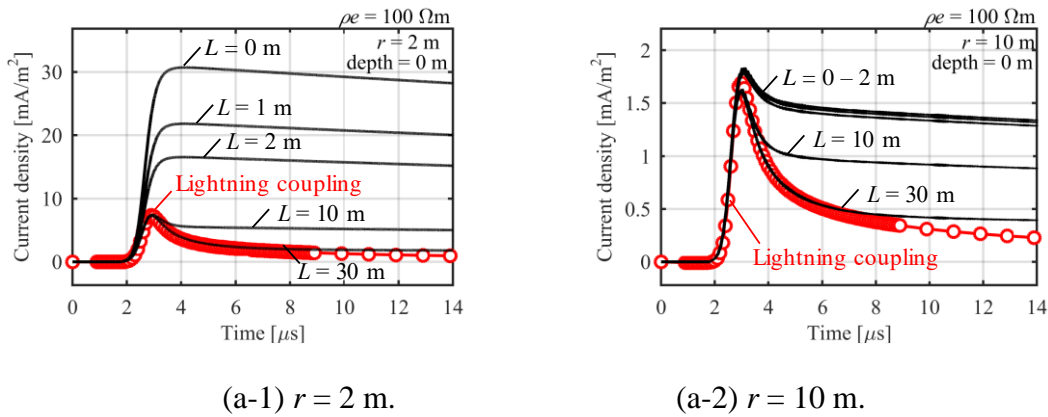
Figure 6.12 Current density peaks as a function of depth  $d$  from the earth surface: current of  $y$  component.

## 6.2.6 Influence of coupling between the lightning and earth

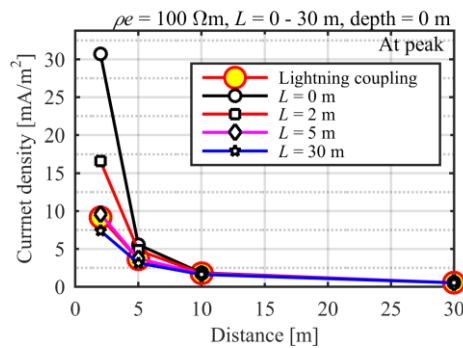
In Figure 6.7 (b) and Figure 6.9 (b), the current and GPR peaks for various electrode lengths  $L$  show almost the same values. This suggests that only the earth-surface or above-ground phenomenon causes the peaks. One possibility is direct electromagnetic coupling between the lightning channel and the earth surface. The lightning radiates an electromagnetic field which causes lightning induced overvoltages on distribution lines as is well known. The electromagnetic field also reaches the earth surface and would influence the current behavior.



An approach to calculate the electromagnetic field radiated from the lightning is explained in [65], [67]. Firstly, the electric field at an arbitrary point of height  $h$  and distance  $r$  is calculated with an assumption of perfectly conducting earth ( $\rho_e = 0 \Omega\text{m}$ ). Then, the Cooray-Rubinstein formula is applied to consider the influence of lossy earth on the electric field. Details are presented in [65], [67]. Finally, the obtained electric field is converted to the current density by (6.1).



(a) Current density waveforms at the earth surface: current of  $y$  component.



(b) Current density peaks as a function of distance  $r$  from the source: current of  $y$  component.

Figure 6.13 Influence of the lightning-to-earth electromagnetic coupling on the earth surface current. The electromagnetic field from the lightning channel to the earth surface is calculated by the Cooray-Rubinstein formula explained in [65], [67], and the current density is calculated by (6.1).

Figure 6.13 shows the influences of the lightning-to-earth electromagnetic coupling on the earth surface current. In Figure 6.13 (a), the current induced by the electric field coupling to the earth agrees well with the initial current peaks observed in FDTD results for large  $L$ . When  $L$  is less than 10 m, conducting current from the grounding electrode into the earth becomes more dominant, and the waveforms become different from the coupling current.

Figure 6.13 (b) shows peak values of the current densities as a function of the distance  $r$ . When  $r$  is less than 5 m, the peak values for small  $L$  differ from that for the coupling current. However, the peak values almost converge at  $r = 10$  m. This indicates that the lightning-to-earth coupling current becomes dominant for the peak value of the earth surface current when  $r$  is greater than 10 m. GPR results also show the same trend as in Figure 6.9. Thus, it is suggested that considering the lightning-to-earth coupling effect is important for more accurate GPR and earth-surface current investigations.

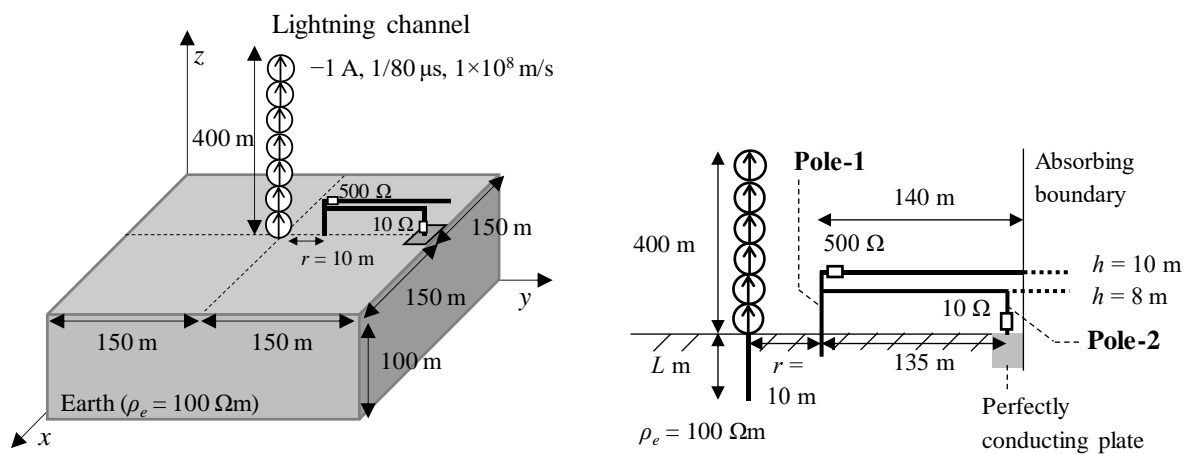
### 6.3 Effect of distribution line

There are a number of papers investigating lightning induced voltages to distribution lines, but only a few papers investigate transient voltages and currents on the lines due to nearby lightning [6], [29]. When lightning strikes the earth near the distribution line, the transients on the line involve both the lightning induced voltages and transient voltages caused by a portion of the lightning current flowing into the line through the distribution-line pole groundings [29] due to GPR. In this section, the current flowing into the distribution line through its grounding and the resultant voltages are investigated considering various grounding structures of the pole.

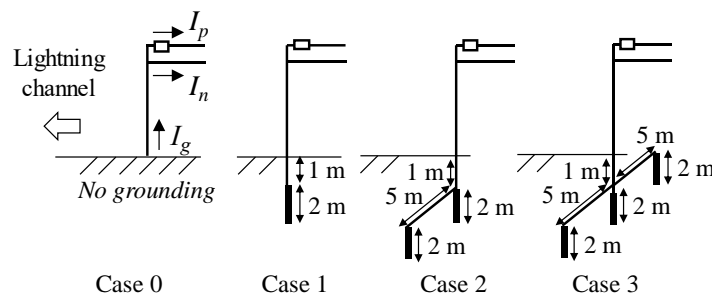
#### 6.3.1 Model circuit

Figure 6.14 (a) illustrates a model circuit for FDTD computations, similar to the model in Figure 6.4. Lightning strikes a structure of which the distance from the nearest distribution pole (Pole-1) is  $r = 10$  m. Note that the lightning-struck structure on the ground is not modeled because no significant difference is observed when the structure height is low. In reality, the lightning could strike, for example, another pole, tower, building or wind turbine near the distribution line.

The distribution line is composed of a phase wire and a neutral wire having horizontal lengths of 140 and 135 m, respectively. The phase wire is terminated by  $500 \Omega$  at Pole-1 and is connected to the absorbing boundary at the other end. The neutral wire is terminated by a grounding resistance of  $10 \Omega$  at a remote pole (Pole-2). The height of the phase wire is 10 m, and that of the neutral wire is 8 m. The structures of Pole-1 grounding are illustrated in Figure 6.14 (b). Case 0 involves no grounding structure (ideal case). Case 1 is a single vertical rod of 2 m with a grounding lead of 1 m. Case 3 has three vertical rods with a 10-m horizontal lead. Table 6.1 gives FDTD computed grounding resistances of the cases.



(a) Model circuit.



(b) Pole-1 groundings.

Figure 6.14 Model circuit for an investigation of a distribution line.

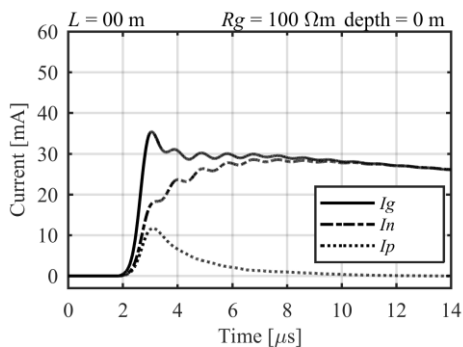
Table 6.1 Grounding resistance

	Case 0	Case 1	Case 2	Case 3
Resistance $\Omega$	51.7	24.9	12.1	8.9

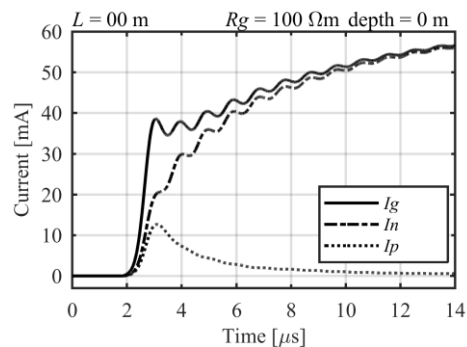
### 6.3.2 Transient current and voltage

In the FDTD simulation, Pole-1 grounding current  $I_g$ , neutral wire current  $I_n$ , and phase wire current  $I_p$  are measured as indicated in Figure 6.14 (b).

Figure 6.15 shows  $I_g$ ,  $I_n$ , and  $I_p$  for Case 0 (ideal case) and Case 3 in Figure 6.14 (b) of which the grounding resistance is  $8.9 \Omega$  as in Table I. It is clear that  $I_g$  and  $I_n$  in Case 3 are greater than those in Case 0 especially over a longer time period. The results indicate that a portion of the lightning current flows into the pole grounding structure of the distribution line. For example,  $I_g = 27$  mA at  $t = 14 \mu\text{s}$  in Case 0 while it reaches 56 mA, more than double, in Case 3. The difference of 29 mA is the portion of the lightning current flowing into the distribution line through the Pole-1 grounding.



(a) Case 0.



(b) Case 3.

Figure 6.15 Currents flowing through a pole grounding ( $I_g$ ), a neutral wire ( $I_n$ ) and a phase wire ( $I_p$ ) for  $L = 0$  m.

Figure 6.16 shows transient GPR waveforms at Pole-1 foot ( $r = 10$  m,  $d = 0$  m) of the distribution line in Figure 6.14 (a) for various pole grounding structures in Figure 6.14 (b). It is observed that the smaller the pole grounding resistance in Table 6.1, the higher the peak GPR, similarly to the higher currents  $I_g$  and  $I_n$  in Figure 6.15 (b). It should be noted that the GPR, which is about 4 V in the case of no distribution line in Figure 6.9 (b), is higher than in the case of the distribution line in Figure 6.16.

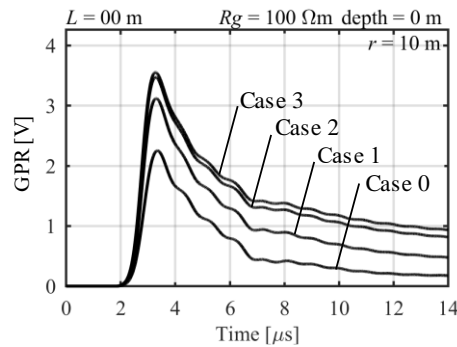


Figure 6.16 Transient GPR waveforms at Pole-1 foot ( $r = 10$ ,  $d = 0$ ) for various grounding structures of Pole 1:  $L = 0$  m.

Figure 6.17 (a) illustrates a map of nodes at which the current density  $J_s$  is calculated, and (b) shows the peak value of the density in the case of no distribution line and the case of the distribution line with Pole-1 grounding of Case 3 in Figure 6.14 (b). It should be recalled that  $J_s$  in the case of no line is independent of the node if the distance “ $r$ ” to the node is the same. It is observed that  $J_s$  in the  $+y$  direction with the line is larger than the others including the case without the line. The result indicates that more current flows in the direction of the distribution line. In other words, a distribution line absorbs lightning current. The phenomenon is clearly observed in Figure 6.18 (a) is for the case of no distribution line, where the current distribution is homogeneous and proportional to  $1/r^2$  from the base following the relation given in (6.2). (b) is for the case of the distribution line. It is observed that the current density becomes higher just in front of Pole-1 of the distribution line. When a perfectly conducting earth ( $\rho_e = 0$   $\Omega$ m) is assumed, the distribution of the

current density is almost independent of the distribution line, and becomes nearly the same as that shown in Figure 6.18 (a). The observation indicates that the earth resistivity should be considered in the simulation of transients on a distribution line due to nearby lightning so that the current flowing into the pole grounding structure and the induced voltage are accurately simulated. In addition, it is suggested that, although lower grounding resistance is generally better to mitigate lightning disturbances, the low-resistivity grounding absorbs more nearby lightning current which may cause surge-current troubles in distribution networks.

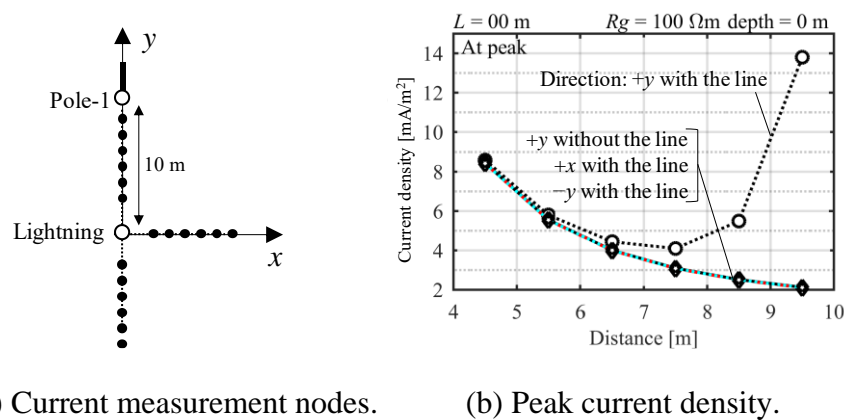


Figure 6.17 Earth-surface current distribution for Case 3 with and without Pole-1 as a function of distance from the lightning base.

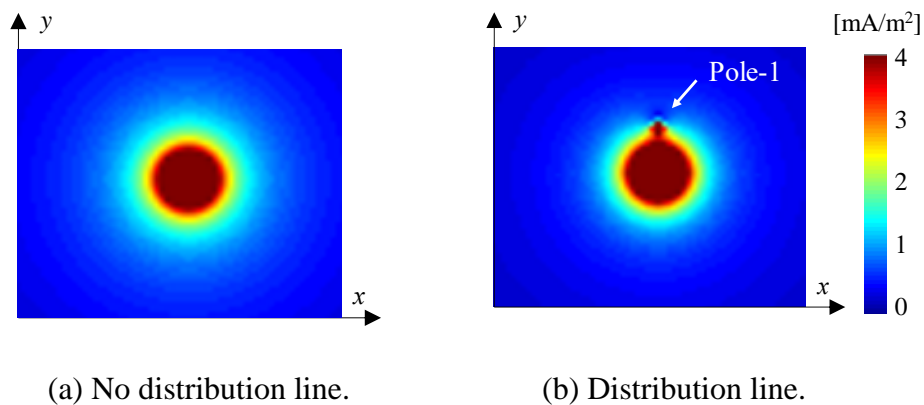


Figure 6.18 Distribution of earth surface current density  $J_s$  in  $x$ - $y$  plane at  $t = 3.6 \mu\text{s}$ : lightning channel base ( $x = 0 \text{ m}$ ,  $y = 0 \text{ m}$ ), Pole-1 of the distribution line ( $x = 0 \text{ m}$ ,  $y = 10 \text{ m}$ );  $\rho_e = 100 \Omega\text{m}$ .

Figure 6.19 shows the peak values of currents  $I_g$ ,  $I_n$  and  $I_p$  at Pole-1 and GPR at the pole foot for various grounding resistances in Table I. It is clear that the lower the grounding resistance, the higher the currents  $I_g$  and  $I_n$ , and GPR.

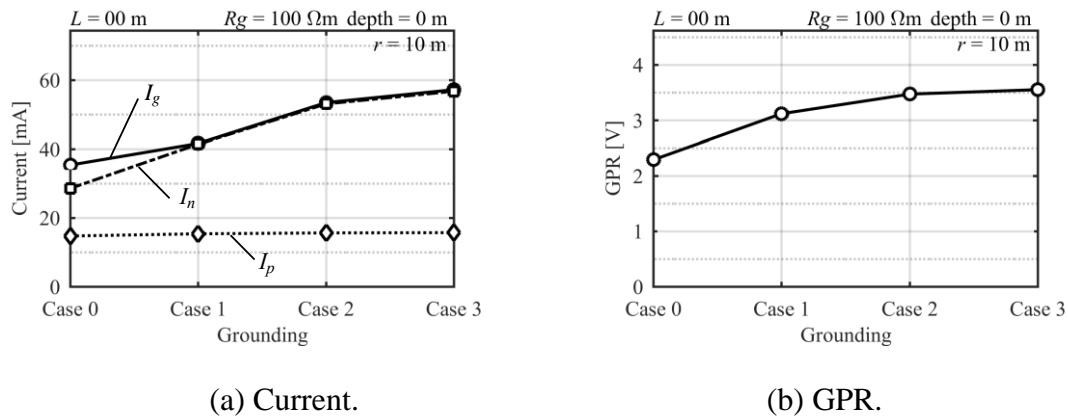


Figure 6.19 GPR peak values of current and GPR at Pole 1:  $L = 0\text{ m}$ .

Figure 6.20 shows the effect of the grounding electrode length “ $L$ ” on the current  $I_g$  at Pole-1.  $I_g$  becomes smaller as length  $L$  becomes larger, because less current flows near the earth surface when the lengths are larger, as already explained in Section 6.2.3.

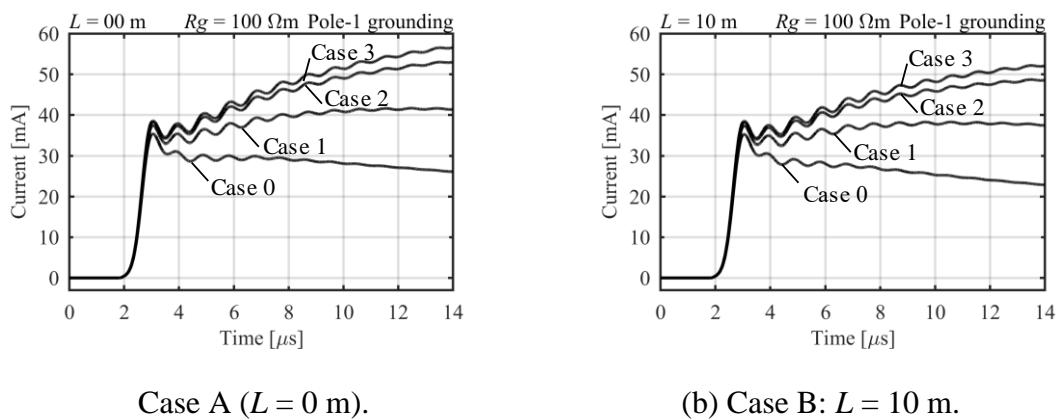


Figure 6.20 Grounding current ( $I_g$ ) waveforms for various electrode length  $L$ .

## 6.4 Concluding remarks

This chapter has investigated the distribution of earth current density  $J$  and GPR due to lightning to the earth surface and to a vertical conductor with a grounding electrode based on measured results and FDTD computations. The following conclusions can be drawn from the investigations.

- (1) FDTD computed results agree reasonably well with measured GPR results. For the current density, larger initial peaks are observed in the measured results while wave-tails show good agreement. Although the initial transient phenomenon requires further study, it is confirmed by comparison with measured results that FDTD can be used to calculate the earth currents and GPRs due to lightning.
- (2) A large portion of the current flows on the earth surface and the remaining portion flows into the earth during a transient period. The current density is approximately proportional to  $1/r^2$  ( $r$ : distance from the lightning base) for the lightning to the earth surface, and  $1/rL$  for the lightning to a vertical conductor with a grounding electrode of length  $L$ .
- (3) Lightning-to-earth electromagnetic coupling influences the initial peaks of the earth surface current. The coupling current becomes more dominant on the current peak when distance  $r$  is greater than 10 m. Consideration of the coupling effect is important for more accurate GPR and earth-surface current investigations.
- (4) When there is a distribution line near the lightning position, a portion of the lightning current is absorbed by the pole grounding structure of the distribution line because of the lower resistivity. Thus, the current density becomes higher toward the distribution pole. It is demonstrated that a low-resistivity grounding absorbs more nearby lightning current, which may cause surge-current troubles in distribution networks.

The fundamental characteristics of the earth current and resulting GPR are revealed. The current distributes hemispherically or cylindrically according to the grounding structure of the lightning-struck object. One important point is that the lightning-to-earth coupling is dominant in inducing the peak earth surface current/GPR. This knowledge can explain the result that the earth surface current and GPR are dependent on the lightning inclination as investigated in Section 3.3.



## **CHAPTER 7      NEARBY LIGHTNING SURGES FLOWING INTO A DISTRIBUTION LINE VIA GROUNDINGS**

The study in the previous chapter reveals the influence of the distribution line groundings on the earth current behavior. In particular, when there is a distribution line near a lightning-struck point, the lightning current is absorbed by the distribution line through its groundings. The current flowing into the line may cause a lightning-current surge problem and may also influence the lightning induced overvoltage.

Several publications are found in the field of lightning induced overvoltages and grounding problems (e.g., [12]-[34]). However, there are only a few publications reporting measured results of transient induced currents/voltages flowing through groundings to distribution lines due to lightning striking nearby ground [6], [29]. In the literature related to the latter reference, measured results of lightning currents flowing into distribution lines due to rocket-triggered lightning are reported in [29] to [32].

The study in this chapter investigates lightning surges on a distribution line reported in [29]. In Section 7.1, FDTD computation results are compared with the test results of [29] to validate the accuracy of the FDTD approach. In Section 7.2, various branch currents and node voltages which were not measured in the test [29] are calculated by FDTD, and the transient current distribution and voltage characteristics are investigated. Then, the effect of the lightning position to the line is studied. Transient currents and voltages are calculated when the lightning channel is inclined but not vertical, and the influence of an inclined lightning channel is analyzed. Further, the effects of pole grounding and neutral wire configuration are investigated. In Section 7.3, an EMTP simulation is performed and the simulation results are compared with measurements [29] and FDTD results.

## 7.1 Experimental circuit

### 7.1.1 Test circuit

Reference [29] has performed transient current measurements from rocket-triggered lightning on a 15-pole distribution line illustrated in Figure 7.1 (a). Phase and neutral wires on the line are in vertical arrangement. Because the heights of conductors are not presented in [29]-[32], three-phase wires (phase-a, b, and c) and a neutral wire of the line are assumed to be placed at heights of 12, 11, 10 and 8 m, respectively. The separation distance between adjacent poles is set to 58 m, which is an average interval distance presented in [29]. The phase wires are terminated by  $500\ \Omega$  resistances at poles 15 and 1 for impedance matching. Arresters with a stray capacitance of 1 nF are installed on Poles 14, 10, 6, and 2. The arrester I-V characteristic is presented in Table 7.1. The arrester characteristic is taken from [31] and the voltage of 47 kV at 1 A is added to limit the arrester current in the low-voltage region.

The resistances, arresters and neutral wire are connected to a vertical ground lead at each pole. A lightning channel of 520 m in height is placed 11 m away from Pole 15, as illustrated in Figure 7.1 (a). A return stroke current,  $I_L$ , of 8.4 kA (Case No.: FPL0350-1 in [29]) as in Figure 7.2, is investigated in this Chapter.

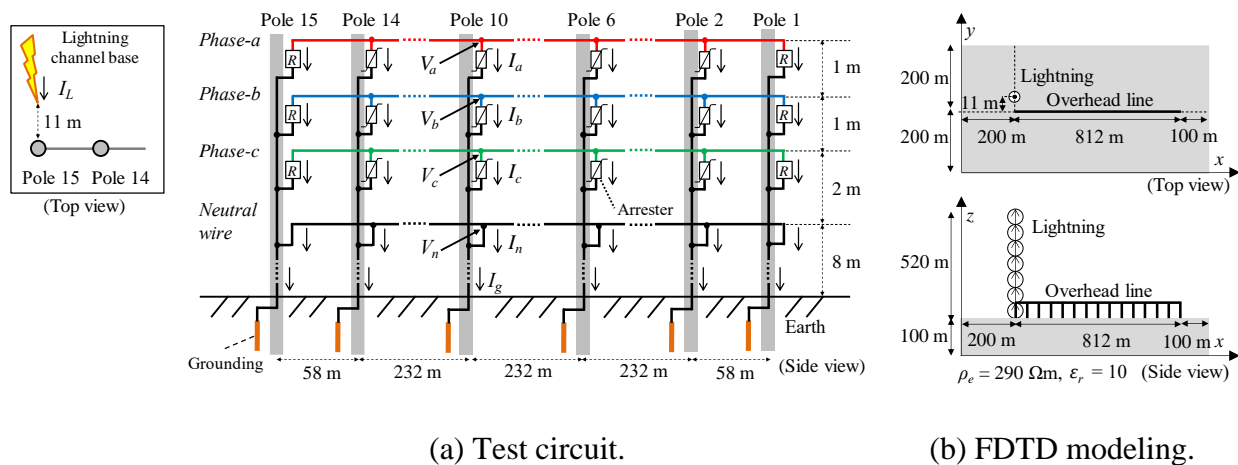
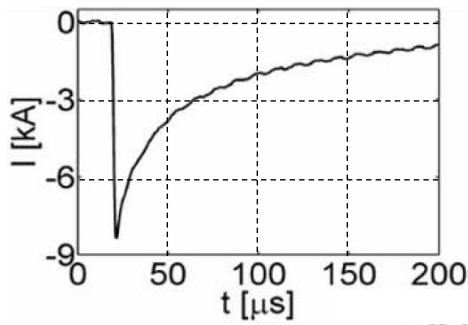


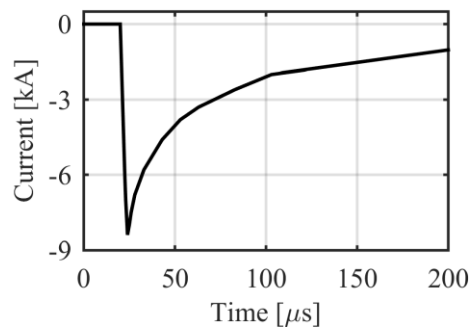
Figure 7.1 Test circuit for transient current measurements due to a lightning strike to ground near a distribution line.

Table 7.1 Arrester characteristic

Current	[A]	1	1500	3000	5000	10000	20000	40000
Voltage	[kV]	47	49	52	55	60	70	82

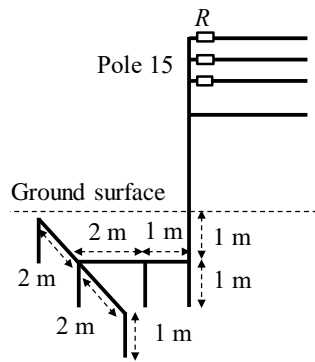


(a) Measured current in [29].

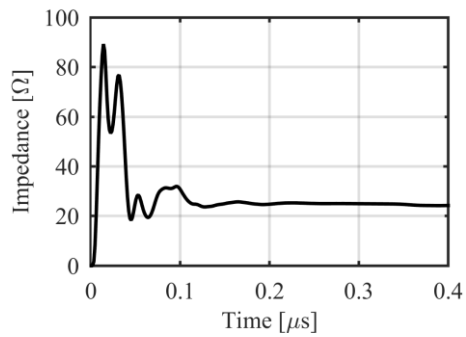


(b) Applied current in FDTD.

Figure 7.2 Return stroke current ( $I_L$ ) of FPL0350-1.



(a) Model of grounding.



(b) Grounding impedance.

Figure 7.3 An example of grounding representation at Pole 15 in FDTD.

Table 7.2 Grounding resistance

Pole		15	14	10	6	2	1
Measured [29]	[Ω]	24	28	18	18	20	24
FDTD	[Ω]	24.3	29.6	18.7	18.7	20.9	24.3

### 7.1.2 FDTD modeling

Figure 7.1 (b) illustrates the FDTD model circuit used to represent the test circuit. Figure 7.2 shows the return stroke current. Figure 7.3 shows a grounding model for Pole 15 in FDTD. Grounding is modeled by vertical and horizontal conductors to represent underground lead wires and grounding rods in [29]. Groundings for the other poles are also modeled in the same manner and their grounding resistances are adjusted by changing the length of the lead wires and the number of rods. Table 7.2 gives the grounding resistance at each pole measured in the test [29] and computed by FDTD when a step current of 1 A is injected into the groundings one by one. Figure 7.3 (b) shows an example of the grounding impedance response at Pole 15 by FDTD. The FDTD results in Table 7.2 show good agreement with the measured results. Earth resistivity  $\rho_e$  is assumed as  $290 \Omega\text{m}$  which gives nearly the same grounding resistance as the measured result at Pole 15. The earth relative permittivity  $\epsilon_r$  is assumed to be 10.

The FDTD working space of  $1112 \text{ m} \times 400 \text{ m} \times 620 \text{ m}$  shown in Figure 7.1 (b) is composed of 1-, 2-, and 4-m cell lengths. The minimum 1-m cell is applied to a region from 180 to 280 m on the  $x$ -axis, 180 to 220 m on the  $y$ -axis, and 80 to 200 m on the  $z$ -axis (20 m underground to 100 m above the ground surface), which includes the lightning channel base, Pole 15 and Pole 14. The largest 4-m cell is applied to the first 140 m on the  $x$ -axis, the first/last 100 m on the  $y$ -axis, and the first 60 m and last 320 m on the  $z$ -axis (40 m underground and 200 m above the ground surface). The 2-m cell is applied to the rest of the space between the minimum- and largest-cell regions. The working space is covered by Liao's absorbing boundary [107]. The depth of earth is taken as 100 m. Ground lead currents at the bottom of the poles ( $I_g$ ) are computed by FDTD. Also, currents flowing from the phase and neutral wires into the ground lead ( $I_a$ ,  $I_b$ ,  $I_c$ , and  $I_n$ ) and voltage differences between the phase wires and neutral wire ( $V_a - V_n$ ,  $V_b - V_n$ , and  $V_c - V_n$ ) are computed. The direction of current injected into the earth is considered as positive. Note that the arrows in Fig. 3 in [29] indicate the direction of the "electron" while the arrows in Figure 7.1 indicate the direction of the current, hence the arrows in Figure 7.1 are opposite to those in [29]. The voltage differences are computed by integration of the electric field intensity from the neutral wire to the phase wire groundings one by one. The FDTD model of the lightning channel is represented by a series of small current sources as a traveling-current-source model [56] to adjust return stroke velocity and to obtain a smooth electromagnetic field. The current is assumed to start rising at 20

$\mu\text{s}$  and reaches its peak at  $24 \mu\text{s}$ . The return stroke velocity is assumed to be  $1 \times 10^8 \text{ m/s}$  (ratio to the speed of light  $\beta = 0.33$ ). One FDTD computation needs about 10 hours on a desktop computer of 4-cores, Intel-i7, 2.8 GHz, with dual channel memory.

### 7.1.3 FDTD simulation in comparison with measured results

Figure 7.4 shows ground lead currents  $I_g$  measured in [29] and computed by FDTD. Also included in this figure with dashed lines are EMTP [70] simulation results (see Section 7.3). Both the polarities and amplitudes of the currents obtained by FDTD agree reasonably well with the measured results. It is stated in [29] that the sum of the currents flowing through all the ground leads except that of Pole 15 was the same as  $I_g$  at Pole 15.

$$I_{g15} = -(I_{g15} + I_{g10} + I_{g6} + I_{g2} + I_{g1}) \quad (7.1)$$

where  $I_{gi}$  is the ground lead current at pole  $i$ .

This has been confirmed in the FDTD results. Only a minor difference at the peak between  $I_{g15}$  and the sum of the currents at the other poles is observed in the FDTD. It would be caused by displacement current, which flows through space instead of the wires in the initial transient.

It is observed in Figure 7.4 that the Pole-14 current reaches zero much faster than the currents at the other poles in the test and FDTD results. This phenomenon is explained by the faster decay of high-frequency current components due to their higher damping [29].

It should be noted that, because Liao's absorbing boundary is originally designed for an electromagnetic field traveling at the speed of light, unintended reflection may occur when the return stroke of  $1 \times 10^8 \text{ m/s}$  reaches the top boundary of the FDTD working space. However, the reflected wave is thought to be negligible because there is no sudden change and fluctuation on the current waveforms at around  $89 \mu\text{s}$  in Figure 7.4, when the reflected wave is estimated to come back to the overhead line. The  $89 \mu\text{s}$  results from the summation of  $20 \mu\text{s}$  (the return stroke starts to rise),  $52 \mu\text{s}$  (the stroke reaches the top boundary after traveling 520 m) and  $17 \mu\text{s}$ . The latter value is the time at which the reflected wave returns to the overhead line at the speed of light, i.e.  $520 \text{ m}/(3 \times 10^8 \text{ m/s})$ .

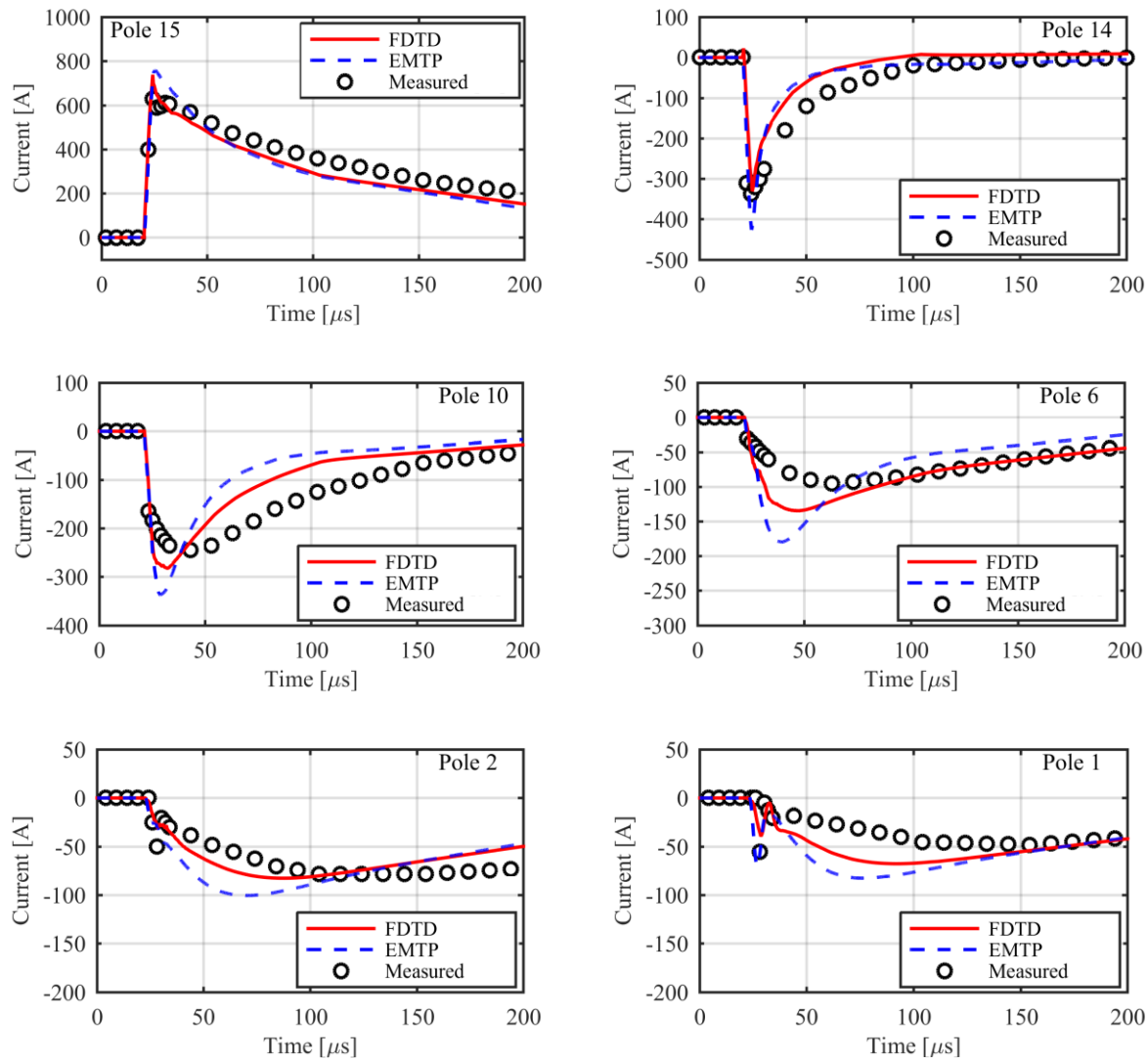


Figure 7.4 Measured and FDTD/EMTP computed results of ground lead current ( $I_g$ ) at each pole.

## 7.2 Investigation of lightning characteristics based on FDTD simulation

In general, transient measurements are expensive and complicated. Consequently, the number of measurements is restricted. If the accuracy of a simulation tool is confirmed in comparison with measured results, the tool can be used to obtain results of transient currents and voltages at various

branches and nodes which were not available in the measurements. In this section, FDTD is adopted to calculate the transient currents and voltages.

### 7.2.1 Current distribution

To investigate the current distribution ( $I_a$ ,  $I_b$ ,  $I_c$ ,  $I_n$ , and  $I_g$ ) at every pole, the currents are separately computed by FDTD. Peak values of the currents and voltages at each pole with the time of occurrence are summarized in Table 7.3. Figure 7.5 shows the current waveforms at Poles 15, 10, and 1. In Figure 7.5, it is confirmed that the sum of  $I_a$ ,  $I_b$ ,  $I_c$ , and  $I_n$  is identical to  $I_g$  except for initial transients.

$$I_g = I_a + I_b + I_c + I_n \quad (7.2)$$

For example, the currents at Pole 15 are

$$\begin{aligned} 617 \text{ A } (I_g) &\approx 610 = 64 + 48 + 39 + 450 \text{ A } (\sum I_{a,b,c,n}) \text{ at } 23 \mu\text{s} \\ 602 \text{ A } (I_g) &= 602 = 4 - 2 - 1 + 601 \text{ A } (\sum I_{a,b,c,n}) \text{ at } 30 \mu\text{s} \end{aligned} \quad (7.3)$$

The small difference at 23  $\mu\text{s}$  is caused by the displacement current as mentioned in Section 7.1.3.

Table 7.3 Peak currents and voltages with the time of occurrence.

Pole no.		15		14		10		6		2		1	
Peak current / time		A	$\mu\text{s}$	A	$\mu\text{s}$	A	$\mu\text{s}$	A	$\mu\text{s}$	A	$\mu\text{s}$	A	$\mu\text{s}$
Measured [29]	$I_g$	630	22	-345	23	-245	38	-95	63	-78	104.0	-80	27
Simulated current	$I_g$	738	24	-330	25	-282	32	-135	46	-83	88	-68	92
	$I_n$	613	26	-308	24	-283	33	-136	46	-83	88	-68	94
	$I_a$	64	23	20	21	9	22	6	23	6	24	18	26
	$I_b$	48	23	14	21	6	22	4	23	3	25	4	26
	$I_c$	39	23	10	21	5	22	4	24	2	25	3	26
Peak voltage / time		kV	$\mu\text{s}$	kV	$\mu\text{s}$	kV	$\mu\text{s}$	kV	$\mu\text{s}$	kV	$\mu\text{s}$	kV	$\mu\text{s}$
Simulated voltage	$V_a - V_n$	31.7	23	25.4	23	12.7	24	10.5	25	9.7	26	9.2	26
	$V_b - V_n$	24.0	23	18.7	23	7.6	23	4.8	24	2.4	25	1.9	26
	$V_c - V_n$	19.4	23	15.2	23	6.0	23	4.0	24	1.8	25	1.4	26

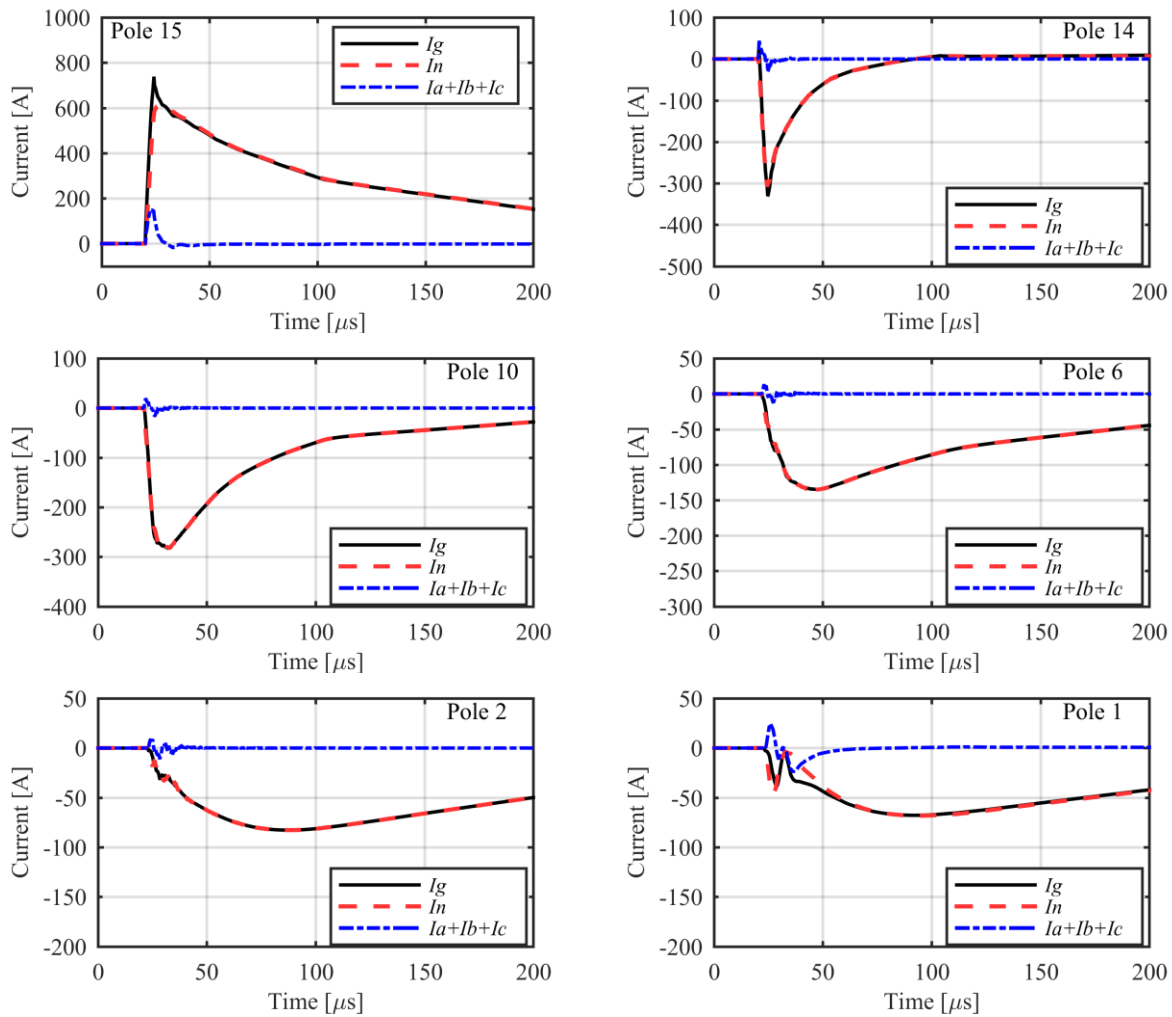


Figure 7.5 Currents  $I_g$ ,  $I_n$ , and  $I_a+I_b+I_c$  at pole 15, 10, and 1 computed by FDTD.

A large part of  $I_g$  comes from the neutral wire, and the phase wire currents contribute only during the initial tens of  $\mu\text{s}$ , because the phase wire currents are produced dominantly by lightning induced voltages to the phase wires. Figure 7.6 shows the phase-to-neutral voltages  $V_a-V_n$ ,  $V_b-V_n$ , and  $V_c-V_n$ . Currents  $I_a$ ,  $I_b$ , and  $I_c$  at Poles 15 and 1 correspond to the values of the voltages divided by the terminating resistance  $500\ \Omega$  as can be seen in Table 7.3. Also, the currents at the other poles, where there are stray capacitances of  $1\ \text{nF}$ , correspond to the value calculated by the following equation.

$$I = C \frac{dV}{dt} \quad (7.4)$$



Figure 7.7 shows an example of the voltage  $V_a - V_n$ , its time-derivative  $dV/dt$ , current  $I_a$ , and capacitance calculated by (7.4) at Pole 14 in the initial transient. The waveforms of  $dV/dt$  and  $I_a$  become identical, which represents the relation (7.4) with a constant  $C$ . The capacitance calculated by  $I_a$  divided by  $dV/dt$  corresponds to 1 nF as plotted with a black dashed line. Note that a spike and fluctuations at 23.3 and 24.3  $\mu\text{s}$  are due to numerical errors where both  $dV/dt$  and  $I_a$  become almost zero.

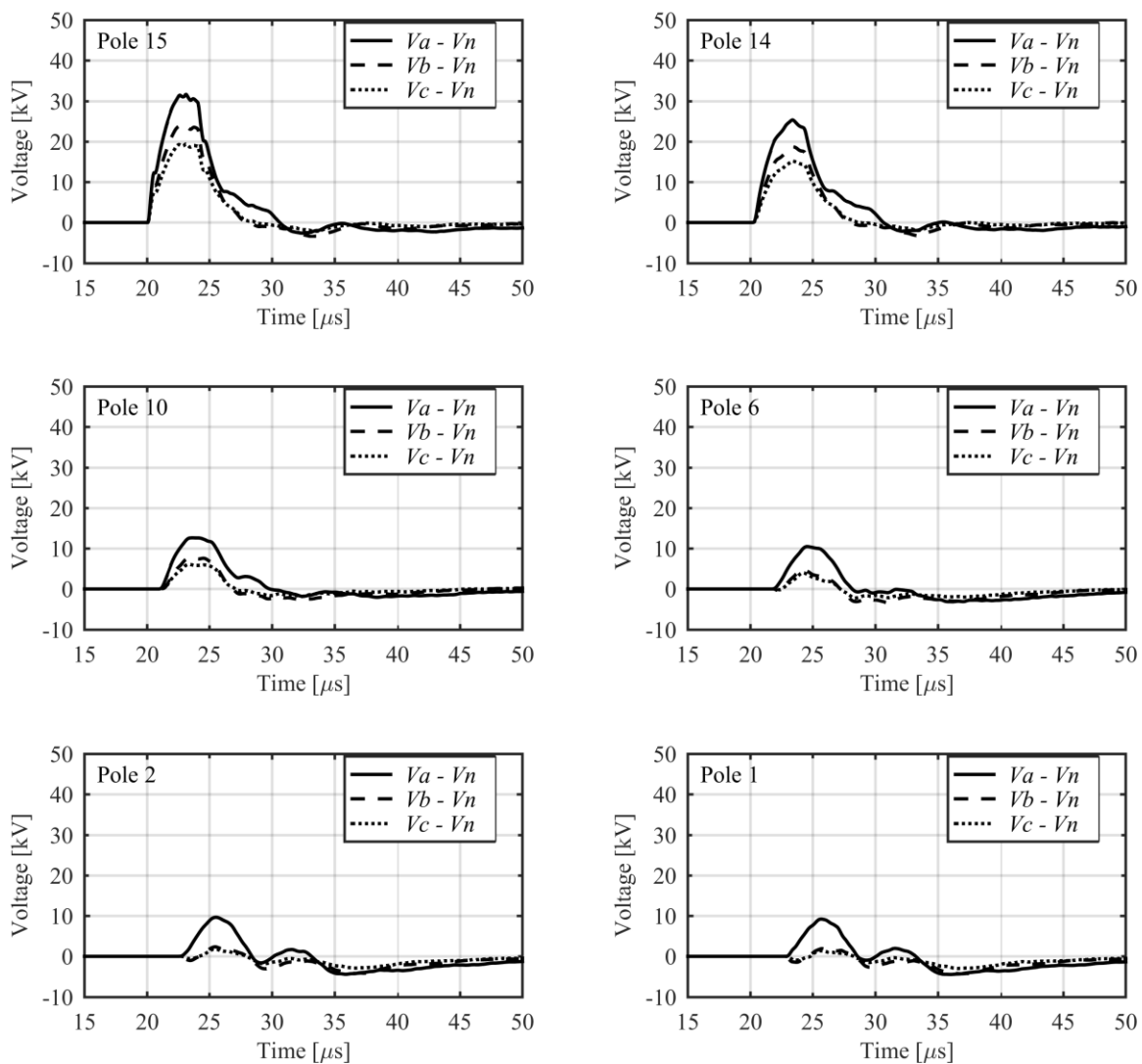


Figure 7.6 Phase-to-neutral voltages ( $V_a - V_n$ ,  $V_b - V_n$ , and  $V_c - V_n$ ) at pole 15, 10, and 1 computed by FDTD.

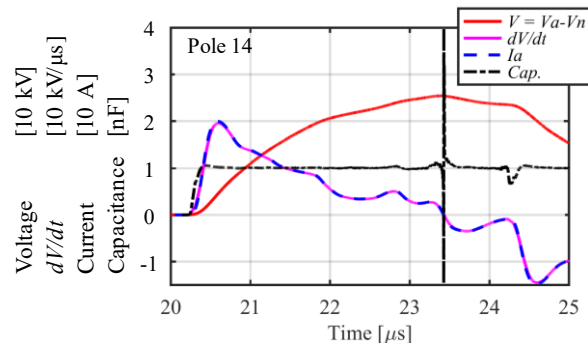
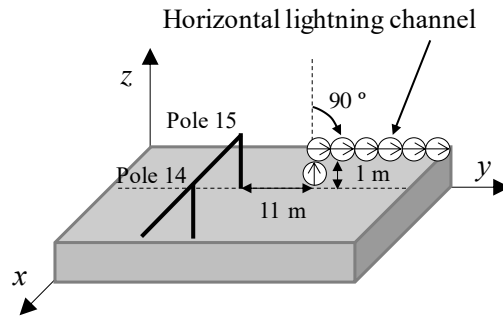


Figure 7.7 Voltage  $V = V_a - V_n$ ,  $dV/dt$ , current  $I_a$ , and arrester capacitance calculated by  $I_a$  divided by  $dV/dt$  at Pole 14 in the initial transient.

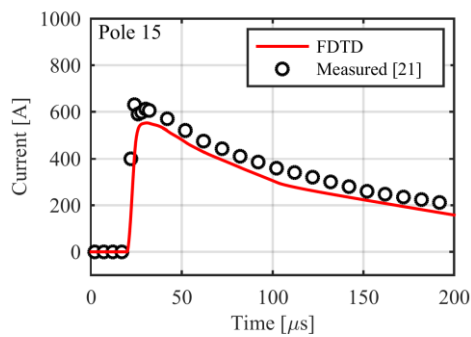
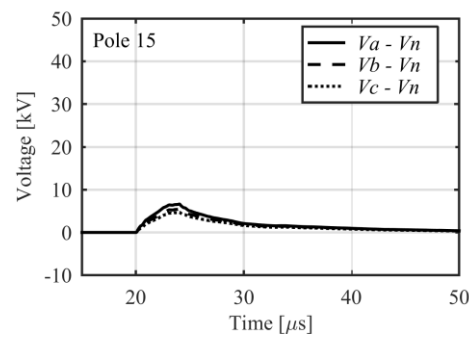
## 7.2.2 Voltage characteristics

In the phase-to-neutral voltages shown in Figure 7.6, the largest and smallest voltages are observed on phase-a and -c, respectively. This can be explained by influences of line height and the distance from the neutral wire. In general, lightning induced voltage becomes proportional to line height in the range of distribution-line height (about 10 to 20 m) [34], [43], and thus the voltage on phase-a should be the largest. In addition, a shorter distance to the neutral wire decreases the induced voltage, as in the case of overhead shield wires.

The voltages do not reach the arrester discharge voltage of 47 kV in this case, and the currents only flow through the terminating resistors and the arrester stray capacitances. To observe the effect of the neutral-wire current on the phase-wire voltage, an FDTD computation is performed by assuming a “horizontal” lightning channel, i.e. the lightning channel is inclined  $90^\circ$  in the opposite direction to the line and placed 1-m above the earth surface as shown in Figure 7.8 (a). Because the channel is perpendicular to the line, the induced voltages become very small. Figure 7.8 (b) shows computed results of the ground lead current and (c) shows phase-wire voltages at Poles 15. The ground lead current is 75 % (552 A) of the original  $I_{g15}$  while the peak phase-a voltage is 21 % (6.7 kV), which indicates that GPR is more dominant for the ground lead and neutral wire currents, and the induced voltage is more significant for the phase voltages and resulting phase-to-neutral currents. A subtraction of the voltages in Figure 7.8 (c) from those in Figure 7.6 is estimated to yield the actual lightning induced voltage.



(a) Horizontal lightning channel (90° inclination).

(b) Ground lead current  $I_g$ .

(c) Phase-to-neutral voltages.

Figure 7.8 Ground lead current and phase-to-neutral voltages at Pole 15 when the lightning channel is inclined 90° in the opposite direction to the line and placed 1-m above the earth surface in the FDTD.

### 7.2.3 Effect of lightning position

In this section, the effect of the lightning position (distance to the nearest pole) is investigated. In [29], the lightning channel base is placed at  $x = 0$  (in front of Pole 15) and  $y = 11$  m as illustrated in Figure 7.1 (Case 0: base case). The following three additional cases are considered.

Case A1:  $x = 0$  m (in front of Pole 15),  $y = 20$  m

Case A2:  $x = 290$  m (in front of Pole 10),  $y = 11$  m

Case A3:  $x = 290$  m (in front of Pole 10),  $y = 20$  m

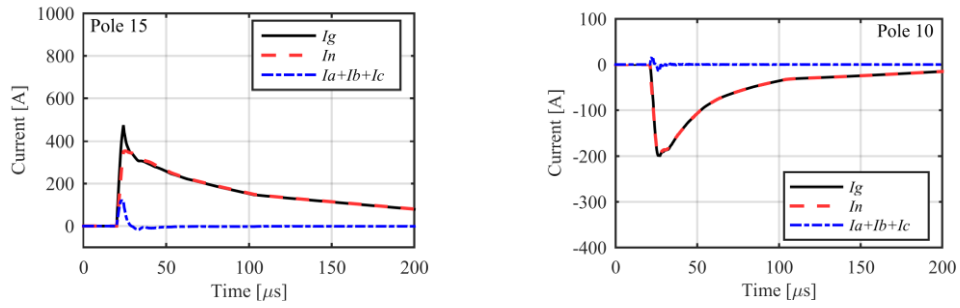
The currents ( $I_a$ ,  $I_b$ ,  $I_c$ ,  $I_n$ , and  $I_g$ ) and phase-to-neutral voltages ( $V_a-V_n$ ,  $V_b-V_n$ , and  $V_c-V_n$ ) in Case 0 are shown in Figure 7.4-Figure 7.6. Those in Case A1 and A2 are presented in Figure 7.9. The peak currents and voltages in Cases 0 and A1 to A3 are summarized in Figure 7.10. It is clear from a comparison of Figure 7.4 and Figure 7.5 (Case 0) with Figure 7.9 (a-1) (Case A1) that the currents become smaller as the distance from the lightning channel base to Pole 15 becomes larger as is easily understood; e.g.  $I_{g15}$  drops to 475 A in Case A1. Also, the voltage shows a similar trend to the current as observed in Figure 7.6 (Case 0) and Figure 7.9 (b-1) (Case A1) because the lightning induced voltage is inversely proportional to the distance.

In Case A2 (the lightning channel base in front of Pole 10), larger currents and voltages appear at Pole 10 as shown in Figure 7.10. The current reaches 850 A which is larger than 738 A at Pole 15 current in Case 0. It is because of 1) the lower grounding resistance at Pole 10 as given in Table 7.2, and 2) larger induced voltages on phase wires as in Figure 7.10 (b). The current at Pole 10 flows to both the left and right poles.

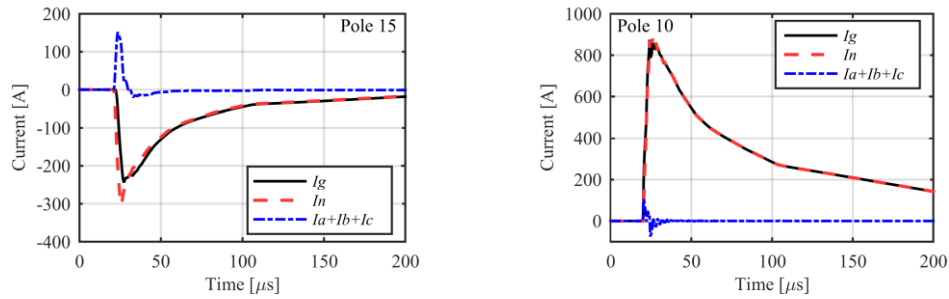
A spike-like current of +150 A is observed in the phase-wire current at Pole 15 in Figure 7.9 (a-2). This current is generated by the induced voltage to the phase wires and thus keeps the same sign as those in Case 0 and A1; i.e. the phase-wire current direction becomes opposite to currents  $I_g$  and  $I_n$  at Pole 15.

The voltage at Pole 10 reaches 47 kV in Case A2 which is much greater than 34 kV at Pole 15 in Case 0, because both  $\pm x$  directions of the distribution line are illuminated by the lightning electromagnetic field which induces the voltage. Note that the phase-a arrester on Pole 10 operates in this case but the influence is minor: the arrester current is less than 45 A and appears only between 20 and 25  $\mu$ s.

It becomes clear that the current and the voltages are quite dependent on the lightning position, the distance from the lightning to the nearest pole, and the pole grounding resistance.

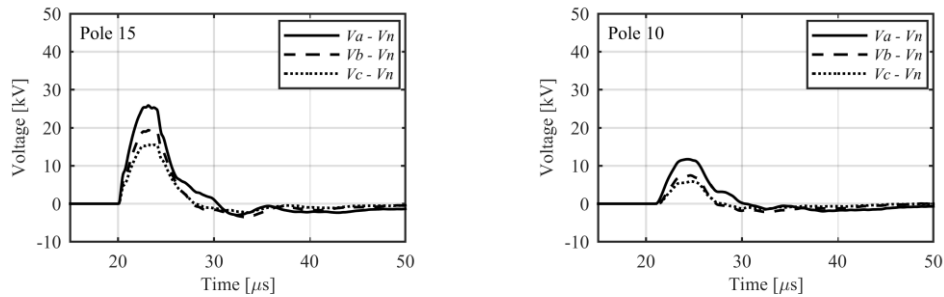


(a-1) Case A1.

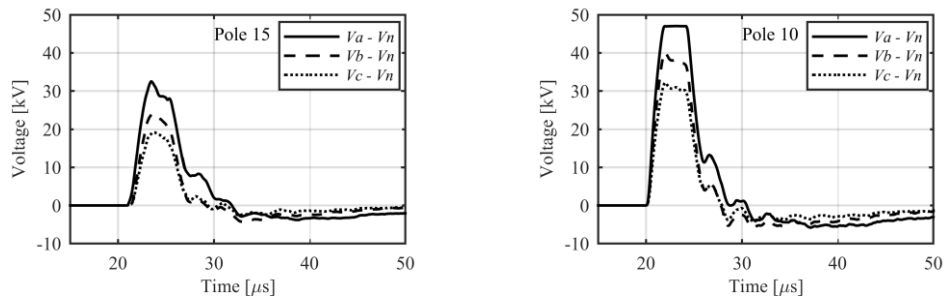


(a-2) Case A2.

(a) Current waveforms.



(b-1) Case A1.



(b-2) Case A2.

(b) Voltage waveforms.

Figure 7.9 Simulated results of currents and voltages in Cases A1 and A2.

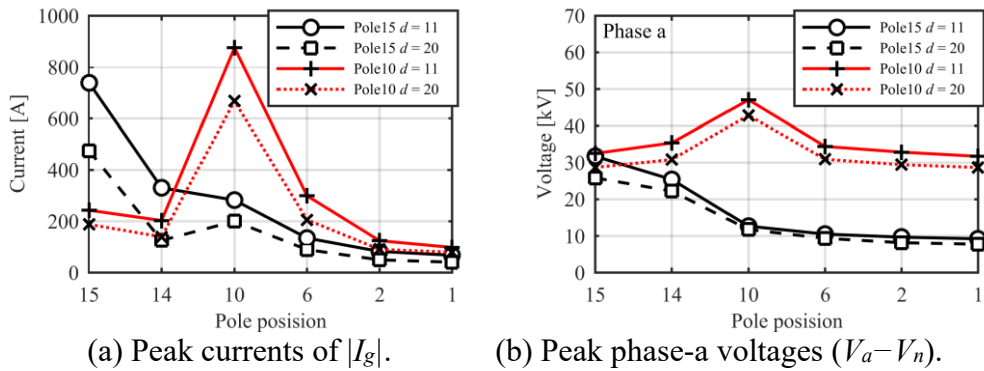


Figure 7.10 Peak currents and phase-a voltages for various lightning positions.

## 7.2.4 Effect of pole grounding resistance

Figure 7.11 illustrates various structures of Pole 15 (nearest to the lightning channel) grounding investigated in this section. From FDTD simulations, the grounding resistances  $R_g$  are evaluated as  $17.9 \Omega$  in Case B1 and  $15.1 \Omega$  in Case B2. It should be recalled that the grounding resistance of Pole 15 in the measurement (Case 0) is  $24.3 \Omega$  as in Table 7.2.

Figure 7.12 shows the currents/voltages at Pole 15 in Case B1 and B2. The current  $I_{g15}$  in Case B2 increases to 879 A. Figure 7.13 summarizes the peak values of ground lead currents and phase-a voltages in Cases 0 to B2. It is clear in Figure 7.13 (a) that the currents increase at every pole as the resistance  $R_g$  decreases. The same trend is observed for the voltage, but the increase is minor as observed in Figure 7.13 (b). Phase-b and -c voltages show the same trend as phase-a, although the peak voltage in phase-a is higher.

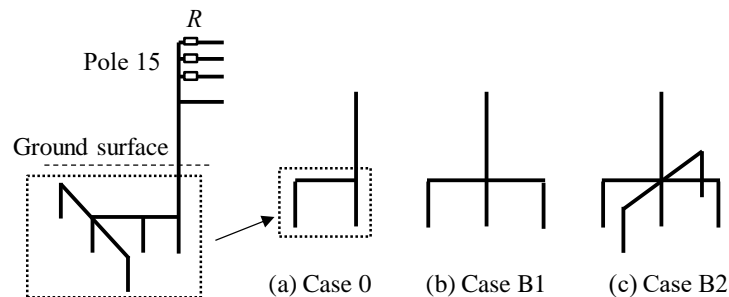
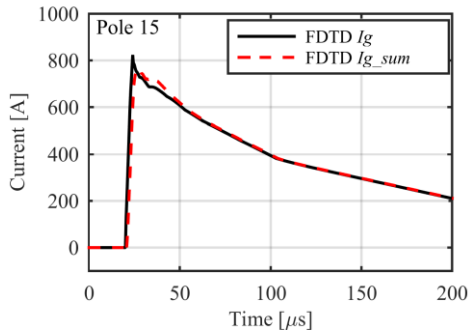
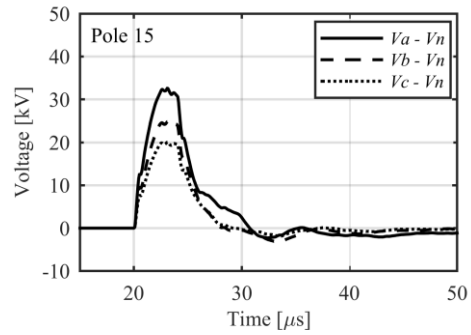


Figure 7.11 Structure of Pole 15 grounding in Cases 0, B1, and B2.

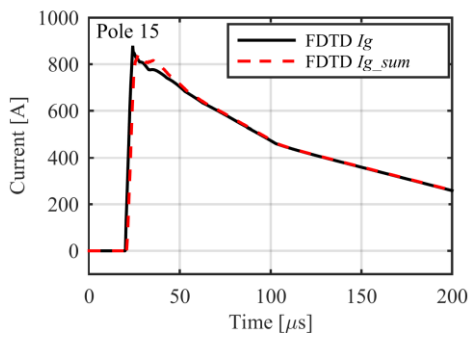


(a-1) Current waveforms.

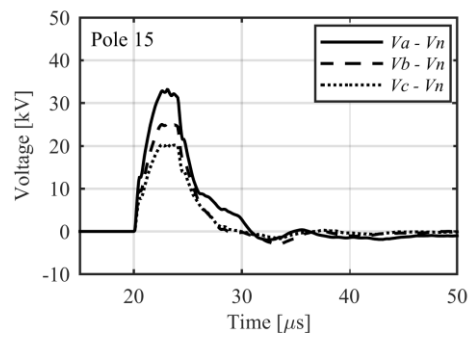


(a-2) Voltage waveforms.

(a) Case B1:  $R_g = 17.9 \Omega$ .



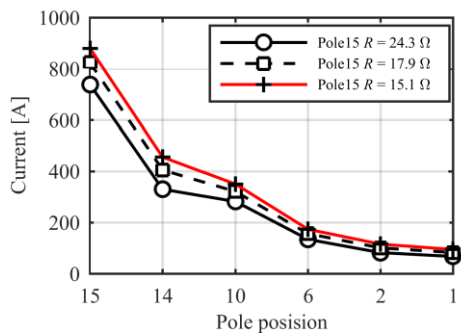
(b-1) Current waveforms.



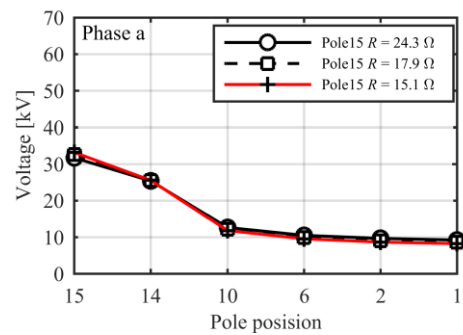
(b-2) Voltage waveforms.

(b) Case B2:  $R_g = 15.1 \Omega$ .

Figure 7.12 Currents and voltages at Pole 15 in Case B1 and B2.



(a) Peak currents of  $|I_g|$ .



(b) Peak phase-a voltages ( $V_a - V_n$ ).

Figure 7.13 Peak ground lead currents and phase-a voltages for different grounding resistances ( $R_g$ ) at Pole 15.

## 7.2.5 Inclined lightning channel

A real lightning channel is not vertical, and an inclined lightning channel influences induced voltages as investigated in the previous chapters. The influence of the inclination on currents flowing from earth to a distribution line due to lightning strikes to the earth near the line, has not been previously investigated. Although the lightning channel in the test [29] is assumed to be vertical, it might be interesting to investigate its influence when it is inclined.

Figure 7.14 illustrates a model circuit for inclined lightning. The lightning channel base is fixed, and two inclined angles are investigated: angle  $\theta$  on the  $yz$  plane for the inclination towards the line, and angle  $\varphi$  on the  $xz$  plane for the inclination along the line. The angles  $\theta$  and  $\varphi$  vary from  $-15^\circ$  to  $+15^\circ$ . A positive sign indicates the channel becoming closer to the line or line center.

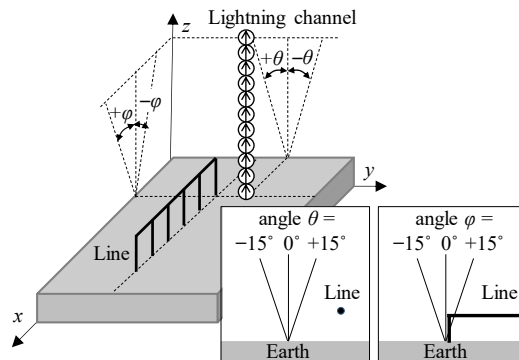


Figure 7.14 Lightning channel inclination.

Figure 7.15 shows the ground lead current ( $I_g$ ) waveforms at Pole 15 with the inclined lightning of  $\theta$  and  $\varphi = \pm 15^\circ$ . As observed in Figure 7.15 (a), the inclined channel causes a minor effect on the entire waveform. A difference due to the inclination is observed only at the wave front in Figure 7.15 (b). The amplitude of the initial peak decreases as the inclined angle decreases. Angle  $\varphi$  shows a much larger influence than that of angle  $\theta$ . It is noticed that the peak current computed by FDTD at  $\varphi = -15^\circ$  becomes nearly the same as the measured result.

Figure 7.16 shows the phase-a voltage waveform at Pole 15 with the inclination. A similar trend to the currents in Figure 7.15 is observed.



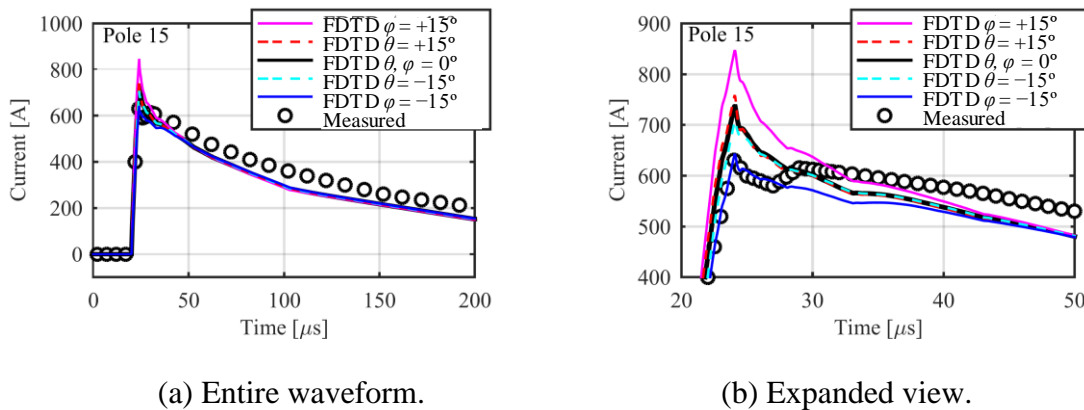


Figure 7.15 Influence of the lightning inclination on the ground-lead current ( $I_g$ ) at Pole 15.

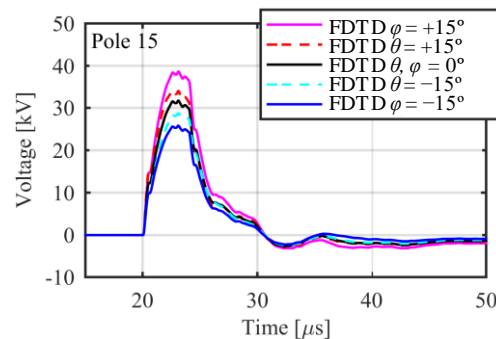


Figure 7.16 Influence of the lightning inclination on the phase-a voltage ( $V_a-V_n$ ) waveform.

Figure 7.17 shows the peak currents and voltages and those at 50  $\mu\text{s}$  as a function of  $\theta$  and  $\phi$ . The peak values are influenced by the angles, but the values at 50  $\mu\text{s}$  show no difference. In summary, the inclined lightning channel influences only the wave front of the current and voltage. When the lightning is inclined along the line (angle  $\phi$ ), vector potential by the return stroke current induces not only a vertical electric field (from the line to ground) but also a horizontal one which contributes to generate a traveling voltage on the line [132]. The lightning channel of  $\phi = +15^\circ$  induces a large traveling voltage in the direction from Pole 14 to 15, which results in the highest current and voltage at Pole 15. When the lightning is inclined toward the line (angle  $\theta$ ), the lightning channel becomes closer ( $\theta = +15^\circ$ ) or farther ( $\theta = -15^\circ$ ). However, the influence of the channel position on the voltage is relatively minor compared to that of angle  $\phi$ .

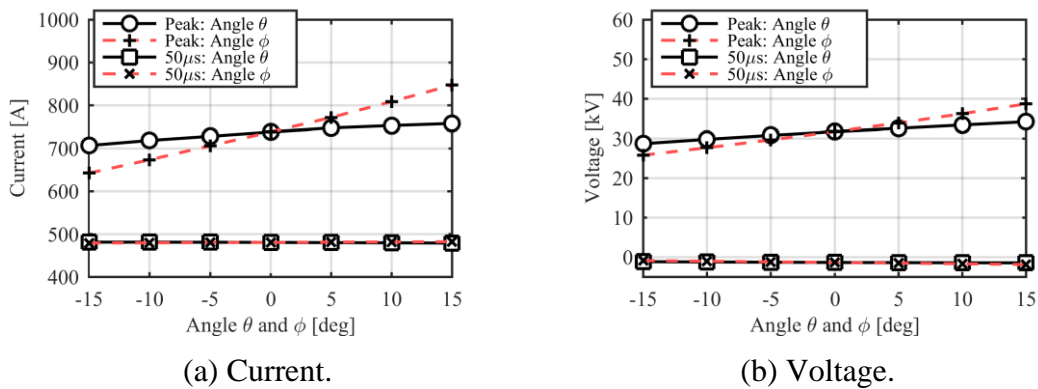


Figure 7.17 Influence of the lightning inclination on the amplitude of the ground lead current ( $I_g$ ) and phase-a voltage ( $V_a - V_n$ ) of Pole 15 at peak and at 50  $\mu$ s.

## 7.2.6 Effect of neutral wire configuration

In this section, the height of the neutral wire is varied and its effect on phase-wire voltages is investigated. Figure 7.18 illustrates the investigated cases. The heights of the phase wires are fixed to those used in the test while that of the neutral wire is varied from  $-1$  m (B1) to 14 m (A14). In case B1, the neutral wire is buried at 1-m beneath the ground surface. Thus, the total grounding resistance of the poles is significantly decreased.

Figure 7.19 shows the peak phase-a voltage at each pole with various neutral wire heights. In Cases A7 to A9, the neutral wire is located under the phase wires and the position of the wire causes a minor effect on the voltage. In Cases A13 and A14, the neutral wire is above the phase wires, the voltages are reduced in comparison with those in Case A7 to A9. The reduction is the largest in Case A13. In Case B1, the voltage becomes the highest at Pole 15 but quickly decreases towards Pole 10. A neutral wire nearest to the phase wires is effective to reduce the voltages, although a larger current flows into it.

Case (A9+A13), where two neutral wires of A9 and A13 are installed at the same time, reduces the voltages significantly around Pole 15 (nearest to the lightning channel base) as in Figure 7.19. However, the voltage peaks at the poles after Pole 10 are nearly the same as those in the single neutral wire cases. This indicates that partially installed double neutral wires are enough to suppress the peak overvoltage which appears at the nearest pole to the lightning. Figure 7.20 (a) illustrates

the double wire structure, and (b) shows FDTD results. The partial double wires are comparable to the complete double wires.

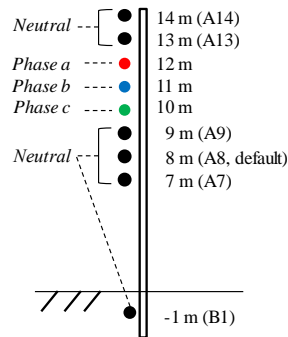


Figure 7.18 Study cases of the neutral wire position.

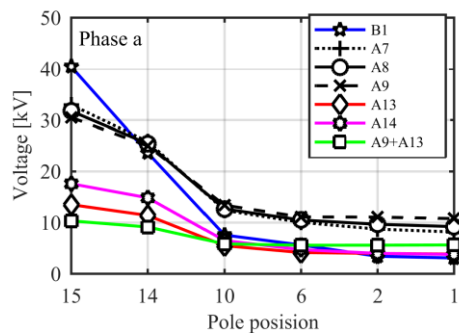
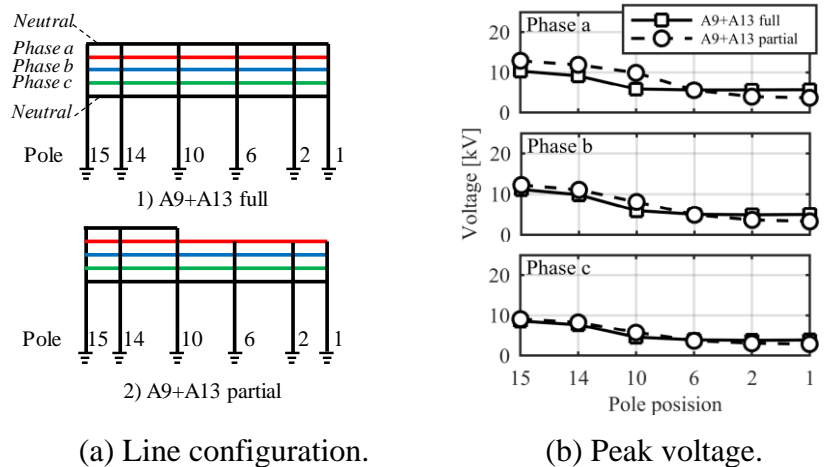


Figure 7.19 Effect of the neutral wire position on the peak phase-a voltage ( $V_a-V_n$ ).



(a) Line configuration.

(b) Peak voltage.

Figure 7.20 Peak phase-to-neutral voltages ( $V_a-V_n$ ,  $V_b-V_n$ , and  $V_c-V_n$ ) in the cases of the neutral wires A9 (full length, Pole 15 to 1) plus: 1) A13 (full length), and 2) A13 (partial length, Pole 15 to 10).

## 7.2.7 Return stroke current of 30 kA

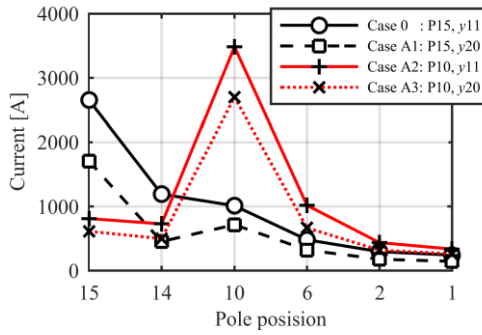
### 7.2.7.1 Effect of lightning position

The investigations in the previous sections are made with the fixed return stroke current  $I_L$  of 8.4 kA based on [29]. However, real lightning current varies from a few kA to more than 100 kA. A larger lightning current easily activates the arresters, which might change the influences discussed in the previous sections. Thus, some additional investigations are made with an average return stroke current of 30 kA [12].

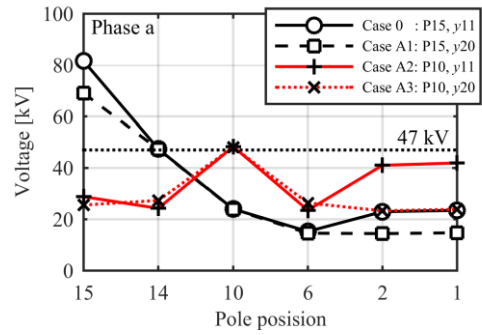
Figure 7.21 shows the influence of the lightning position on the peak current and voltage when  $I_L = 30$  kA. Although the voltages in Figure 7.21 (b) are limited to 47 kV at Pole 14 and 10 by the arresters, the influences of the lightning position and distance from the line are clearly observed. The current distribution in Figure 7.21 (a) looks similar to those in Figure 7.10. The largest current is observed at Pole 10 in Case A2. Figure 7.22 shows the current and voltage waveforms at Pole 10 in Case A2. The neutral wire current  $I_n$  is still dominant in the grounding current  $I_g$ , but the sum of the phase-to-neutral (arrester) currents  $I_a+I_b+I_c$  contributes almost half of the  $I_g$ -peak.

In Figure 7.21, one difference from Figure 7.10 is that the peak voltages at Pole 2 and 1 are larger than that at Pole 6 in Case 0 and A2. This can be explained by the influence of the larger arrester current at Pole 14 or 10. When  $I_L$  is 8.4 kA and the arrester currents are small, the induced voltages at Pole 1 show relatively simple waveforms with positive polarity as presented in Figure 7.23 (a). Correspondingly, the phase-to-neutral currents flow from the phase wires to the Pole-1 grounding. On the other hand, when  $I_L$  is 30 kA and the arrester currents are large, the voltage waveforms fluctuate, and negative peaks appear as shown in Figure 7.23 (b). Because the large arrester currents flow from the other poles to Pole 10 (the grounding to the phase wire at Pole 1), the current directions at Pole 1 become opposite if the currents by the arrester discharge are larger than those by the induced voltages at Pole 1.

In summary, even when  $I_L = 30$  kA and the arresters are clearly activated, the current and voltage distributions are dependent on the lightning position and distance from the line. The current distribution is similar to the one of  $I_L = 8.4$  kA. However, the phase-to-neutral current directions and voltage polarities become different due to the arrester discharge.

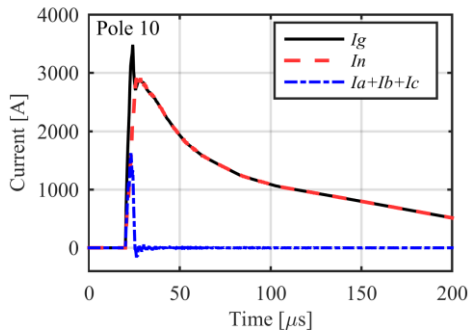


(a) Peak currents of  $|I_g|$ .

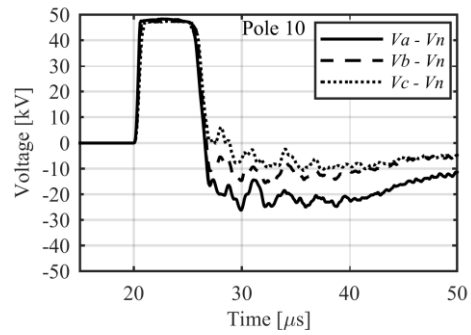


(b) Peak phase-a voltages  $|V_a - V_n|$ .

Figure 7.21 Peak currents and phase-a voltages for various lightning positions with a return stroke current of 30 kA.

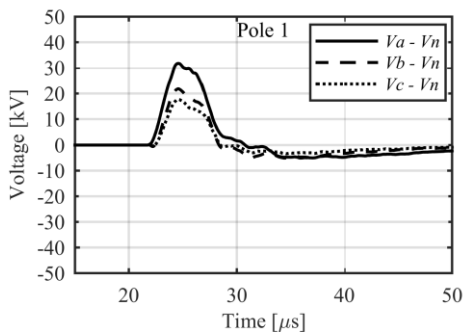


(a) Current waveforms.

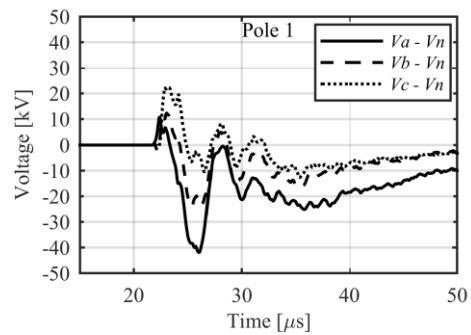


(b) Voltage waveforms.

Figure 7.22 Current and voltage waveforms at Pole 10 in Case A2 with a return stroke current of 30 kA.



(a) Case A2, 8.4 kA.

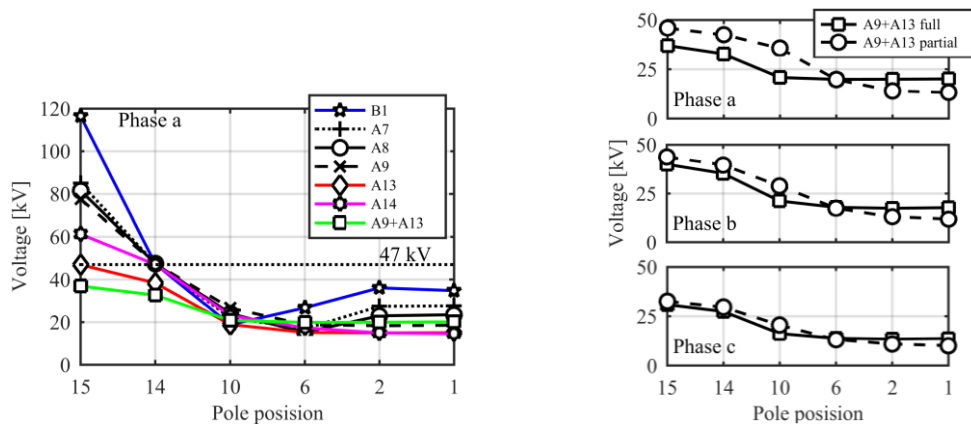


(b) Case A2, 30 kA.

Figure 7.23 A comparison of the voltage waveforms at Pole 1 in Case A2 between return stroke currents of 8.4 and 30 kA.

### 7.2.7.2 Effect of neutral wire position

Because the characteristics of the phase-to-neutral currents and voltages are influenced by the  $I_L$  amplitude and arrester discharge, effect of neutral wire configuration is also investigated with  $I_L = 30$  kA. Figure 7.24 shows the results. Although the arresters at Pole 14 are activated and the voltages are limited to 47 kV, the voltage trend at Pole 15 becomes the same as that in Figure 7.19. The voltage at Pole 15 is significantly suppressed in Case A9+13, as in Figure 7.19, and the voltage at Pole 14 does not reach the discharge voltage of 47 kV. The result clearly indicates that the double neutral-wire configuration can effectively suppress the induced voltage even when  $I_L = 30$  kA. In addition, the partially-installed double neutral wires are still useful as illustrated in Figure 7.24 (b).



(a) Peak phase-a voltages  $|V_a - V_n|$ .

(b) Voltages in Case A9+A13.

Figure 7.24 Effect of the neutral wire position on the peak phase-a voltage  $|V_a - V_n|$  with a return stroke current of 30 kA.

## 7.3 EMTP Simulation

### 7.3.1 Modeling of test circuit

Figure 7.25 illustrates the test circuit for EMTP simulation. It is straightforward to model the distribution line with arresters in EMTP. The line can be represented either by a frequency

dependent (FD) line model [166] or by a constant parameter (CP) line model [7]. Note that lightning induced voltage is not considered in this EMTP simulation.

### 7.3.1.1 Pole grounding

There is no subroutine to calculate grounding impedance in EMTP. The pole grounding resistances are evaluated from FDTD simulation results as shown in Table 7.2. The resistances can be used to represent the pole groundings.

### 7.3.1.2 Lightning channel base to poles

As explained in [29], GPR at the lightning channel base and GPR generated by the lightning to nearby equipment can be modeled by a mutual impedance circuit. Based on this approach, the circuit from the lightning channel base to the pole groundings is represented as shown in Figure 7.25. The resistance between the lightning channel base and Pole 15 is estimated by FDTD.

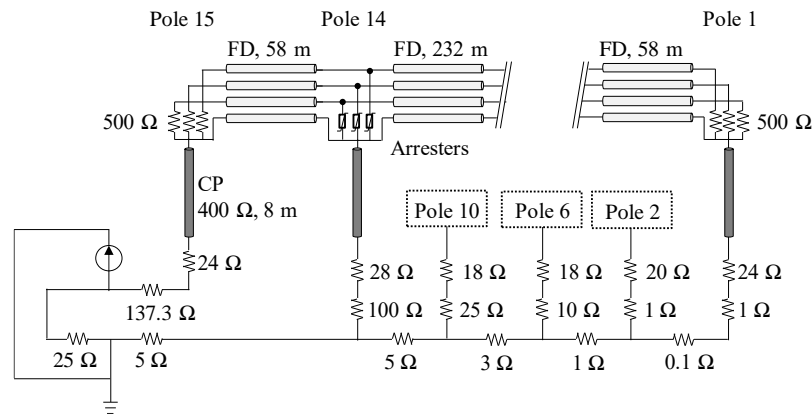


Figure 7.25 EMTP model circuit.

## 7.3.2 Simulation results

Figure 7.4 shows EMTP simulation results in comparison with the test and FDTD results. The EMTP results are observed to agree satisfactorily with the FDTD results at Poles 15 and 14. A discrepancy from the test and FDTD results is noticeable at the other poles, although qualitatively acceptable. Because GPR is more dominant for the ground lead and neutral currents as explained

in Section 7.2.2, neglecting induced voltages would not make large differences to the overall waveforms (at least in this case). The result suggests that EMTP can be used to approximately simulate lightning surge currents on a distribution line due to nearby lightning. However, parameters such as the resistance between the lightning and pole would be required to be estimated by another method.

## 7.4 Concluding remarks

Measured currents from rocket-triggered lightning near a test distribution line reported in a reference have been simulated by FDTD, and the simulation results agree reasonably well with the measured results. Transient currents and voltages in the distribution line are computed by FDTD, and currents/voltages not measured in the test are shown. Further, the effects of the lightning position, pole grounding, inclined lightning channel, and neutral wire configuration are investigated. Also, EMTP simulations are performed and compared with the test and FDTD results.

Based on the above observations, it is validated that FDTD is effective for the analysis of transients on a distribution line due to nearby lightning considering both induced voltages and lightning currents flowing into the line by GPR. It is confirmed that the lightning current flowing into the nearest pole is dependent on the lightning position, distance from the lightning to the pole, and pole grounding resistance. The influences of the lightning position and distance are also confirmed when the lightning current amplitude is changed from 8.4 to 30 kA. In addition, the following concluding remarks can be made.

- (1) A large part of the phase-to-neutral wire voltage is lightning induced voltage. Correspondingly, a large part of the phase-wire current is produced by the induced voltage and appears as a spike-like current with time duration of less than 10  $\mu$ s. The spike-like current superposes onto the neutral wire current at the wave front and gives the peak in the ground lead current.
- (2) When the lightning channel is inclined but not vertical to the earth surface, the peak current and voltage vary by  $\pm 10\%$  depending on the inclined angle, but the overall wave shape shows only a minor difference except on the wave front.



- (3) The neutral wire height under the phase wires causes a minor difference to the phase voltages. If double neutral wires under and above the phase wires are installed, the voltage at the pole near the lightning channel is significantly reduced.
- (4) EMTP simulation results agree qualitatively well with test and FDTD results. EMTP can be used to approximately simulate lightning surge currents on a distribution line due to nearby lightning by adopting a mutual impedance circuit.

## CHAPTER 8 CONCLUSIONS

### 8.1 Summary of thesis

The main objective of this thesis is to reveal and summarize (1) the influences of non-vertical lightning on the lightning induced overvoltages in the distribution systems and (2) lightning current behaviour in a lossy earth, for an accurate evaluation of the induced voltages.

The most important remarks of this thesis are summarized below.

#### 8.1.1 Influences of non-vertical lightning on lightning induced overvoltages

FDTD model circuits to represent non-vertical lightning channels are built and the influences of non-vertical lightning are investigated with various conditions such as lightning parameters, lightning channel geometry, earth condition, voltage measuring point, and distribution-line configuration including a realistic three-phase line with poles, arresters, and groundings. In addition, the FDTD results are compared with an analytical formula and the mechanism of the changes is discussed. The following concluding remarks can be made.

- (1) Lightning induced overvoltages are significantly influenced by inclined lightning, especially by the inclination toward a distribution line (angle  $\theta$ ). The peak voltages at  $\theta = +45^\circ$  reach values that are more than two times larger than those obtained by vertical lightning when a fast-rise lightning current is assumed.
- (2) Lightning inclination along the line (angle  $\varphi$ ) shows only a minor difference on the peak induced voltage. However, it makes the voltage profile along the line asymmetric due to the influence of the inclination on the induced traveling-wave voltages.
- (3) The voltage increase ratio by the angle  $\theta$  increases with decreasing earth resistivity and the rise-time of the lightning current becomes shorter.
- (4) When a three-phase line with a shield wire is assumed, the increase ratio of the voltage by the angle  $\theta$  shows a similar trend to that for the single-phase line. The influence of the angle

$\theta$  is clearly observed even when arresters are installed on the line. However, the arresters decrease both the induced voltages and the increase ratio of the voltages caused by the angle  $\theta$ .

- (5) It is confirmed by using a computationally-generated lightning-like (zig-zag) channel that realistic non-vertical lightning can be represented by simply-inclined lightning. Therefore, the obtained knowledge by the above-mentioned inclined-lightning studies is reasonable and applicable to real induced-voltage problems.

The knowledge obtained from the studies carried out in this thesis clearly indicates that the influences of non-vertical lightning should be considered for an accurate evaluation of lightning induced overvoltage.

### 8.1.2 Earth current behavior

FDTD model circuits are validated in comparison with experimental results in published papers and the influences of lightning distance, lightning-struck position to the line, grounding structure, neutral wire position, and lightning inclination are investigated using FDTD. Further, lightning current behavior due to lightning near a distribution line is studied and the following concluding remarks can be made.

- (1) When lightning strikes the earth or a pole with a grounding electrode, a large portion of the current flows on the earth surface and the remaining portion flows into the earth during a transient period. The current density is approximately proportional to  $1/r^2$  ( $r$ : distance from the lightning base) for the lightning to the earth surface, and  $1/rL$  for the lightning to the pole with the grounding electrode of length  $L$ .
- (2) Lightning-to-earth electromagnetic coupling influences the initial peaks of the earth surface current and resulting GPR. The coupling current becomes more dominant on the current peak when distance  $r$  is greater than 10 m. For more accurate GPR and earth-surface current evaluation, the coupling effect should be considered.
- (3) It is also confirmed that the lightning inclination increases the earth-surface current amplitude and resulting GPR.

- (4) When lightning strikes a distribution line, a portion of the lightning current flows into the pole grounding structure of the distribution line due to the lower impedance. Thus, the current density becomes higher toward the distribution pole. It is observed that current larger amount of the nearby lightning current is absorbed by a low-resistance grounding. This could cause surge-current troubles in distribution networks.
- (5) In the case of the lightning near a three-phase line with a neutral wire and groundings, it is observed that a large part of the voltage difference between the phase and neutral wires is caused by the lightning induced overvoltage. Further, a large current flows into the neutral wire via the groundings. The induced voltage produces a spike-like current in short time duration and superposes onto the neutral-wire current, which gives the peak lightning current flowing into the distribution line via the groundings.

The basic characteristic of earth current distribution is summarized, and the influence of the lightning-to-earth coupling is clearly demonstrated. The coupling effect should be considered for accurate earth current/GPR estimations.

## **8.2 Future work**

### **8.2.1 Correction method for existing standards**

Existing standards, including IEEE standards, adopt the vertical lightning assumption to calculate the lightning induced overvoltages. A correction method to consider the influence of the non-vertical lightning on induced voltages might be valuable for designing lightning protection schemes. For this purpose, the derivation of a correction term or a correction formula to modify the standard evaluation results of the induced voltage is one of the important future topics.

### **8.2.2 Further verification and comparison with field test results**

For any numerical computations, a comparison with field tests is the best way to validate the calculated results and refine the model circuit. Further comparisons of the influences of non-vertical lightning especially on the induced voltage and earth surface current (lightning-to-earth coupling) should be performed in the future.

### **8.2.3 Statistical analysis of the non-vertical lightning influences**

One technical hurdle for the study of non-vertical lightning is that availability of data related to real non-vertical lightning geometry is quite limited. By collaborating with lightning-observation researchers, lightning channel geometry (and in particular, lightning inclination angles at low altitude) could be summarized, and statistical analyses of the non-vertical lightning should be performed.

## BIBLIOGRAPHY

- [1] S. B. Smith and R. B. Standler, "The effects of surges on electronic appliances," *IEEE Trans. Power Del.*, vol. 7, no. 3, pp. 1275-1282, Jul. 1992.
- [2] M. Kawahito, "Investigation of lightning overvoltages within a house by means of an artificial lightning experiment," *R&D News Kansai Electric Power*, pp. 32-33, Sep. 2001.
- [3] Y. Imai, N. Fujiwara, H. Yokoyama, T. Shimomura, K. Yamaoka, and S. Ishibe, "Analysis of lightning overvoltages on low voltage power distribution lines due to direct lightning hits to overhead ground wire," *IEE Jpn. Trans. PE 113-B*, pp. 881-888, 1993.
- [4] T. Hosokawa, S. Yokoyama, and T. Yokota, "Study of damages on home electric appliances due to lightning," *IEE Jpn. Trans. PE 125-B*, pp. 221-226, Feb. 2005. (in Japanese)
- [5] Y. Nagai and H. Sato, "Lightning surge propagation and lightning damage risk across electric power and communication system in residential house," *IEICE Japan, Research Meeting*, EMC-05-18, 2005.
- [6] A. Ametani, K. Matsuoka, H. Omura, and Y. Nagai, "Surge voltages and currents into a customer due to nearby lightning," *Electr. Power Syst. Res.*, vol. 79, pp. 428-435, 2009.
- [7] A. Ametani, N. Nagaoka, Y. Baba, and T. Ohno, "Power System Transients: Theory and Applications," CRC Press, N.Y, 2013.
- [8] CIGRE WG C4.408, "Lightning Protection of Low-Voltage Networks," *CIGRE Technical Brochure*, no. 550, 2013.
- [9] P. Wang, L. Li, and V. A. Rakov, "Calculation of current distribution in the lightning protective system of a residential house," *IEEE Trans. Magn.*, vol. 50, no. 2, Article Sequence Number: 7005404, 2014.
- [10] C. A. Charalambous, N. D. Kokkinos, and N. Christofides, "External lightning protection and grounding in large-scale photovoltaic applications," *IEEE Trans. Electromagn. Compat.*, vol. 56, no. 2, pp. 427-434, 2014.
- [11] J. C. Hernández, P. G. Vidal, and F. Jurado, "Lightning and surge protection in photovoltaic installations," *IEEE Trans. Power Deliv.*, vol. 23, no. 4, pp. 1961-1971, 2008.

- [12] IEEE Guide for Improving the Lightning Performance of Electric Power Overhead Distribution Lines, IEEE Standard 1410, 2010.
- [13] IEC-60071-2, Insulation co-ordination - Part 2: Application guide, 1996.
- [14] IEC Protection against lightning Part 1: General principles, IEC Standard 62305-1, 2011.
- [15] JEC-0102-2010, Testing voltage standard, 2010. (in Japanese)
- [16] CIGRE WG C4.402, "Protection of MV and LV Networks against Lightning. Part I: Common Topics," *CIGRE Technical Brochure* no. 287, 2005.
- [17] CIGRE WG C4.501, "Guideline for Numerical Electromagnetic Analysis Method and its Application to Surge Phenomena," *CIGRE Technical Brochure*, no. 543, 2013.
- [18] CIGRE WG C4.26, "Evaluation of Lightning Shielding Analysis Methods for EHV and UHV DC and AC Transmission-lines," *CIGRE Technical Brochure*, no. 704, 2017.
- [19] H. Koga, T. Motomitsu, and M. Taguchi, "Lightning surge waves induced on overhead lines," *Trans. IECE of Japan*, vol. E62, no. 4, pp. 216-223, 1979.
- [20] S. Yokoyama, K. Miyake, H. Mitani, and A. Takanishi, "Simultaneous measurement of lightning induced voltages with associated stroke currents," *IEEE Trans. Power App. Syst.*, vol. 102, no. 8, pp. 2420-2429, 1983.
- [21] C. A. Nucci, "Lightning-induced voltages on overhead power lines. Part I: return stroke current models with specified channel-base current for the evaluation of the return stroke electromagnetic fields, Part II: coupling models for the evaluation of the induced voltages," *ELECTRA*, no. 162, pp. 74-102, 1995.
- [22] A. De Conti, E. Perez, E. Soto, F. H. Silveira, S. Visacro, and H. Torres, "Calculation of lightning-induced voltages on overhead distribution lines including insulation breakdown," *IEEE Trans. Power Del.*, vol. 25, no. 4, pp. 3078-3084, 2010.
- [23] J. O. S. Paulino, C. F. Barbosa, I. J. S. Lopes, and C. C. Miranda, "Time-domain analysis of rocket-triggered lightning-induced surges on an overhead Line," *IEEE Trans. Electromagn. Compat.*, vol. 51, no. 3, pp. 725-732, 2009.

- [24] P. P. Barker, T. A. Short, A. R. Eybert-Berard, and J. P. Berlandis, "Induced voltage measurements on an experimental distribution line during nearby rocket triggered lightning flashes," *IEEE Trans. Power Del.*, vol. 11, no. 2, pp. 980-980, 1996.
- [25] F. Rachidi, "A review of field-to-transmission line coupling models with special emphasis to lightning-induced voltages on overhead lines," *IEEE Trans. Electromagn. Compat.*, vol. 54, no. 4, pp. 898-911, 2012.
- [26] C. F. Wagner and A. R. Hileman, "A new approach to the calculation of the lightning performance of transmission lines III a simplified method: stroke to tower," *AIEE Power App. Syst.*, Part III, vol. 79, no. 3, pp. 589-603, 1960.
- [27] R. Lundholm, R. B. Finn Jr, and W. S. Price, "Calculation of transmission line lightning voltages by field concepts," *AIEE Power App. Syst.*, Part III, vol. 76, no. 3, pp. 1271-1281, 1958.
- [28] S. Yokoyama, K. Miyake, and S. Fukui, "Advanced observations of lightning induced voltage on power distribution lines (II)," *IEEE Trans. Power Del.*, vol. 4, no. 4, pp. 2196-2203, 1989.
- [29] J. Schoene, M. A. Uman, V. A. Rakov, J. Jerauld, K. J. Rambo, D. M. Jordan, G. H. Schnetzer, M. Paolone, C. A. Nucci, E. Petrache, and F. Rachidi, "Lightning currents flowing in the soil and entering a test power distribution line via its grounding," *IEEE Trans. Power Del.*, vol. 24, no. 3, pp. 1095-1103, 2009.
- [30] V. A. Rakov, C. T. Mata, M. A. Uman, K. J. Rambo, and A. G. Mata, "Review of triggered-lightning experiments at the ICLRT at Camp Blanding, Florida," *Power Tech Conference Proceedings*, Bologna, 2003.
- [31] J. Schoene *et al.*, "Direct lightning strikes to test power distribution lines - Part I: experiment and overall results," *IEEE Trans. Power Deliv.*, vol. 22, no. 4, pp. 2236-2244, 2007.
- [32] J. Schoene *et al.*, "Direct lightning strikes to test power distribution lines - Part II : measured and modeled current division among multiple arresters and grounds," *IEEE Trans. Power Deliv.*, vol. 22, no. 4, pp. 2245-2253, 2007.



- [33] C. F. Wagner and G. D. McCann, "Induced voltages on transmission lines," *AIEE Trans.* Vol. 61, no. 12, pp. 916-930, 1942.
- [34] S. Rusck, "Induced lightning overvoltages on power transmission lines with special reference to the overvoltage protection of low voltage networks," *Trans. of the Royal Institute of Technology*, Stockholm. Sweden, no. 120, pp. 1-118, 1958.
- [35] C. D. Taylor, R. S. Satterwhite, and W. Jr. Harrison, "The response of terminated two-wire transmission line excited by a non-uniform electromagnetic field," *IEEE Trans. Antennas Propagat.*, vol. AP-13, pp. 987-989, 1965.
- [36] R. F. Harrington, *Field Computation by Moment Methods*, New York, NY, USA: Macmillan, 1968.
- [37] M. N. O. Sadiku, "A simple introduction to finite element analysis of electromagnetic problems," *IEEE Trans. Education*, vol. 32, no. 2, pp. 85-93, 1989.
- [38] K. S. Yee, "Numerical solution of initial boundary value problems involving Maxwell's equations in isotropic media," *IEEE Trans. Antennas Propagat.*, vol. 14, no. 3, pp. 302-307, 1966.
- [39] P. Chowdhuri, "Parametric effects on the induced voltages on overhead lines by lightning strokes to nearby ground," *IEEE Trans. Power Del.*, vol. 4, no. 2, pp. 1185-1194, 1989.
- [40] P. Chowdhuri and E. T. B. Gross, "Voltage surges induced on overhead lines by lightning strokes," *Proc. Inst. Elect. Eng.*, vol. 114, no. 12, pp. 1899-1907, 1967.
- [41] A. C. Liew and S. C. Mar, "Extension of the Chowdhuri-Gross model for lightning induced voltage on overhead lines," *IEEE Trans. PowerSyst.*, vol. PWRS-1, no. 2, pp. 240-247, 1986.
- [42] H. K. Høidalen, "Analytical formulation of lightning-induced voltages on multiconductor overhead lines above lossy ground," *IEEE Trans. Electromagn. Compat.*, vol. 45, no. 1, pp. 92-100, 2003.

- [43] A. Andreotti, D. Assante, F. Mottola, and L. Verolino, "An exact closed-form solution for lightning-induced overvoltages calculations," *IEEE Trans. Power Del.*, vol. 24, no. 3, pp. 1328-1343, 2009.
- [44] M. Darveniza, "A practical extension of Rusck's formula for maximum lightning-induced voltages that accounts for ground resistivity," *IEEE Trans. Power Del.*, vol. 22, no. 1, pp. 605-612, 2007.
- [45] J. O. S. Paulino, C. F. Barbosa, I. J. S. Lopes, and W. C. Boaventura, "An approximate formula for the peak value of lightning-induced voltages in overhead lines," *IEEE Trans. Power Del.*, vol. 25, no. 2, pp. 843-851, 2010.
- [46] A. Andreotti, A. Pierno, and V. A. Rakov, "An analytical approach to calculation of lightning induced voltages on overhead lines in case of lossy ground - Part I: Model development," *IEEE Trans. Power Del.*, vol. 28, no. 2, pp. 1213-1223, 2013.
- [47] A. Andreotti, A. Pierno, and V. A. Rakov, "An analytical approach to calculation of lightning induced voltages on overhead lines in case of lossy ground - Part II: comparison with other models," *IEEE Trans. Power Del.*, vol. 28, no. 2, pp. 1224-1230, 2013.
- [48] A. Piantini and S. Member, "Extension of the Rusck model for calculating lightning-induced voltages on overhead lines considering the soil electrical parameters," *IEEE Trans. Electromagn. Compat.*, vol. 59, no. 1, pp. 154-162, 2017.
- [49] F. Rachidi, S. L. Loyka, C. A. Nucci, and M. Ianoz, "A new expression for the ground transient resistance matrix elements," *Electric Power Syst. Res.*, vol. 65, pp. 41-46, 2003.
- [50] M. J. Master and M. A. Uman, "Transient electric and magnetic fields associated with establishing a finite electrostatic dipole," *Ant. J. Phys.*, no. 51, pp. 118-126, 1983.
- [51] A. K. Agrawal, H. J. Price, and S. H. Gurbaxani, "Transient response of multiconductor transmission lines excited by a nonuniform electromagnetic field," *IEEE Trans. Electromagn. Compat.*, vol. 22, no. 2, pp. 119-129, 1980.
- [52] M. A. Uman and D. K. McLain, "Magnetic field of the lightning return stroke," *J. Geophys. Res.*, vol. 74, pp. 6899-6910, 1969.

- [53] V. A. Rakov and A. A. Dulzon, "Calculated electromagnetic fields of lightning return stroke," *Tekh. Elektrodinam.*, no. 1, pp. 87-89, 1987.
- [54] C. A. Nucci, C. Mazzetti, F. Rachidi, and M. Ianoz, "On lightning return stroke models for LEMP calculations," *Proc. 19th Int. Conf. Lightning Protection*, Graz, Austria, 1988.
- [55] E. R. Bruce and R. H. Golde, "The lightning discharge," *J. Inst. Elect. Eng.—Pt. 2*, vol. 88, pp. 487-520, 1941.
- [56] F. Heidler, "Traveling current source model for LEMP calculation," *Proc. 6th Int. Zurich Symp. Electromagn. Compat.*, Zurich, Switzerland, pp. 157-162, 1985.
- [57] V. A. Rakov and M. A. Uman, "Review and evaluation of lightning return stroke models including some aspects of their application," *IEEE Trans. Electromagn. Compat.*, vol. 40, no. 4, pp. 403-426, 1998.
- [58] M. Rubinstein and M. A. Uman, "Methods for calculating the electromagnetic fields from a known source distribution: Application to lightning," *IEEE Trans. Electromagn. Compat.*, vol. 31, no. 2, pp. 183-189, 1989.
- [59] C. A. Nucci and F. Rachidi, "Interaction of electromagnetic fields generated by lightning with overhead electrical networks," *The Lightning Flash*, London, U.K.: IEE Press, pp. 425-478, 2003.
- [60] A. Sommerfeld, "Über die ausbreitung der wellen in der drahtlosen telegraphie," *Ann. Phys.*, vol. 28, pp. 665, 1909. (in German)
- [61] M. Thomson, P. J. Medelius, M. Rubinstein, M. A. Uman, J. Johnson, and J. W. Stone, "Horizontal electric fields from lightning return strokes," *J. Geophysical Res.*, vol. 93, pp. 2429-2441, 1988.
- [62] V. Cooray, "Horizontal fields generated by return strokes," *Radio Sci.*, vol. 27, pp. 529-537, 1992.
- [63] M. Rubinstein, "Voltages induced on a test power line from artificially initiated lightning: theory and experiment," Ph. D. dissertation, University of Florida, Gainesville, 1991.

- [64] M. Rubinstein, "An approximate formula for the calculation of the horizontal electric field from lightning at close, intermediate, and long range," *IEEE Trans. Electromagn. Compat.*, vol. 38, no. 3, pp. 531-535, 1996.
- [65] V. Cooray, "Lightning-induced overvoltages in power lines. Validity of various approximations made in overvoltage calculations," *22nd Int. Cons Lightning Protect.*, Budapest, Hungary, 1994.
- [66] C. A. Nucci, F. Rachidi, M. V. Ianoz, and C. Mazzetti, "Lightning-induced voltages on overhead lines," *IEEE Trans. Electromagn. Compat.*, vol. 35, no. 1, pp. 75-86, 1993.
- [67] F. Rachidi, C. A. Nucci, M. Ianoz, and C. Mazzetti, "Influence of a lossy ground on lightning-induced voltages on overhead lines," *IEEE Trans. Electromagn. Compat.*, vol. 38, no. 3, pp. 250-264, 1996.
- [68] M. Paolone *et al.*, "Lightning electromagnetic field coupling to overhead lines: theory, numerical simulations, and experimental validation," *IEEE Trans. Electromagn. Compat.*, vol. 51, no. 3, pp. 532-547, 2009.
- [69] LIOV code, [online]. Available: <http://www.liov.ing.unibo.it/introduction.html>.
- [70] J. Mahseredjian, S. Dennerrière, L. Dubé, B. Khodabakhchian, and L. Gérin-Lajoie, "On a new approach for the simulation of transients in power systems," *Electr. Power Syst. Res.*, vol. 77, no. 11, pp. 1514-1520, 2007.
- [71] LIOV Toolbox, [online]. Available: <https://www.emtp-software.com/en/products/liov-toolbox>.
- [72] J. R. Carson, "Wave propagation in overhead wires with ground return," *Bell Syst. Tech. J.*, vol. 5, pp. 539-554, 1926.
- [73] F. Pollaczek, "Über das feld einer unendlich langen wechselstrom durchlossenen einfachleitung," *E.N.T.*, vol. 3, pp. 339-359, 1926. (in German)
- [74] E. D. Sunde, "Earth conduction effects in transmission systems," Dover publications, New York, 1968.
- [75] E. F. Vance, "Coupling to shielded cables", Wiley Interscience, New York, 1978.

- [76] J. R. Wait, "Theory of wave propagation along a thin wire parallel to an interface," *Radio Sci.*, vol. 7, pp. 675-679, 1972.
- [77] G. Bridges, O. A. Atta, and L. Shafai, "Solution of discrete modes for wave propagation along multiple conductor structures above a dissipative earth," *Can J. Phys.*, vol. 66, pp. 428-438, 1988.
- [78] F. M. Tesche, M. Ianoz, and T. Karlsson, "EMC Analysis Methods and Computational Models," J. Wiley&Sons, New York, 1996.
- [79] A. Ametani, T. Yoneda, Y. Baba and N. Nagaoka, "An investigation of earth-return impedance between overhead and underground conductors and its approximation," *IEEE Trans. Electromag. Compat.*, vol. 51, pp. 860-867, 2009.
- [80] F. Rachidi, C. A. Nucci, and M. Ianoz, "Transient analysis of multiconductor lines above a lossy ground," *IEEE Trans. Power Deliv.*, vol. 14, no. 1, pp. 294-302, 1999.
- [81] A. Timotin, "Longitudinal transient parameters of a unifilar line with ground return," *Rev. Roum. Sc. Tech., Electrotech. Energie*, vol. 12, no. 4, pp. 523-535, Bucarest, 1967
- [82] E. Petrache, F. Rachidi, M. Paolone, C. A. Nucci, V. Rakov, and M. Uman, "Lightning induced disturbances in buried cables—Part I: theory," *IEEE Trans. Electromagn. Compat.*, vol. 47, no. 3, pp. 498-508, 2005.
- [83] M. Paolone *et al.*, "Lightning induced disturbances in buried cables - Part II : experiment and model validation," vol. 47, no. 3, pp. 509-520, 2005.
- [84] F. Delfino, R. Procopio, F. Rachidi, and C. A. Nucci, "An algorithm for the exact evaluation of the underground lightning electromagnetic fields," *IEEE Trans. Electromagn. Compat.*, vol. 49, no. 2, pp. 401-411, 2007.
- [85] F. Delfino, R. Procopio, and M. Rossi, "Lightning return stroke current radiation in presence of a conducting ground: 1. Theory and numerical evaluation of the electromagnetic fields," *J. Geophys. Res.*, vol. 113, pp. D05110-1-D05110-10, 2008.

- [86] F. Delfino, R. Procopio, M. Rossi, F. Rachidi, and C. A. Nucci, "Lightning return stroke current radiation in presence of a conducting ground: 2. Validity assessment of simplified approaches," *J. Geophys. Res.*, vol. 113, pp. D05111-1-D05111-11, 2008.
- [87] A. Shoory, A. Mimouni, F. Rachidi, V. Cooray, R. Moini, and S. H. H. Sadeghi, "Validity of simplified approaches for the evaluation of lightning electromagnetic fields above a horizontally stratified ground," *IEEE Trans. Electromagn. Compat.*, vol. 52, no. 3, pp. 657-663, 2010.
- [88] A. E. Ruehli, "Equivalent circuit models for three-dimensional multiconductor systems," *IEEE Trans. Microw. Theory Techn.*, vol. 22, no. 3, pp. 216-221, 1974.
- [89] S. Visacro and A. Soares Jr., "HEM: A model for simulation of lightning related engineering problems," *IEEE Trans. Power Delivery*, vol. 20, no. 2, pp. 1206-1207, 2005.
- [90] M. Ishii and Y. Baba, "Numerical electromagnetic field analysis of tower surge response," *IEEE Trans. Power Deliv.*, vol. 12, no. 1, pp. 483-488, 1997.
- [91] Y. Baba, and M. Ishii, "Numerical electromagnetic field analysis of lightning current in tall structures," *IEEE Trans. Power Deliv.*, vol. 16, no. 2, pp. 324-328, 2001.
- [92] L. Grcev, "Time- and frequency-dependent lightning surge characteristics of grounding electrodes," *IEEE Trans. Power Deliv.*, vol. 24, no. 4, pp. 2186-2196, 2009.
- [93] C. Vilachá, A. F. Otero, J. C. Moreira, and E. Míguez, "Analysis of a grounding system under a lightning stroke," *IEEE Trans. Ind. Appl.*, vol. 51, no. 6, pp. 4907-4911, 2015.
- [94] A. Shoory, R. Moini, S. H. H. Sadeghi, and V. A. Rakov, "Analysis of lightning-radiated electromagnetic fields in the vicinity of lossy ground," *IEEE Trans. Electromagn. Compat.*, vol. 47, no. 1, pp. 131-145, 2005.
- [95] S. Bonyadi-Ram, R. Moini, S. H. H. Sadeghi, and V. A. Rakov, "On representation of lightning return stroke as a lossy monopole antenna with inductive loading," *IEEE Trans. Electromagn. Compat.*, vol. 50, no. 1, pp. 118-127, 2008.

- [96] R. K. Pokharel, M. Ishii, and Y. Baba, "Numerical electromagnetic analysis of lightning-induced voltage over ground of finite conductivity," *IEEE Trans. Electromagn. Compat.*, vol. 45, no. 4, pp. 651-656, 2003.
- [97] H. Janani, R. Moini, and S. H. H. Sadeghi, "Evaluation of lightning-induced voltage on overhead lines with nonlinear load using the scattering theory," *IEEE Trans. Power Deliv.*, vol. 27, no. 1, pp. 317-324, 2012.
- [98] M. Akbari, K. Sheshyekani, A. Pirayesh, F. Rachidi, M. Paolone, A. Borghetti, and C. A. Nucci, "Evaluation of lightning electromagnetic fields and their induced voltages on overhead lines considering the frequency dependence of soil electrical parameters," *IEEE Trans. Electromagn. Compat.*, vol. 55, no. 6, pp. 1210-1219, 2013.
- [99] K. Sheshyekani and M. Akbari, "Evaluation of lightning-induced voltages on multiconductor overhead lines located above a lossy dispersive ground," *IEEE Trans. Power Deliv.*, vol. 29, no. 2, pp. 683-690, 2014.
- [100] K. Sheshyekani and J. Paknahad, "Lightning electromagnetic fields and their induced voltages on overhead lines: The effect of a horizontally stratified ground," *IEEE Trans. Power Deliv.*, vol. 30, no. 1, pp. 290-298, 2015.
- [101] J. Paknahad, K. Sheshyekani, M. Hamzeh, D. Li, and F. Rachidi, "The influence of the slope angle of the ocean - land mixed propagation path on the lightning electromagnetic fields," *IEEE Trans. Electromagn. Compat.*, vol. 57, no. 5, pp. 1086-1095, 2015.
- [102] K. Sheshyekani and J. Paknahad, "The effect of an ocean-land mixed propagation path on the lightning electromagnetic fields and their induced voltages on overhead lines," *IEEE Trans. Power Deliv.*, vol. 30, no. 1, pp. 229-236, 2015.
- [103] J. Paknahad, K. Sheshyekani, F. Rachidi, M. Paolone, and A. Mimouni, "Evaluation of lightning-induced currents on cables buried in a lossy dispersive ground," *IEEE Trans. Electromagn. Compat.*, vol. 56, no. 6, pp. 1522-1529, 2014.
- [104] J. Paknahad, K. Sheshyekani, and F. Rachidi, "Lightning electromagnetic fields and their induced currents on buried cables. Part I: The effect of an ocean-land mixed propagation path," *Electromagn. Compat. IEEE Trans.*, vol. 56, no. 5, pp. 1137-1145, 2014.

- [105] J. Paknahad, K. Sheshyekani, F. Rachidi, and M. Paolone, "Lightning electromagnetic fields and their induced currents on buried cables. Part II: The effect of a horizontally stratified ground," *IEEE Trans. Electromagn. Compat.*, vol. 56, no. 5, pp. 1146-1154, 2014
- [106] Y. Baba and V. A. Rakov, "Electromagnetic fields at the top of a tall building associated with nearby lightning return strokes," *IEEE Trans. Electromagn. Compat.*, vol. 49, no. 3, pp. 632-643, 2007.
- [107] Z. P. Liao, H. L. Wong, B. P. Yang, and Y. F. Yuan, "A transmission boundary for transient wave analysis," *Sci. Sinica*, vol. A27, no. 10, pp. 1063-1076, 1984.
- [108] C. Yang and B. Zhou, "Calculation methods of electromagnetic fields very close to lightning," *IEEE Trans. Electromagn. Compat.*, vol. 46, no. 1, pp. 133-141, 2004.
- [109] Y. Baba and V. A. Rakov, "On the mechanism of attenuation of current waves propagating along a vertical perfectly conducting wire above ground: application to lightning," *IEEE Trans. Electromagn. Compat.*, vol. 47, no. 3, pp. 521-532, 2005.
- [110] T. Noda, "A tower model for lightning overvoltage studies based on the result of an FDTD simulation," *IEEEJ. Trans. Power Energy*, vol. 127, no. 2, pp. 379-388, 2007.
- [111] K. Tanabe, "Novel method for analyzing dynamic behavior of grounding systems based on the finite-difference time-domain method," *IEEE Power Eng. Rev.*, vol. 21, no. 9, pp. 55-57, 2001.
- [112] G. Ala, P. L. Buccheri, P. Romano, and F. Viola, "Finite difference time domain simulation of earth electrodes soil ionisation under lightning surge condition," *IET Sci., Meas. Technol.*, vol. 2, no. 3, pp. 134-145, 2008.
- [113] Y. Baba and V. A. Rakov, "Voltages induced on an overhead wire by lightning strikes to a nearby tall grounded object," *IEEE Trans. Electromagn. Compat.*, vol. 48, no. 1, pp. 212-224, 2006.
- [114] H. M. Ren, B. H. Zhou, V. A. Rakov, L. H. Shi, C. Gao, and J. H. Yang, "Analysis of lightning-induced voltages on overhead lines using a 2-D FDTD method and agrawal coupling model," *IEEE Trans. Electromagn. Compat.*, vol. 50, no. 3, pp. 651-659, 2008.



- [115] H. Sumitani, T. Takeshima, Y. Baba, N. Nagaoka, A. Ametani, J. Takami, S. Okabe, and V. A. Rakov, "3-D FDTD computation of lightning-induced voltages on an overhead two-wire distribution line," *IEEE Trans. Electromagn. Compat.*, vol. 54, no. 5, pp. 1161-1168, 2012.
- [116] T. H. Thang, Y. Baba, N. Nagaoka, A. Ametani, N. Itamoto, and V. A. Rakov, "FDTD simulations of corona effect on lightning-induced voltages," *IEEE Trans. Electromagn. Compat.*, vol. 56, no. 1, pp. 168-176, 2014.
- [117] A. Tatematsu and T. Noda, "Three-dimensional FDTD calculation of lightning-induced voltages on a multiphase distribution line with the lightning arresters and an overhead shield wire," *IEEE Trans. Electromagn. Compat.*, vol. 56, no. 1, pp. 159-167, 2014.
- [118] Q. Zhang, V. Tang, J. Gao, L. Zhang, and D. Li, "The Influence of the horizontally stratified conducting ground on the lightning-induced voltages," *IEEE Trans. Electromagn. Compat.*, vol. 56, no. 2, pp. 435-443, 2014.
- [119] T. H. Thang, Y. Baba, V. A. Rakov, and A. Piantini, "FDTD computation of lightning-induced voltages on multiconductor lines with surge arresters and pole transformers," *IEEE Trans. Electromagn. Compat.*, vol. 57, no. 3, pp. 442-447, 2015.
- [120] E. M. Rizk, F. Mahmood, M. Lehtonen, E. A. Badran, and M. H. Abdel-rahman, "Influence of highly resistive ground parameters on lightning-induced overvoltages using 3-D FDTD method," *IEEE Trans. Electromagn. Compat.*, vol. 58, no. 3, pp. 792-800, 2016.
- [121] E. M. Rizk, F. Mahmood, M. Lehtonen, E. A. Badran, and M. H. Abdel-rahman, "Computation of peak lightning-induced voltages due to the typical first and subsequent strokes considering high ground resistivity," *IEEE Trans. Power Deliv.*, vol. 32, no. 4, pp. 1861-1871, 2017.
- [122] K. Yamamoto, T. Noda, S. Yokoyama, and A. Ametani, "Experimental and analytical studies of lightning overvoltages in wind turbine generator systems," *Electric Power Syst. Res.*, vol. 79, no. 3, pp. 436-442, 2009.

- [123] K. Yamamoto, J. Takami, and S. Okabe, "Overvoltages on dc side of power conditioning system caused by lightning stroke to structure anchoring photovoltaic panels," *IEEJ Trans. Power Energy*, vol. 132, no. 11, pp. 903-913, 2012.
- [124] N. Nagaoka, H. Morita, Y. Baba, and A. Ametani, "Numerical simulations of lightning surge responses in a seismic isolated building by FDTD and EMTP," *IEEJ Trans. Power Energy*, vol. 128, no. 2, pp. 473-478, 2008.
- [125] M. Levine and R. Meneghini, "Simulation of radiation from lightning return strokes: The effect of tortuosity," *NASA Technical Reports*, Document ID 19770023740, 1977.
- [126] A. Sakakibara, "Calculation of induced voltage on overhead lines caused by inclined lightning strokes," *IEEE Trans. Power Del.*, vol. 4, no. 1, p. 683-693, 1989.
- [127] S. Wu and W. Hsiao, "Characterization of induced voltages on overhead power lines caused by lightning strokes with arbitrary configurations," *1994 Int. Conf. on Systems, Man and Cybernetics*, vol. 3, pp. 2706-2710, 1994.
- [128] K. Michishita, M. Ishii, and Y. Hongo, "Induced voltage on an overhead wire associated with inclined return-stroke channel-model experiment on finitely conductive ground," *IEEE Trans. Electromagn. Compat.*, vol. 38, no. 3, pp. 507-513, 1996.
- [129] T. Yamada, A. Mochizuki, J. Sawada, E. Zaima, T. Kawamura, A. Ametani, M. Ishii, and S. Kato, "Experimental evaluation of a UHV tower model for lightning surge analysis," *IEEE Trans. Power Deliv.*, vol. 10, no. 1, pp. 393-402, 1995.
- [130] A. Ametani, "Wave propagation on a nonuniform line and its impedance and admittance," *Sci.&Eng. Review of Doshisha Univ.*, pp. 11-23, 2002.
- [131] A. Ametani and T. Kawamura, "A method of a lightning surge analysis recommended in Japan using EMTP," *IEEE Trans. Power Deliv.*, vol. 20, no. 2, pp. 867-875, 2005.
- [132] I. Matsubara and S. Sekioka, "Analytical formulas for induced surges on a long overhead line caused by lightning with an arbitrary channel inclination," *IEEE Trans. Electromagn. Compat.*, vol. 51, no. 3, pp. 733-740, 2009.

- [133] N. Rameli, M. Z. A. A. Kadir, M. Izadi, C. Gomes, and J. Jasni, "On the influence of inclined lightning channel on lightning induced voltage evaluation," *2012 31st Int. Conf. Light. Prot. ICLP 2012*, pp. 1-5, 2012.
- [134] N. Rameli, M. Z. A. A. Kadir, M. Izadi, C. Gomes, and J. Jasni, "Evaluation of lightning induced over-voltage due to variations of channel angle," *2013 IEEE 7th International Power Engineering and Optimization Conf.*, no. June, pp. 184-187, 2013.
- [135] S. I. Abouzeid, G. Shabib, and A. Z. E. D. Mohamed, "Induced voltages on overhead transmission lines because of nearby included lightning channel," *IET Gener. Transm. Distrib.*, vol. 9, no. 1, pp. 1672-1680, 2015.
- [136] G. Lupò, C. Petrarca, V. Tucci, and M. Vitelli, "EM fields associated with lightning channels: On the effect of tortuosity and branching," *IEEE Trans. Electromagn. Compat.*, vol. 42, no. 4, pp. 394-404, 2000.
- [137] T. X. Song, Y. H. Liu, and J. M. Xiong, "Computations of electromagnetic fields radiated from complex lightning channels," *Prog. Electromagn. Res.*, vol. 73, pp. 93-105, 2007
- [138] A. Andreotti, C. Petrarca, V. A. Rakov, and L. Verolino, "Calculation of voltages induced on overhead conductors by nonvertical lightning channels," *IEEE Trans. Electromagn. Compat.*, vol. 54, no. 4, pp. 860-870, 2012.
- [139] A. Andreotti, C. Petrarca, and A. Pierno, "On the effects of channel tortuosity in lightning-induced voltages assessment," *IEEE Trans. Electromagn. Compat.*, vol. 57, no. 5, pp. 1096-1102, 2015.
- [140] A. Andreotti, A. Piantini, A. Pierno, and R. Rizzo, "Lightning-induced voltages on complex power systems by using CiLIV : The effects of channel tortuosity," *IEEE Trans. Power Deliv.*, vol. 33, no. 2, pp. 680-688, 2018.
- [141] G. Lupò, C. Petrarca, V. Tucci, and M. Vitelli, "EM fields generated by lightning channels with arbitrary location and slope," *IEEE Trans. Electromagn. Compat.*, vol. 42, no. 1, pp. 39-53, 2000.

- [142] R. Moini, S. H. H Sadeghi, B. Kordi, and F. Rachidi, "An antenna-theory approach for modeling inclined lightning return stroke channels," *Electr. Power Syst. Res.*, vol. 76, pp. 945-952, 2006.
- [143] M. Izadi, M. Z. A. A. Kadir, and C. Gomes, "Evaluation of electromagnetic fields associated with inclined lightning channel using second order FDTD-hybrid methods," *Prog. Electromagn. Res.*, vol. 117, no. May, pp. 209-236, 2011.
- [144] M. Izadi, M. Z. A. A. Kadir, C. Gomes, and W. F. H. W. Ahmad "Analytical expressions for electromagnetic fields associated with the inclined lightning channels in the time domain," *Electr. Power Components Syst.*, vol. 40, no. 4, pp. 414-438, 2012.
- [145] A. Gomes, V. Cooray, and M. Z. A. A. Kadir, "Vertical electric fields and field change parameters due to partly inclined lightning leader channels," *Prog. Electromagn. Res.*, vol. 135, no. October, pp. 55-80, 2013.
- [146] A. Nemamcha and M. Houabes, "Electromagnetic fields produced by inclined return stroke channel," *J. Electr. Eng.*, vol. 65, no. 3, pp. 151-156, 2014
- [147] S. I. Abouzeid, G. Shabib, and A. Z. E. Dine, "Analysis of electromagnetic fields generated by inclined lightning channel," *Arab. J. Sci. Eng.*, vol. 40, no. 9, pp. 2585-2608, 2015.
- [148] Z. D. Jiang, B. H. Zhou, S. Qiu, and L. H. Shi, "Evaluation of electric fields radiated by lightning stepped leaders on finitely conductive ground," *IEEE Trans. Electromagn. Compat.*, vol. 57, no. 5, pp. 1070-1078, 2015.
- [149] H. Motoyama, "Electromagnetic transient response of buried bare wire and ground grid," *IEEE Trans. Power Deliv.*, vol. 22, no. 3, pp. 1673-1679, 2007.
- [150] A. Ametani, T. Chikara, H. Morii and T. Kubo, "Impedance characteristics of grounding electrodes on the earth surface", *Electr. Power Syst. Res.*, vol.85, pp.38-43, 2012.
- [151] K. Yamamoto, Y. Kubo, and S. Sumi, "Transient grounding characteristic of wind turbines affecting back-flow lightning current into distribution system," *Light. Prot. (ICLP), 2016 33rd Int. Conf.*, Estoril, Portugal, 2016.

- [152] J. C. Willett, D. M. Le Vine, and V. P. Idone, "Lightning return stroke current waveforms aloft from measured field change, current and channel geometry," *J. Geophys. Res. Atmos.*, vol. 113, no. D7, pp. 1-45, 2008.
- [153] J. D. Hill, J. Pilkey, M. A. Uman, D. M. Jordan, W. Rison, and P. R. Krehbiel, "Geometrical and electrical characteristics of the initial stage in Florida triggered lightning," *J. Geophys. Res. Atmos.*, vol. 39, no. 9, pp. 1-7, 2012.
- [154] W. R. Gameraota *et al.*, "An 'anomalous' triggered lightning flash in Florida," *J. Geophys. Res. Atmos.*, vol. 118, no. 8, pp. 3402-3414, 2013.
- [155] A. A. Tsonis and J. B. Elsner, "Fractal characterization and simulation of lightning," *Beitr. Phys. Atmosph.* vol. 60, no. 2, pp. 187-192, 1987.
- [156] B. C. Graham-Jones, "The fractal nature of lightning: an investigation of the fractal relationship of the structure of lightning to terrain," MS. thesis, *Dept. Mathematics*, Florida State University, Tallahassee, 2006.
- [157] G. F. Tagg, "Earth Resistances", G. Newens, 1964.
- [158] E. D. Sunde, "Earth Conduction Effect in Transmission Systems", Dover, 1968.
- [159] T. A. Short, "Electric Power Distribution Handbook, Second Edition", CRC press, 2016.
- [160] J. M. Nahman and V. B. Djordjevic, "Maximum step voltages of combined grid-multiple rods ground electrodes," *IEEE Trans. Power Deliv.*, vol. 13, no. 3, pp. 757-761, 1998.
- [161] O. E. Gouda and A. Z. E. Dein, "Ground potential rise of faulty substations having equal and unequal spacing grounding grids conductors," *IET Gener. Transm. Distrib.*, vol. 11, no. 1, pp. 18-26, 2017.
- [162] H. Motoyama, "Transient resistance characteristics of vertical grounding electrodes", *IEE Japan technical meeting on high voltage engineering*, HV-11-085, 2011 (in Japanese).
- [163] A. P. S. Meliopoulos, "Power System Grounding and Transients," Marcel Dekker, 1988.
- [164] J. He, "Methodology and Technology for Power System Grounding," Wiley, 2012.

- [165] K. Yamamoto, S. Sumi, S. Sekioka, and J. He, "Derivations of effective length formula of vertical grounding rods and horizontal grounding electrodes based on physical phenomena of lightning surge propagations," *IEEE Trans. Ind. Appl.*, vol. 51, no. 6, pp. 4934-4942, 2015.
- [166] I. Kocar and J. Mahseredjian, "Accurate frequency dependent cable model for electromagnetic transients", *IEEE Trans. Power Deliv.*, vol. 31, no. 3, pp. 1281-1288, 2016.

## APPENDIX A LIST OF PUBLICATIONS

### Journal publications

1. **M. Natsui**, A. Ametani, J. Mahseredjian, S. Sekioka, and K. Yamamoto, “FDTD analysis of distribution line voltages induced by inclined lightning channel,” *Electr. Power Syst. Res.*, vol. 160, pp. 450-456, 2018.
2. **M. Natsui**, A. Ametani, J. Mahseredjian, S. Sekioka, and K. Yamamoto, “FDTD analysis of nearby lightning surges flowing into a distribution line via groundings,” *IEEE Trans. Electromagn. Compat.*, vol. 62, no. 1, pp. 144-154, 2020.
3. **M. Natsui**, A. Ametani, J. Mahseredjian, and H. Motoyama, “Earth current and GPR distributions due to lightning and effect of a distribution line,” *IEEE Trans. Electromagn. Compat.*, DOI: 10.1109/TEMPC.2019.2954719.
4. **M. Natsui**, A. Ametani, J. Mahseredjian, S. Sekioka, and K. Yamamoto, “3D-FDTD analysis of lightning induced voltages in distribution lines due to inclined lightning,” *IEEE Trans. Electromagn. Compat.*, (accepted on July 4th, 2020).
5. A. Ametani, H. Xue, **M. Natsui**, and J. Mahseredjian, “Electromagnetic disturbances in gas-insulated substations and VFT calculations”, *Electr. Power Syst. Res.*, vol. 160, pp. 191-198, 2018.
6. **M. Natsui**, A. Ametani, J. Mahseredjian, S. Sekioka, and K. Yamamoto, “FDTD analysis of distribution line voltages induced by non-vertical lightning,” *Electr. Power Syst. Res.*, (submitted on February 28th, 2020, under the review).

### Conference publications

1. **M. Natsui**, A. Ametani, J. Mahseredjian, S. Sekioka, and K. Yamamoto, “FDTD analysis of distribution line voltages induced by inclined lightning channel,” *International Conference on Power System Transients (IPST) 2017*, Seoul, South Korea, Paper-ID 101, 2017.

2. **M. Natsui**, S. Sekioka, A. Ametani, K. Yamamoto, and J. Mahseredjian, "Comparison of FDTD and analytical calculations of distribution line voltages induced by inclined lightning," *Annual Conference on IEEJ B-Dept. 2017*, Tokyo, Japan, Paper-ID 302, 2017.
3. **M. Natsui**, A. Ametani, and J. Mahseredjian, "A study on lightning induced overvoltage caused by inclined lightning," *International Symposium on EMC and Transients (ISET) 2017*, Kyoto, Japan, ISET-05, 2017.
4. **M. Natsui**, A. Ametani, and J. Mahseredjian "A study on very fast transients in a gas-insulated bus circuit by FDTD," *High voltage technical meeting on IEEJ*, HV-18-29, 2018.
5. **M. Natsui**, S. Sekioka, A. Ametani, K. Yamamoto, and J. Mahseredjian, "Nonhomogeneous line - Problem associated with a circuit theory and EMTP," *Annual Conference on IEEJ B-Dept. 2018*, Tokushima, Japan, Paper-ID 302, 2018.
6. **M. Natsui**, A. Ametani, J. Mahseredjian, S. Sekioka, and K. Yamamoto, "FDTD analysis of distribution line voltages caused by non-vertical lightning," *International Conference on Power System Transients (IPST) 2019*, Perpignan, France, Paper-ID 51, 2019.
7. H. Xue, **M. Natsui**, A. Ametani, J. Mahseredjian, H. Tanaka, and Y. Baba, "Comparison of transient simulations on overhead cables by EMTP and FDTD," *International Conference on Power System Transients (IPST) 2017*, Seoul, paper-ID 5, 2017.
8. A. Ametani, H. Xue, **M. Natsui**, and J. Mahseredjian, "Electromagnetic disturbances in gas-insulated substations and VFT calculations," *International Conference on Power System Transients (IPST) 2017*, Seoul, paper-ID 72, 2017.
9. A. Ametani, H. Xue, **M. Natsui**, and J. Mahseredjian, "Effect of elbow part of Gas-Insulated Bus on Surge Propagation in GIS," *High voltage technical meeting of IEEJ*, HV-18-095, 2018.